2006

Development of capillary electrophoresis-based microfluidic devices for future medical diagnostics: separation and detection of DNA adducts and other related biomarkers

Abdulilah Abdulqader Dawoud
Iowa State University

Development of capillary electrophoresis-based microfluidic devices for future medical diagnostics: separation and detection of DNA adducts and other related biomarkers

by

Abdulilah Abdulqader Dawoud

A dissertation submitted to the graduate faculty

in partial fulfillment of the requirements for the degree of

DOCTOR OF PHILOSOPHY

Major: Physical Chemistry (Chemical Instrumentation)

Program of Study Committee:
Ryszard Jankowiak, Co-major Professor
Mark Gordon, Co-major Professor
Edward Yeung
Mark Hargrove
Mei Hong

Iowa State University

Ames, Iowa

2006

Graduate College
Iowa State University

This is to certify that the doctoral dissertation of

Abdulilah Abdulqader Dawoud

has met the dissertation requirements of Iowa State University

Signature was redacted for privacy.

Co-major Professor

Signature was redacted for privacy.

Co-major Professor

Signature was redacted for privacy.

For the Major Program

In the memory of my mother, to my father, my wife Elham, my sons Abdulqader and Abdulhadi, my sisters and brothers, and to everybody I love.

TABLE OF CONTENTS

LIST OF ABBREVIATIONS

Ade, adenine
CEC, capillary electrochromatography
CE, capillary electrophoresis
CE-AD, capillary electrophoresis- amperometric detection
CE-ED, capillary electrophoresis- electrochemical detection
CGE, capillary gel electrophoresis
CIEF, capillary isoelectric focusing
CZE, capillary zone electrophoresis
CA, catechol
CEQ, catechol estrogen quinones
DEP, dielectrophoresis
DMEG, dynamic multiple equilibrium gradients
DGS, dynamic gradient sedimentation
DA, dopamine
ED, electrochemical detection
EDL, electric double layer
EOF, electro-osmotic flow
EKC, electrokinetic chromatography
ESI, electrospray ionization
E, estrogen,
E_1, estrone
E_2, estradiol
EG, electrophoretic ground
EGM, equilibrium gradient method
EHD, electro-hydrodynamic
GSH, glutathione
Gua, guanine
HPLC, high performance liquid chromatography
8-OH-dG, 8-Hydroxy-deoxyguanocine
IEF, isoelectric focusing
ITP, isotachophoresis
LIF, laser-induced fluorescence
L-DOPA, L-dihydroxyphenylalanine
LOD, limit of detection
MALDI, matrix-assisted laser desorption ionization
MEKC, micellar electrokinetic chromatography
μ-TAS, micro total analysis system
MES, 2-[N-morpholino] ethanesulfonic acid
NacCys, N-acetylcysteine
NACE, Non-aqueous capillary electrophoresis
OS, oxidative stress

PAH, polycyclic aromatic hydrocarbons
PDMS, poly (dimethylsiloxane)
PE, polyethylene
PET, polyethylene terephthalate
PMMA, Poly (methyl methacrylate)
ROS, reactive oxygen species
R, resolution
SEM, scanning electron microscopy
SDS, sodium dodecyl sulfate
UV, ultraviolet
WE, working electrode

ACKNOWLEDGMENT

First and for most, I should thank and express my gratitude and obedience to Allah the great from whom I receive guidance and help.

My sincere gratitude and appreciation to my father and family, especially my wife Elham, for their support and encouragement over the long years of my schooling.

I would like to offer my special thanks to my research advisor, Prof. Ryszard Jankowiak, and my previous advisor Prof. Gerald J. Small, for all the support and commitment to my education and scientific achievement, and to all previous and present members of Prof. Jankowiak' and Prof. Small's groups.

Also, I would like to express my thanks to Dr. Toshikazu Kawaguchi for offering his vast experience and assistance in electrochemistry and microfabrication through out my research time.

Lastly, I would like to thank and acknowledge the Department of Chemistry at Iowa State University for Science and Technology for giving me the opportunity to peruse my PhD and for the financial support.

ABSTRACT

Genotoxic carcinogens can react covalently with DNA to form DNA adducts, which can lead to mutations in critical genes and subsequently to the development of diseases such as cancer. Consequently, the role of DNA damage and their subsequent biomarkers are considered important in studies involving cancer and other aging-related diseases. Analytical methods with high resolving power and sensitive detection are needed to detect neurotransmitters (e.g. dopamine (DA) and DA-derived DNA adduct), catechol estrogen-derived DNA adducts, and 8-hydroxy-deoxyguanosine DNA adduct in human fluids, as their presence is difficult to determine by standard chromatography with UV absorbance detection. Furthermore, these DNA adducts are weakly fluorescent at room temperature. Thus, native fluorescence detection methods are ineffective with this class of biomarkers. Interestingly, capillary electrophoresis (CE) combined with electrochemical detection (ED) has been found to be a sensitive, selective technique for analyzing a large number of compounds including these analytes. Therefore, a CE-based PDMS/glass hybrid microfluidic device for free solution electrophoresis with totally integrated gold electrodes and simplified gated sample injection were fabricated to separate and detect various DNA adducts and other related biomarkers. Various arrangements of the ED system were tested and evaluated including in-channel and end-channel detection. The best electrode configuration was optimized based on in-channel detection with an *in situ* fabricated palladium decoupler serving as the electrophoretic ground located inside the microchannel. With these microdevices, excellent separation of the above analytes can be accomplished in relatively short times (< 2 minutes); with a limit of detection (LOD) in the sub-femto mole range. Different buffer systems were

used including 2-[N-morpholino] ethanesulfonic acid (MES), phosphate, and borate buffers. Interestingly, significant improvement in the resolution was achieved by using borate buffer, where injecting a mixture of five analytes yield only two peaks with MES buffer, whereas five well-resolved peaks were obtained with borate buffer. These results show that these microdevices have promising separation resolving power and sensitivity for future medical diagnostics.

CHAPTER 1: CAPILLARY ELECTROPHORESIS-BASED MICROFLUIDIC SYSTEMS

1.1 Overview and Dissertation Organization

Microfluidic chips, which first appeared in the early 1990s, are revolutionizing the analytical science landscape [1-9]. Since the initial introduction of the concept, lab-on-a-chip or micro total analysis system (μ-TAS), by Manz et al in 1990 [1], there has been tremendous interests in integrating lab-on-a chip technologies with commonly used separation methods such as capillary electrophoresis (CE). CE is a ubiquitous analytical separation technique with many applications in biomedical, environmental, pharmaceutical, and chemical sciences. Since the first highly efficient separations with CE that was demonstrated by Jorgenson and Lukacs in the early 1980s [10,11], CE have been utilized for various applications, such as the analysis of inorganic ions [12,13], drugs [14,15], peptides [16], proteins, [17,18], DNA [19,20], DNA adducts [21,22], and single cells [23]. In conventional CE, the separation process is performed using a fused-silica capillary, whereas the separation on microchip is performed in a microchannel created on the surface of planar substrate made of glass or polymeric materials. Current technologies offer "laboratories on a chip" that have already demonstrated several advantages over conventional CE systems, including minimal reagent and sample consumption [4,5], higher efficiency [7,8], speed and throughput, portability, integration, and increased parallelism and automation [4,24-27]. The key principle behind developing and manufacturing these μ-TAS's is using well-established fabrication techniques that were developed in the semiconductor industry.

Microfluidic chips with an integrated electrochemical detection (ED) system exploit many of the advantages of miniaturization. In addition, they are more easily and quickly fabricated than chips with integrated optical detection. EC detection also provides a precise method of analytical precision for sensing molecules that are difficult to detect with spectroscopic techniques, such as estrogens-derived and 8-OH-deoxyguanosine DNA adducts [28-30]. In this thesis, the development of CE-microfluidic devices integrated with electrochemical/ amperometric detection for the separation and detection of different DNA adducts and other related metabolites are discussed and presented.

Chapter 1 provides general overview and the motivations underlying the development of CE-based integrated microfluidic chips. Section 1.2 presents the fundamentals of electrokinetic phenomenon and the principle of CE and related analytical parameters. In Section 1.3, the principles of microchip format and other considerations, such as sample introduction (injection), detection, and applications are presented. Also, a summary of previously accomplished developments regarding these issues is provided as well. Chapter 2 provides a brief description of microfabrication and micromachining that are used to manufacture these microfluidic chips. The main emphasis in this chapter is on manufacturing of microfluidic chips by utilizing different materials such as glass (Section 2.1), and poly dimethyl siloxane (PDMS) (Section 2.2) that have been developed in our labs. Chapter 3 provides a brief description of the DNA adducts that are considered as potential biomarkers for cancer diagnostics.

Chapter 4 presents published results by the candidate on the development of integrated microfluidic devices with electrochemical/ amperometric detection, which utilizes the principle of end-channel working electrode arrangement, for the separation and detection

of dopamine-derived DNA adducts and related neurotransmitters. Likewise, Chapter 5 presents results that are submitted for publication by the candidate that utilize the principle of in-channel detection by *in situ* fabrication of palladium decoupler. These microfluidic devices were then used for the separation and detection of 8-OH-dG adduct and related analytes. In Chapter 6, the application of integrated microfluidic devices with palladium decoupler for the separation and detection of different estrogen-derived DNA adducts is presented. In Appendix A, previously published results on Dynamic Multiple Equilibrium Gradients (DMEG) Approach, as a hyper selective separation technique, are presented.

1.2 Principles of Capillary Electrophoresis

1.2 .1 Electrokinetic Phenomenon

Most solids acquire an electric surface charge upon coming into contact with polar liquid, or more specifically electrolytes [31-33]. This surface charge attracts counter ions from the electrolyte solution to form a very thin layer that is known as the *Stern layer*. Then under the influence of the Stern layer, a diffuse layer is formed, that is known as the *Gouy-Chapman layer*. This diffusion layer contains excess charges of the same sign as those in the Stern layer but is thicker than the Stern layer. Both, the Stern and the Gouy-Chapman layers, form what is known as the electric double layer (EDL) [31,32]. The Stern layer has no net charge because of charge proximity, thus the application of any external electric field has no influence on it, i.e. the Stern Layer is fixed in place. On the other hand, the Gouy-Chapman layer has a net charge, which permits it to move under the influence of an external electric field, which is defined as electro-osmosis [31-33]. The movement of the diffuse layer under the influence of the external electric field creates an imaginary surface at the boundary between the two layers called the shear plane. Two potentials are generated within the EDL,

one at the wall surface, which is defined as the wall potential (ψ_o), and a second potential at the shear plane, defined as the zeta potential (ξ), figure 1.1 [31,32].

Assuming a Boltzmann charge distribution at the EDL and that the electrolyte is symmetric, the relation between the charge density (ρ_E) and the potential (ψ) is governed by the following equation, which is known as Poisson-Boltzmann equation [33]:

$$\frac{d^2\psi}{dy^2} = \frac{2Fzc_\infty}{\varepsilon}\sinh\left(\frac{zF\psi}{KT}\right) \qquad 1.1$$

Where c_∞ is the ions' concentration far from the surface, z is the charge of each ion, ε is the dielectric constant, and F is the Faraday constant (96,458C/mol). Applying the Debye-Hückel approximation, Equation 2.1 can be simplified to

$$\frac{d^2\psi}{dy^2} = \frac{\psi}{\lambda_D^2} \qquad 1.2$$

where λ_D is the Debye length of the electrolyte and is given by the following equation

$$\lambda_D^2 = \sqrt{\frac{\varepsilon KT}{2z^2F^2c_\infty}} \qquad 1.3$$

The solution for the differential equation 2.2 is:

$$\psi = \psi_0 \exp\left(-\frac{y}{\lambda_D}\right) \qquad 1.4$$

The flow caused by the electro-osmotic effect, u_{EOF}, can be determined by introducing this potential into Navier-Stock equation, and assuming the flow is fully developed in the y-direction [33]:

$$\eta\frac{d^2u_{eof}}{dy^2} = \varepsilon E_{el}\frac{d^2\psi}{dy^2} \qquad 1.5$$

where η is viscosity of the solution. Solving the above differential equation leads to Helmholtz-Smoluchowski equation [31-33]:

$$u_{EOF} = \frac{\varepsilon E_{el} \xi}{\eta} \qquad 1.6$$

2.1.2 Electrophoresis

Electrophoresis is defined as the migration of an electrically charged species (ions) under the influence of an electric field [31-37]. The electro-osmotic mobility (μ_e) is defined by:

$$\mu_e = \frac{u_{EOF}}{E_{el}} \qquad 1.7$$

The movement of charged particles under the influence of electric field is due to Lorentz force, which is governed by the equation:

$$F_E = qE_{el} \qquad 1.8$$

where q is the ion charge. The overall movement of the fluid has a frictional force on spherical ion, which is called viscous Stokes drag [32,37]:

$$F_F = -6\pi\eta r v \qquad 1.9$$

where r is the ion radius, and v is the ion velocity. During electrophoresis the ion moves at a constant speed, i.e. under steady state conditions, thus the balance of F_E and F_F is attained. Equalizing F_F by F_E and substituting in Equation 7 yields an equation that expresses the mobility with physical parameters of the ions; q, k, and r [37]:

$$\mu_e = \frac{q}{6\pi\eta r} \qquad 1.10$$

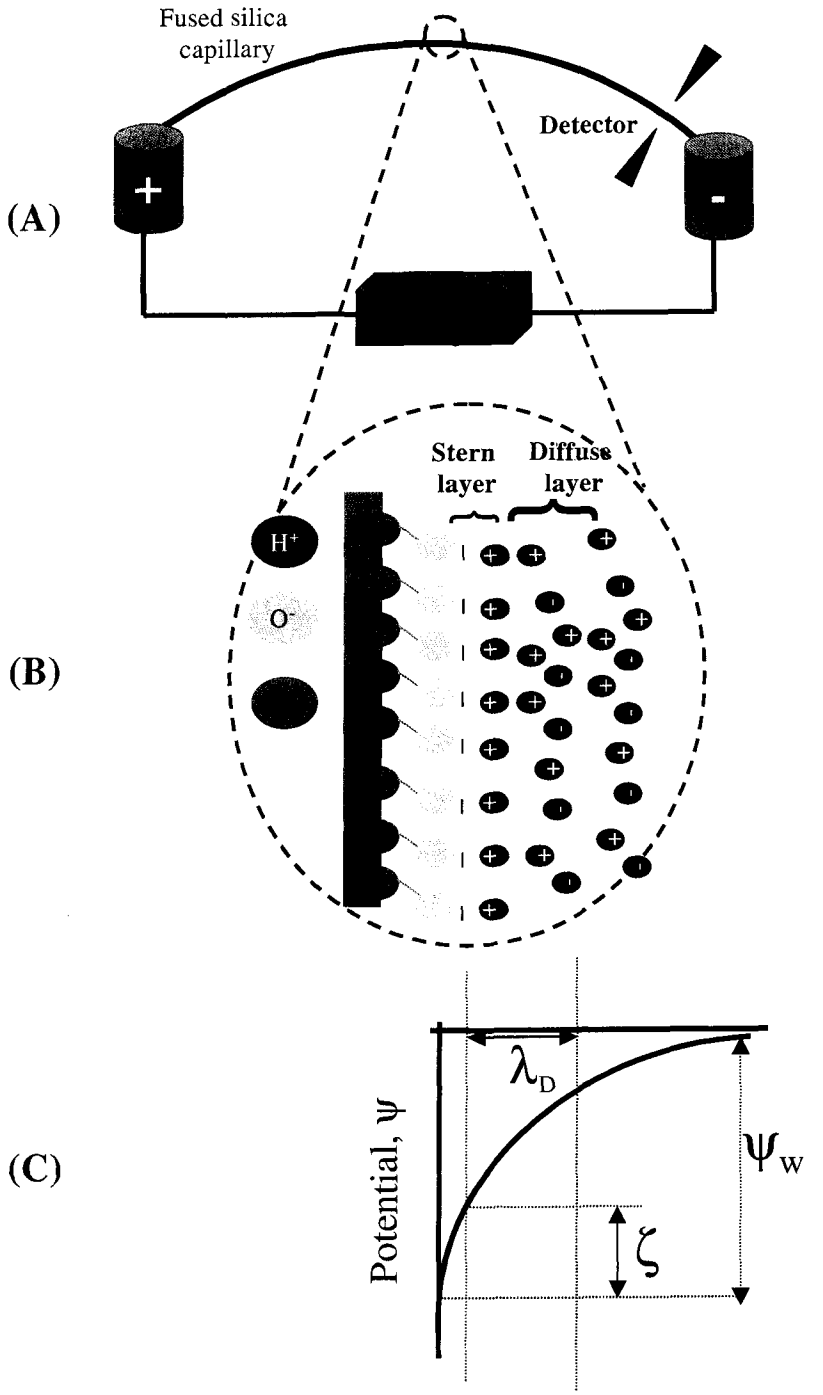

Figure 1.1 Principle of capillary electrophoresis; (A) Schematic of CE instrumentation, (B) Negatively charged fused silica surfaces and EDL, (C) Potential distribution

Capillary electrophoresis is an electrophoretic process that is accomplished in a capillary tube made of fused silica (SiO_2), which bears abundant silanol groups (SiOH) that can be ionized into anionic form (SiO^-) under electrolytic conditions [37,38]. Thus, the tube tends to have negatively charged surface whereas the EDL is positively charged, figure 1.1. The EOF is a consequence of applying electric field on the solution EDL for CE operation, where the solvated cations, forming the diffuse layer, are attracted toward the cathode and drag the bulk solution inside the capillary toward the cathode [35-37]. Molecules of different sizes and charges will migrate toward the cathode regardless of their charges. The difference among them is the migration velocities, where the smaller and positively charged molecules migrate faster, whereas larger and negatively charged molecules migrate slower, i.e. migration velocity merely depends on the molecule's charge-to mass ratio.

The driving force of the EOF is uniform all over the capillary, which ensures that there is no pressure drop across the capillary. This uniformity grants the flow its unique feature and that is its flat profile. A flat profile guarantees a sharp solute zone, which is in contrast to the solute zone in laminar flow that is due to hydrodynamic deriving forces, which has a broad zone [32,37]. Figure 1.2 shows the difference between the flows' profiles and the corresponding solute zones of EOF and laminar flow [37].

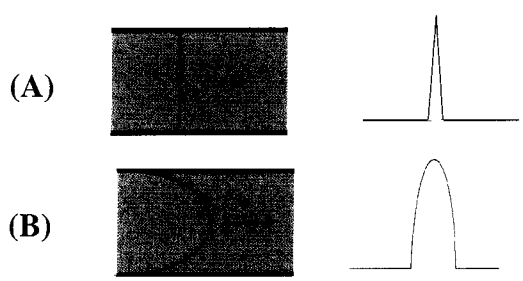

Figure 1.2 Flow profiles in microchannel; EOF (A) and Laminar (B), and the corresponding solute zones.

Controlling the EOF is essential for obtaining high quality separation process. As it can be seen from the equation above, the EOF depends on the applied electric field, solution viscosity and permitivity, and zeta potential, which correspond to the surface charge density [35-37]. In some cases it is desired to have slow EOF for the separation to occur, which can be achieved by either decreasing the applied field or by lowering the pH of the solution, which will decrease the zeta potential. The drawback of lowering the pH is the adsorption of cationic species, such as proteins, via coulombic interaction [37,39,40]. In summary, different adjustments can be made in order to achieve the optimum EOF, which results in the best separation conditions. These include the parameter optimization (electric field, buffer pH, ionic strength, temperature), organic modifier and/or surfactant addition to the running buffer, and covalent coating of the surface channel walls, see section 1.2.3 (below) for more details.

Similar to other separation techniques, such as column chromatography, the analytical performance of capillary electrophoresis is evaluated by numerous analytical parameters. The first analytical parameters is the apparent solute mobility, μ_a, which is governed by the following equation [35,37]:

$$\mu_a = \frac{l}{tE} = \frac{lL}{tV} \qquad 1.11$$

where l is the effective capillary length, L is the total capillary length, E is the electric field, t is the migration time, and V is the applied voltage. Frequently, the apparent mobility and the EOF are used to calculate the effective mobility, μ_e [35-37]:

$$\mu_a = \mu_e + \mu_{EOF} \qquad 1.12$$

The EOF usually is determined by either injecting neutral analytes, such as rhodamine B

[41] or by the current monitoring method [42,43]. Selecting the right neutral analytes depends on the incorporated detection mode, whereas the current monitoring method is simpler and can be done regardless of the detection mode. For the current monitoring method, basically, the current at high buffer concentration is recorded, then is replaced by a lower buffer concentration (the same buffer), and the time that is needed for the current to drop to a lower value is recorded since this is the time that is needed for the buffer to migrate from one end to the other end across the capillary:

$$v_{EOF} = \frac{\Delta t}{L} \qquad 1.13$$

Another analytical parameter, which is related to the efficiency of the separation process, is the number of theoretical plates; N. Different equations have been developed to calculate the number of theoretical plates, but the simplest one, can be determined directly from the electropherogram [37]:

$$N = 5.54\left(\frac{t}{w_{1/2}}\right)^2 \qquad 1.14$$

where t is the migration time, and $w_{1/2}$ is the peak width at half height. The corresponding height equivalent to theoretical plate, H, is given by:

$$H = \frac{l}{N} \qquad 1.15$$

The ultimate goal for any separation process is to achieve the best separation resolution, which depends on the resolving power of the system. The resolution, R, can be simply determined from the electropherogram based on the following equation [35-37]:

$$R = \frac{2(t_2 - t_1)}{w_1 + w_2} \qquad 1.16$$

where w is the peak width, and subscripts 1 and 2 refer to the two solutes.

1.2.3 Capillary Electrophoresis Operation Modes

Capillary electrophoresis has numerous modes of operation that depends on the background electrolyte system. Each operation mode has its own characteristic separation mechanism. In this section a brief description for each operation mode is presented along with its separation mechanism.

Capillary Zone Electrophoresis (CZE): it is the simplest and the most frequently used separation mode of capillary electrophoresis. The separation mechanism relies on the dissociation of acidic groups or the protonation of basic groups of the analytes, hence the separation occurs because of differences in the charge-to-mass ratio of the analytes [37]. Experimentally, the capillary is filled with a certain buffer, then a constant electric filed is applied across the capillary [10,11].

Capillary Isoelectric Focusing (CIEF): in this operation mode, a pH gradient is generated along the capillary, thus an amphoteric compound, such as proteins; migrate into a region where they become uncharged, i.e. isoelectric point (pI) [37,44]. At the pI, the analytes do not migrate and the sample is focused into a very narrow zone. The most frequent application of CIEF is separation and determination of proteins' pIs [44,45].

Capillary Gel Electrophoresis (CGE): Polymers in solution, such as polyacrylamide, are incorporated inside the capillary and function as molecular sieve [37,46,47]. CGE is used to separate molecules that are similar in their size to charge ratio, but differ in their sizes. The

most frequent application of this operation mode is molecular weight analysis of proteins and DNA sequencing and genotyping [19,20].

Isotachophoresis (ITP): the main application of this operation mode is sample focusing to lower the limit of detection (LOD). The sample zone is sandwiched between two electrolytes, the leading and the terminating electrolytes [37]. The sample has intermediate mobility between the leading and the termination electrolyte; hence the sample is focused into a sharp zone [37,48].

Electrokinetic Chromatography (EKC): this is a combination of electrophoresis and chromatography, in which a surfactant, such as sodium dodecyl sulfate (SDS) [49], or chiral selector, such as cyclodextrin [50], is added to the running buffer. The interaction of the solutes with the additives enhances the separation process, however, the solutes still migrate under the influence of the EOF [37]. The most frequent application of this mode is chiral separation. Furthermore, the introduction of the surfactant to the running buffer is a special mode of EKC that is known as micellar electrokinetic chromatography (MEKC) [37,49].

Capillary Electrochromatography (CEC): this is a combination of electrophoresis and liquid chromatography [51]. The mobile phase migrates through a packed bed under the influence of the EOF rather than hydraulic pressure. This mode is mainly used for concentrating the sample before separation via CZE.

Non-Aqueous Capillary Electrophoresis (NACE)): this operation mode is mainly analogous to CZE, but rather than preparing aqueous solutions, the samples and the running buffer are made in organic solvents [52]. The most popular buffer systems and organic solvents used in association with NACE is acetonitrile are acetic acid/ammonium acetate and acetonitrile, respectively.

1.3 Equilibrium Gradient Methods (EGM)

The advantages of EGM in physics [53] have been known since 1950s; however their potential and applicability in chemical and separation sciences have not been effusively explored. For instance, EGM has been established by applying a linear field intensity gradient in which analytes are brought to unique equilibrium points by a force gradient and counter force (a hydrodynamic flow from a pump) a long separation pathway, which has been described theoretically and demonstrated experimentally [53-57]. The equations relating the operating parameters with separation performance show that higher peak capacities in the separation process can be obtained [54]. In the devices demonstrated thus far, the electric field gradient was established using an array of electrodes for which voltages have to be individually adjusted and controlled [56,57]. The gradient of the external filed intensity can be expressed as $q(x) = -\partial E(x)/\partial x$, where E(x) is the intensity of the external field at point x, and the axis of transport is the x-coordinate. In general, the translation velocity of the analyte at point x is given by $v(x) = \mu E(x) + u$, where u is velocity of the bulk flow and μ is the electrophoretic mobility of the analyte.

The basic theory of EGM with a field gradient can be derived from the general equation [52]:

$$J = v(x)c(x) - D_T \frac{\partial c(x)}{\partial x} \qquad 1.17$$

where J is the flux density of the analyte, v(x) and c(x) are translational velocity and concentration of analyte at point x, and D_T is the effective diffusion coefficient. In EGM each analyte is focused into a steady-state band [53,54]. It has been shown theoretically [54,56] that the focused band follows a Gaussian distribution with a standard deviation of:

$$\sigma = \sqrt{\frac{D_T}{\mu q(x_{po})}} \qquad 1.18$$

where x_{po} is the focusing position of the analyte. In order to obtain a focused band, a positive value of $\mu q(x_{po})$ is required, and thus steeper gradient will produce a sharper peak. It has been shown that the resolution can be expressed approximately as [54]:

$$R_S = \frac{|x_{po} - x_p|}{\sqrt{\mu q(x_{po}) D_T}} \qquad 1.19$$

where x_p and x_{po} are the focusing positions of the first and second analytes, respectively. A drawback of the simple EGM approach, as shown by equations 1.18 and 1.19, is that resolution and peak width cannot be improved simultaneously. Previous experimental designs utilizing EGM with 50 wire- based electrodes that maintained a simple field gradient along the separation chamber and a constant hydrodynamic force opposing the electric field gradient were limited in resolving power because of a simple stair-step electric field gradient with discontinuities at the electrodes [55,56,58]. In these experiments, the first 49 electrodes were anodes while the last electrode was a cathode set to ground and the electric field was linear. Such experimental design is not sensible and allows separation for a limited number of analytes [55]. Also, it is not easy to keep the profile constant over a long distance of the separation column and extended separation time, as the opposing hydrodynamic flow and his breading effects significantly hamper the extent of electrofocusing.

Other, well-known equilibrium gradient methods include isoelectric focusing (IEF) [44,45,54] and density gradient sedimentation (DGS) [57, 59]. In isoelectric focusing, a pH gradient is established along the separation channel; the analyte still moves along the separation channel under the influence of an electric field, and its migration stops at the pH

value where it becomes neutral and consequently focused into narrow zone. In a DGS approach, a density gradient it typically established along the tube applied with a centrifugal force [60]. However, in both IEF and DGS methodologies, it is not trivial to change the gradient once it has formed. Although some of the above mentioned technologies provide good separation of macromolecules, such as proteins, with their own advantages and disadvantages, but they are not efficient enough for biomarker discovered in very complex samples [44,45].

Dynamic Multiple Equilibrium Gradients (DMEG). In this methodology, running waveforms (e.g. sine or saw-tooth waves) with continuously increasing and variable amplitude are applied to multiple (~ 500) microelectrodes insulated from the buffer solution with a dielectric material, such as silicon dioxide or silicon nitride. The microelectrodes are located along the top and bottom of microfluidic channel (or capillary). The resulting propagating electric waves along the electric material above and below the separation channel then induce *propagating* multiple electric field gradients along the separation channel. Appropriate (running) multiple steep gradients tightly focus and separate analytes of different electrophoretic mobilities using different amplitudes of electric filed strength, E_{eff} that varies along the channel pathway, thereby, fulfilling the equilibrium gradient condition for each analyte:

$$\upsilon_p = \mu_i(E_{eff}) \qquad 1.20$$

where υ_p is the phase velocity of the running gradients, and μ_i is electrophoretic mobility of analyte i (i= 1...n) labels the analyte to be separated). E_{eff}. The DMEG separation pathway with the same phase velocity is given by $\upsilon_p = f\lambda$, where f and λ are the frequency and

wavelength of the running waves. The resulting effective field strength that varies along the separation pathway for an analyte i (i=1…n) can be written as:

$$[E_{eff}(x)]_i = f\lambda / \mu_i \qquad 1.21$$

The profile of E_{eff} has to be calculated as it strongly depends on the complexity of the electrode architecture and applied waveforms. This approach is still a new technique, hence, the focusing and separation resolution are still under investigation and development (see App. A).

Current technologies and methods remain largely inadequate to meet the need of biochemical sciences, such as proteomics, especially with respect to resolution and quantitative and real time measurements. However, with the miniaturization and development of various advanced microfluidic devices, many will find many future applications in biomedical fields.

1.4 Microchip Format

Recently, numerous designs of microchips for capillary electrophoreses have been developed [1-9, 24-27]. The design merely relies on the applications that the microchip will be used for, as it can be designed with single separation channel to multiple channels of various geometries. In this section, we provide brief description for the main issues that must be considered regarding the main components of the microchip layout, sample injection, and detection mode integrated or incorporated with the microchip.

1.4.1 Microchip: The Layout

The standard microchip layout for capillary electrophoresis separation consists of two cross channels, referred to as the T-design, and four reservoirs as can be seen in Figure 1.3.

From the intersection point there are four extended channels, which are used for sample injection and the separation process. Two reservoirs are used for sample and buffer solutions; whereas the other two are used as waste reservoirs. The configuration of the reservoirs and the microchannels merely depends on the injection mode that is used to introduce the sample into the separation channel as discussed later.

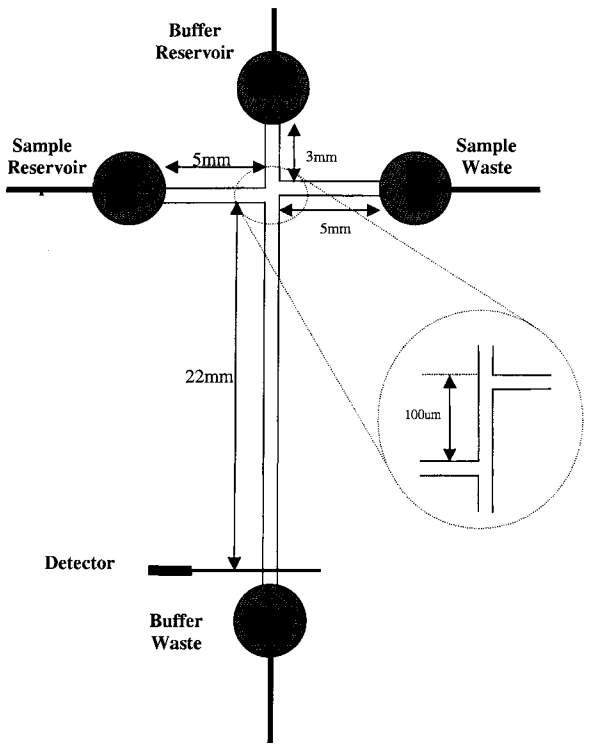

Figure 1.3 Standard microchip layout.

The optimal microchannel depth and width are in the range 15-50 μm and 40-100 μm, respectively, whereas the length strongly depends on the separation process, which is in the range 3-8 cm. Under certain circumstances, such as increasing the injected sample volume, a double T-design can be used instead of the single T-design, where the distance between the two intersections is in the 50-200 μm range.

Multi-channel microchip have been designed and fabricated to perform 2-D [61,62] separation or multiple separation processes on one platform [63]. For example, Mathies et al have developed a platform with 96 separation channels, which is capable of performing 96 independent separation processes for genotyping [63].

1.4.2 Sample introduction (injection)

The most frequent injection technique associated with capillary electrophoresis on microchip is electrokinetic injection [1-9.24-27]. However, some other injection techniques, such as hydrodynamic [64], also can be considered. Electrokinetic injection can be carried out via three different modes: simplified (un-pinched), pinched injection, and gated injection. For the un-pinched injection, a certain voltage is applied between the sample and the waste reservoir, to fill the injection channel with the sample, and then the voltage is switched to the buffer reservoir and other waste reservoir, where the sample plug is carried through the separation channel. Figure 1.4 illustrates the configuration for un-pinched injection and the corresponding images for real injection of fluorescein solution. Due to the presence of the sample solution in the injection channel, the sample leaks, via diffusion, into the separation channel, which can cause some problems, such as peak tailing and increasing the background signal (Figure 1.4). To solve the problem of sample leakage into the separation channel, pinched injection can be applied. In pinched mode, a pushback voltage is applied to carry the sample back to the sample and waste reservoirs. One drawback of these injection modes is that the sample volume is fixed. Having double T-design can be applied to increase the sample volume, but still has fixed injection volume though. Gated injection provides variable sample volume by floating the buffer voltage for a short time. The sample volume merely

depends on the floating time, where shorter times provide smaller sample volumes. See Chapter 4 for more details regarding the gated injection mode.

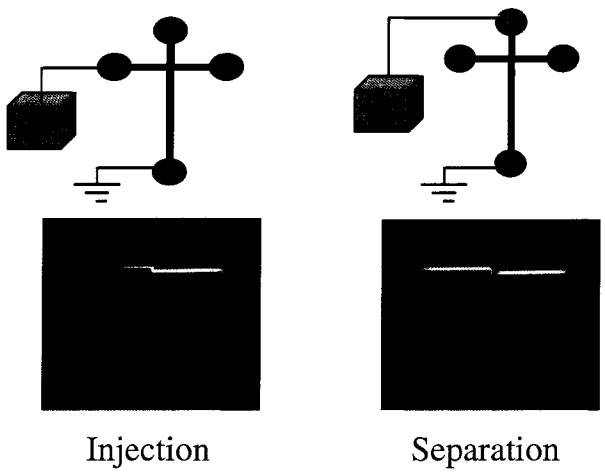

Figure 1.4 Un-pinched injection of fluorescein; top: schematic, bottom: experimental data

1.4.3 Detection

1.4.3.1 Electrochemical detection (ED)

Different electrochemical-based systems and methodologies have been developed to separate and detect various analytes of interests. ED has three different modes: amperometry, conductometry, and potentiometry. In this section we present a description of amperometry, whereas only a brief description conductometry is presented. Potentiometry is rarely used in integration with CE, therefore no description is provided.

Amperometry is the most frequently applied ED mode coupled with CE on a microchip [6,24,27,65-69]. In Amperometry, the detection system consists of three electrodes; working, reference, and counter electrode, which are controlled by a potentiostat. In principle, amperometric detection is accomplished by applying a certain potential to the

working electrode and then measuring the oxidation or the reduction current of the analytes [27,70]. In association with separation process, the current is measured as a function of time.

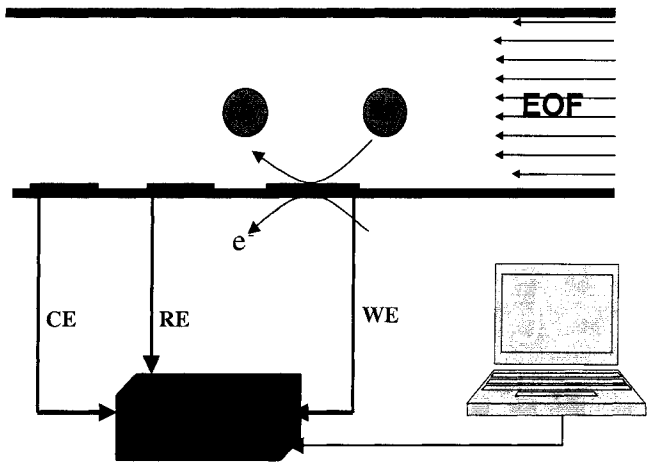

Figure 1.5 Principles of amperometry

Figure 1.5 illustrates the principle of amperometric detection inside the channel. The current that results from either the oxidation or reduction process is proportional to the molar concentration of analyte, which is governed by Faraday's law [27,70]:

$$i_t = dQ / dt = nF (dN / dt) \qquad 2.17$$

where i_t is the current generated after the oxidation process or consumed after the reduction process at time t. Q is the charge at the electrode surface, F is the Faraday constant, n is number of moles of electrons involved in the oxidation or the reduction reaction of the analyte, and N is the number of moles of analyte reduced or oxidized. The resultant current (i_t) strongly depends on the applied potential, where each analyte has its characteristic redox potential. The optimum oxidation or reduction potential is determined by constructing of the hydrodynamic voltammogram, which can be accomplished by varying the applied potential while keeping all other parameters constant.

Two important factors play a significant role in obtaining high performance of CE with ED (CE-ED). First, although full advantage of miniaturization can be achieved with CE, integrating amperometric detection with capillary electrophoresis can be problematic because of the detection current-electrophoretic current (DC-EC) coupling. The Second factor is the position of the WE relative to the capillary. Thus, electrode configuration and alignment are crucial for the separation process.

The development of CE-EC has been restricted by handling difficulties related to classical electrode alignment procedures and by difficulty in decoupling the detection current from the electrophoretic current. In this regard, different electrode arrangements and configurations have been developed to solve these two problems. The detection system can be either on-chip or off-chip [6,27]. For the on-chip construction, the working electrode is integrated with the microchip, i.e. it is a component of the chip, whereas the off-chip amperometric detection is not integrated within the chip. For the on-chip construction, the working electrode can be located either in the channel or at the end channel, i.e. inside the waste reservoir. Each construction has its advantages and disadvantages. Although the off-chip and on-chip/end channel detection both could be considered a solution to minimize the DE-EC, they suffer from sample diffusion after the working electrode at once it exits the separation channel, which leads to peak tailing and decreased sensitivity [71]. Positioning the working electrode too close to the channel exits can minimize the peak tailing, but this causes the DE-EC coupling to increase, and thus a decrease in sensitivity. Locating the working electrode inside the separation channel could solve the problem completely, but the DC-EC coupling would increase significantly, which could be problematic and cause damage to the electronics. An elegant solution for all of these problems is the decoupling the two currents.

Full details regarding the decoupling significance and how it can be accomplished are presented and discussed in Chapter 5.

Secondly, the electrode material is also an important factor in obtaining high performance CE separation with ED. Different materials have been used for working electrode fabrication. Metal electrodes, such as gold (Au) and platinum (Pt), are still the most popular material for integrated electrodes [24,65], but carbon electrodes of different kind such as carbon fibers [66], carbon paste [67], screen-printed carbon [68], and carbon nanotube [69], have been incorporated with microchip as well. Carbon electrodes are more sensitive than metal electrodes; however, there are some problems associated with the fabrication protocols and the expenses. While metals are less sensitive than carbon for electrochemical measurements, they are much easier to fabricate and less expensive as well.

For more details regarding the integration and fabrication of amperometric detection with CE-based microfluidic devices, see the introductory sections of Chapters 4 and 5

Conductometry is a 2-electrode configuration detection scheme [27,70], which can be accomplished by applying a potential (V) between the two electrodes and measuring the resultant current (i), then the conductance or the resistance (R) of the solution can be determined by applying Ohm's law, $V = IR$ [27,70]. However, the redox reaction on the electrodes' surfaces can interfere with the conductivity measurements, which can be suppressed by applying an A.C. voltage at a frequency of typically 1 kHz. The solution conductivity (L) can be related to the sample concentration via the equation [27,70]:

$$L = \frac{A}{I} \sum (\lambda_i c_i) \qquad 2.18$$

where A is the electrode surface area, I is the distance between the two electrodes, c_i and λ_i are the concentration and the molar conductivity of the ion i, respectively.

Contactless conductometric measurements also are an alternative to avoid any redox reaction on the electrode's surface [72]. In this construction, an isolation layer, such as silicon dioxide or silicon nitride is deposited on the top of the detection electrodes. While amperometric detection is more sensitive and selective than conductometric detection; nonetheless, conductometric measurements have wide applications for metallic ions detection, where amperometric detection might result in metal deposition on the electrodes surfaces [72].

1.4.3.2 Spectroscopic Detection:

Laser induced fluorescence (LIF) has been the most frequently used detection mode for CE on microchip applications [1,6-9,61-63,73-77]. Figure 1.6 shows the basic experimental setup used for LIF detection. A light excitation source, such as laser or xenon arc lamp, is used in order to increase the fluorescence signal, which is directed to appoint near the end of the separation channel via a reflection mirror. Band-bass emission filters, positioned in a cube with dichroic mirror, are used to reduce the amount of the excitation light that enters the photo detector, such as photomultiplier tube (PMT) or a CCD camera.

LIF is applied for fluorescent molecules, which could be a problematic for non-fluorescent molecules, and thus either a labeling protocol or indirect fluorescence detection is applied [77]. Due to the large-scale instrumentation associated with LIF, full benefits of miniaturization are not granted in comparison with electrochemical detection. Nevertheless, integrated fluorescence detection system has been reported by Chabinyc et al [73], but due to

the relatively difficult and costly fabrication procedure it has limited application in most laboratories. Due to the large-scale instrumentation associated with LIF, full benefits of miniaturization are not granted in comparison with electrochemical detection.

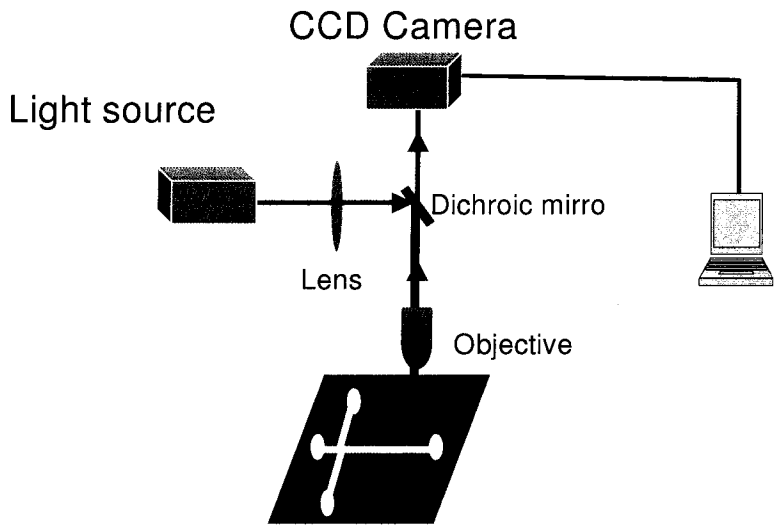

Figure 1.6 Schematic of the LIF detection

Absorbance detection strongly depends on the optical path length, which makes it much less sensitive than other techniques such as LIF. Due to its lack of sensitivity, different techniques have been applied to increase the sensitivity of absorbance detection. For example, the optical path length is maximized on microchip by fabricating a U-shaped detection cell [78]. Collimating lenses and a detection slits have been also integrated into PDMS microchip [79], which reduces scattered light collection and interference. In another approach, a photo sensor array was integrated on acrylic chip to improve the light collection

[80]. Having a deeper channel, such as ~100 μm, also increases the optical light path, but it could be problematic because of the huge electrophoretic current that leads to large joule heating and can eventually damage the chip [81].

Mass spectrometry has become progressively more popular as a detection mode incorporated with CE because of its high selectivity. In order to interface mass spectrometry detection with the microchip, the microfluidic chip has been coupled with various ionization sources, such as ESI [82] and MALDI [83], and different mass analyzers, such as single quadrupole and ion-trap [82,83]. Although the difficulty in using mass spectrometry detection is its large size, its advantageous selectivity as a detector makes it very useful and applicable where portability is not necessary. Because of its unique characteristic feature of compatibility with aqueous solutions and non-volatile compounds, electrospray ionization (ESI) is the most frequently used ionization source for mass spectrometry interfaced with microfluidic chips [82]. Lazar et al have developed complete set of components, such as concentrator and pumps on a microfluidic chips interfaced with mass spectrometer [84]. The outlet of the separation channel was connected with a conductive tip that operates at high voltage, ~6 kV, which function as the electrospray source. Also, matrix-assisted laser desorption ionization (MALDI) has been interfaced with microfluidic chips [83]. The main applications of microfluidic devices interfaced with mass spectrometry have been related with proteins and peptides separation for protemics analysis [82-86].

In addition to the previously mentioned detection modes, some other detection schemes have been interfaced with microfluidic chips such as H^1-NMR spectroscopy [87], Raman spectroscopy [88], FT-IR spectroscopy [89], and refractive index spectroscopy [90].

1.4 Applications:

In this section we present brief review regarding the applications and associated protocols for the separation and detection various kinds of molecules of diverse interests.

Neurotransmitters and related compounds: Different electrochemical-based systems and methodologies have been developed to separate and detect neurotransmitters because of their importance for brain research and understanding neurodegenerative diseases [91,92]. Neurotransmitters exhibit very weak fluorescence, and thus this is not the best mode for detection. Nevertheless, they exhibit strong electrochemical properties, and hence amperometric detection is the optimal detection mode for neurotransmitters. Accordingly, in addition to its importance as neurotransmitter, dopamine is often chosen as a model compound for electrochemical measurements because of its moderate redox potential [93-98]. Many research groups have utilized CE on microchip to separate and electrochemically detect dopamine and other related analytes, where catechol and dopamine have been the most popular mixture for many research groups [93-95]. Other related analytes such as hydroquinone, adrenaline, histamine, epinephrine, L-DOPA, and tyrosine have also been analyzed [96-98]. Different microchip materials, such as glass and glass/PDMS, electrode materials, and electrodes alignments have been utilized to perform these analyses [93-98].

Nucleic acids analysis has been one of the leading applications of capillary electrophoresis on microchip, which can be classified into three main areas of analysis: nucleic acid sizing [63,99], genotyping [100,101], and DNA sequencing [102]. Numerous research groups have applied microchip CE for separation and sizing of oligonucleotides and restriction fragments of DNA molecules, such as ΦX174 *Hae*III fragments [103]. For example, seminal work has been published by Mathies et al. in which they developed a 384

lane capillary analyzer on a radial chip for ultrahigh simultaneous genotyping of the hemochromatosis-linked H63D mutation in less than 6 minutes [104]. Also, microfabricated silicon PCR reactor, which can perform rapid thermal cycling, and sieving matrices, such as hydroxyoropyl cellulose (HPC) and hydroxyethyl cellulose (HEC), have been integrated on a single microfluidic chip [105].

Proteins and peptides: numerous methods and protocols have been applied to separate and detect proteins and peptides on microchip; this includes: capillary SDS electrophoresis in sieving matrix [106], capillary isoelectric focusing (CIEF) [107], multidimensional separation [61,62], enzymatic assays [108], and immunoaffinity [109].

Other applications: Many other compounds of diverse interests (clinical, environmental, forensic) have been analyzed by utilizing capillary electrophoresis on microchip; this includes explosive residues, such as TNT [110], illegal and narcotic drugs, such as amphetamine [111], sulfur-containing compounds, such as homocystein [112,113], clinical assays of uric acid and ascorbic acid [114-116], and many others.

1.5 References:

1. A. Manz, N. Grabner, H.M. Widmer, *Sens. Actuators B.* 1 (1990), 244-248.
2. A. Manz, D.J. Harrison, J.C. Rettinger, E. Verpoorte, H. Ludi, H.M. Widmer, Transducers 91, Digest of Technical Papers, IEEE 91 CH2817; IEEE: New York (1990), 939-941.
3. D.J. Harrison, A. Manz, P.J. Glavina, Transducers 91, Digest of Technical Papers, IEEE 91-CH2817-5; IEEE: New York (1990), pp 792-795.
4. G.J. Bruin, *Electrophoresis* 21 (2000), 3931-3951.
5. A. Mello, *Lab. on a Chip* 2 (2002), 48N-54N.

6. N.A. Lacher, K.E. Garrison, R.S. Martin, S.M. Lunte, *Electrophoresis* 22 (2001), 2526-2536.

7. D.J. Harrison, A. Manz, Z. Fan, H. Lüdi, H.M. Widmer, *Anal. Chem.* 64 (1992), 1926-1932.

8. A.T. Woolley, R.A. Mathies, *Anal. Chem.* 67 (1995), 3676-3680.

9. M.A. Burns, B.N. Johnson, S.N. Brahmasandra, K. Handique, D.T. Burke, *Science* 282 (1998), 484-487.

10. J.W. Jorgenson, and K.D. Lukacs, *Anal.Chem.* **53** (1981), 1298.

11. J.W. Jorgenson, and K.D. Lukacs, *Science* **222** (1983), 266.

12. W.R. Jones, and P. Jandik, *Am. Lab.* **6** (1990), 51.

13. P. Doble, and P.R. Haddad, *Anal. Chem.* **71** (1999), 15.

14. V.C. Trenerry, J. Robertson, and R.J. Wells, *Eletcrophoresis* **15** (1994), 103.

15. H. Nishi, and S. Terabe, *J. Chromatogr.* **735** (1996), 3.

16. C. Schwer, and F. Lottspeich, *J. Chromatogr.* **623** (1992), 345.

17. E. Semo-Alfonso, M. Conti, C. Gelfi, and P.G. Righetti, *J. Chromatogr.* **689** (1995), 85.

18. K. Ganzler, K.S. Greve, A.S. Kohen, B.L. Garger, A. Guttman, and A.S. Cook, *Anal. Chem.* **64** (1992), 2665.

19. A. Guttman, A.S. Kohen, D.N. Heiger, and B.L. Garger, *Anal. Chem.* **62** (1990), 137.

20. Y. He, H.-M Pang, and E.S. Yeung, *J. Chromatogr . A.* **894** (2000), 179.

21. K.P. Robert, C.-H. Lin, R. Jankowiak, and G.J. Small, *J. Chromatogr. A.* **853** (1999), 159.

22. J.P. Barry, C. Narwood, and P. Vourous, *Anal. Chem.* **68** (1996), 1432.

23. G.Y. Chen, P.F. Gavini, G.A. Luo, and A.G. Ewing, *Neuroscience* **15** (1995), 7747.

24. R. Wilke, S. Büttgenbach, *Biosens. Bioelect.* 1 (2003), 149-153.

25. V. Dolník, S. Liu, S.J. Vladisl, *Electrophoresis* 21 (2000), 41- 54.
26. M.P. Hughes, *Electrophoresis* 23 (2002), 2569-2582.

27. W. R. Vandaveer, S.A. Pasas-Farmer, D.J. Fischer, C.N. Frankenfeld, and S.M. Lunte, *Electrophoresis* **25** (2004), 3528-3549.

28. S. Adachi, M. Zeisig and L. Moller, *Carcinogenesis* **16** (1995), 253-258.

29. T. Hofer and L. Moller, *Chem. Res. Toxicol.*, 2002, **15**, 426-432

30. P. Devanesan, R. Todorovic, J. Zhao, M.L. Gross, E.G. Rogan, , and E.L. Cavalieri, *Carcinogenesis* **22** (2001), 489-497.

31. R.J. Hunter, *Zeta Potential in Colloid Science: Principles and Applications*, Academic Press, New York (1981), pp 1-56.

32. A. V. Delgado, *Interfacial Electrokinetics and Electrophoresis*, Marcel Dekker, New York (2002), pp 1-54.

33. N-T Nguyen, and S.T. Wereley, *Fundamentals and Applications of Microfluidics*, Artech House, Boston (2004), Chap.2.

34. S.F.Y. Li, *Capillary Electrophoresis: Principles, Practice, and Applications*, Elsevier Science, Amsterdam, 1992, Chap.1.

35. A. Weston, and P.R. Brown, *HPLC and CE: Principles and Practice*, Academic Press, San Diego, 1997, Chap.4.

36. T.J. Bruno, *Chromatographic and Elecrophoretic Methods*, Prentice-Hall, New Jeresy, 1991, Chap.5.

37. D.N. Heiger, *High Performance Capillary Electrophoresis*,Hewlett-Packard GmbH, Germany, 1992, Chap.2.

38. C. Schwer, and E.Kendler, *Chromatographia* **30** (1990), 3898.

39. H.L. Lauer, and D. McManigill, *Anal. Chem.* **58** (1986), 166-70.

40. E.A. Doherty, R.J. Meagher, M.N. Albarghouthi, A.E. Barron, *Electrophoresis* **24** (2003), 34-54.

41. J.L. Pittman, S.D. Gilman, and K.F. Schrum, *Analyst* **126** (2001), 1240-1247.

42. X. Huang, M.J. Gordon, and R.N. Zare, *Anal. Chem.* **60** (1988), 1837.

43. J.L. Pittman, C.S. Henry, S.D. Gilman, *Anal. Chem.* **75** (2003), 361-370.

44. S. Hjerten, and M.D.Zhu, *J. Chromatogr.* **346** (1985), 265.

45. Q. Mao, and J. Pawliszyn, *J Biochem. Biophys. Meth.* **39** (1999), 93-110.

46. S. Hjerten *J. Chromatogr.* **270** (1983), 1.

47. S. Hjerten, *J. Chromatogr.* **347** (1985), 191.

48. P. Gebauer, and P. Bocek, *Electrophoresis* **18** (1997), 2154-2161.

49. S. Terabe, *Trends Anal. Chem.* 8 (1989), 129-134.

50. Guebitz, Gerald; Schmid, Martin G. *Mol. Biotech.* (2006), 32, 159-179.

51. Wanders, B. J.; Van de Goor, A. A. A. M.; Everaerts, F. M. *J. Chromatogr.* (1989), 470, 89-93.

52. M.-L. Riekkola, M. Jussila, S.P. Porras, and I.E. Valko, *J. Chromatogr. A* **892** (2000), 155-170

53. J.C. Giddings, *Sep. Sci. Technol.* **14**, (1979), 871-882.

54. H.D. Tolley, Q. Wang, D.A. LeFebre, and M.L. Lee, *Anal. Chem.* **74** (2002), 4456-4463

55. C.F. Ivory, *Sep. Sci. Technol.* 53 (2000), 1777-1793.

56. Z. Huang, and C.F. Ivory, *Anal. Chem.* **71** (1999), 300-309.

57. A.J. Link, J. Eng, D.M. Schieltee, E. Carmack, G.J. Mize, D.R. Morris, B.M. Garvik, and J.R. Yates, *Nat. Biotechnology* **17** (1999), 676.

58. A Kolin, In Electrofocusing and Isotachophoresis, B.J. Radola, and D Graesslin, Eds; de Gruyter: Berlin, 3-33 (1977)

59. Y. Shen, F. Xiang, T.D. Veenstra, E.N. Fung, and A.D. Smith, *Anal. Chem.* **71** (1999), 5348.

60. M. Meselson, F.W. Stahl, and J.Vinograd, Proc. Natl. Acad. Sci. **43** (1957), 581-588.

61. S.-W. Tsai, M.K. Loughran, and I. Karube, *J. Micromech. Microeng.* **14** (2004), 1693-1699.

62. H. Shadpour, and S.A. Soper, *Anal. Chem.* **78** (2006), 3519-3527.

63. Y. Shi, P.C. Simpson, J.R. Scherer, D.S. Wexler, C. Skibola, M.T. Smith, AND R.A.Mathies, *Anal. Chem.* **71** (1999), 5354-5361.

64. Y.-H. Lin, G.-B. Lee, C.-W. Li, G.R. Huang, and S.H. Chen, *J. Chromatogr. A* **937** (2001), 115-125.

65. A.T. Woolley, K. Lao, A.N.Glazer, and R.A. Mathies, *Anal. Chem* **70** (1998), 684-688.

66. J.-J. Xu, Y. Peng, N. Bao, X.-H. Xia, and H.-Y. Chen, *Electrophoresis* **26** (2005), 3615-3621.

67. A. J. Gawron, R.S. Martin, and S.M. Lunte, *Electrophoresis* **22** (2001), 242-248.

68. W. Wang, B. Tian, and E. Sahlin, *Anal. Chem* **71** (1999), 5436-5440.

69. J. Wang, G. Chen, M.D. Chatrathi, and M. Musameh, *Analy. Chem* **76** (2004), 298-302.

70. S.M. Lunte, C.E. Lunte, P.T. Kassinger, *Laboratory Techniques in Electroanalytical Chemistry*, 2nd ed., Marcel Dekker, New York 1996, pp 813-853.

71. D. Osbourn, and C.E. Lunte, *Anal. Chem* **75** (2003), 2710-2714.

72. P. Kuban, and P.C. Hauser, *Lab on a Chip* **5** (2005), 407-415.

73. M.L. Chabinyc, D.T. Chiu, J.C. McDonald, A.D. Stroock, J.F. Christian, A.M. Karger, and G.W. Whitesides, *Anal. Chem* **73** (2001), 4491-4498.

74. J.-L. Fu, Q. Fang, T. Zhang, X.-H. Jin, and Z.-L. Fang, *Anal. Chem.* **78** (2006), 3827-3834.

75. M. Yamauchi, M. Tokeshi, J. Yamaguchi, T. Fukuzawa, A. Hattori, A. Hibara, and T. Kitamori, Takehiko, *J. Chromatogr. A* **1106** (2006), 89-93.

76. S.-L. Wang, X.-F. Fan, Z.-R. Xu, and Z.-L. Fang, *Electrophoresis* **26** (2005), 3602-3608.

77. C.G. Bailey C G, and S.R. Wallenborg, *Electrophoresis* **21** (2000), 3081-3087.

78. K.B. Mogensen, N.J. Petersen J. Hubner, and J.R. Kutter, *Electrophoresis* **22** (2001), 3930-3938.

79. K.W. Ro, K. Lim, B.C. Shim, and J.H. Hahn, *Anal. Chem.* **77** (2005), 5160-5166.

80. Y. Mizukami, D. Rajniak, A. Rajniak, and M. Nishimura, *Sens. Actuators B* **B87** (2002), 211.

81. H Salimi-Moosavi, Y. Jiang, L. Lester, G. McKinnon, and D.J. Harrison, *Electrophoresis* **21** (2000), 1291-1299.

82. J. Li, P. Thibault, N.H. Bings, C.D. Skinner, C. Wang, C. Colyer, and D. Harrison *Anal. Chem.* **71** (1999), 3036-3045.

83. A.R. Wheeler, H. Moon, C.-J. Kim, J.A. Loo, and R.L. Garrell, *Anal. Chem.* **76** (2004), 4833-4838.

84. I.M. Lazar, and B.L. Karger, *Anal. Chem.* **74** (2002), 6259-6268.

85. N. Lion, J.O. Gellon, H. Jensen, and H.H. Girault, *J. Chromatogr. A* **1003** (2003), 11-19.

86. A.R. Wheeler, H. Moon, C.A. Bird, R.R. Ogorzalek Loo, C.-J. Kim, J.A. Loo, and R.L. Garrell, *Anal. Chem.* **77** (2005), 534-540.

87. C. Massin, F. Vincent, A. Homsy, K. Ehrmann, G. Boero, P.-A. Besse,A. Daridon, E. Verpoorte, N.F. de Rooij, and R.S. Popovic, *J. Magn. Reson.* **164** (2003), 242-255.

88. P.A. Walker, M.D. Morris, M.A. Burns, and B.N. Johnson, *Anal. Chem.* **70** (1998), 3766-3769.

89. T. Pan, R.T. Kelly, M.C. Asplund, and A.T. Woolley, *J. Chromatogr. A* **1027** (2004), 231-235.

90. N. Burggraf, B. Krattiger, N.F. de Rooij, A. Manz, and A.J. de Mello, *Analyst* **123** (1998), 1443-1447.

91. G. Levay, and W.J. Bodell, *Carcinogenesis* **14** (1993), 241-1245.

92. G. Levay, Q. Ye, and W.J. Bodell, *Exp. Neurol.* **146** (1997), 570-574.

93. N.A. Lacher, S.M. Lunte, and R.S. Martin, *Anal. Chem.*, **76** (2004), 2482-2491.

94. M.L. Kovarik, M.W. Li, and S.R. Martin, *Electrophoresis*, **26** (2005), 202-210.

95. M. Schwarz, and P.C. Hauser, *Anal. Chem.*, **75** (2003), 4691-4695.

96. R.S. Keynton, T.J. Roussel, M.M. Crain, D.J. Jackson, D.B. Franco, J.F. Naber, K.M. Walsh, and R.P. Baldwin, *Anal. Chimica Acta*, (**50**) 2004, 95-105.
97. Q.L. Zhang, J.J. Xu, H.Z. Lian, X.Y. Li, and H.Y. Chen, *Anal. Bioanal. Chem.*, **384** (2000), 265-270.

98. A.J. Blasco, I. Barrigas, M.C. Gonzalez, and A. Escarpa, *Electrophoresis*, **26** (2005), 4664-4673.

99. A. Cantafora, I. Blotta, E. Pino, L. Pisciotta, S. Calandra, and S. Bertolini, *Electrophoresis* **25** (2004), 3882-3889.

100. I. Medintz, W.W. Wong, G. Sensabaugh, and R.A. Mathies, *Electrophoresis* **21** (2000), 2352-2358.

101. K. Karasawa, H. Arakawa, T. Igarashi, N. Goto, M. Maeda, and T. Masako, *J. Chromatogr.B* **810** (2004), 41-47.

102. E.T. Lagally, and R.A. Mathies, *J. Phys.: Appl. Phys.* **37** (2004), R245-R261.

103. R.M. McCormic, R.J. Nelson, M.G. Alonso-Amigo, J. Benvegnu, and H.H. Hooper, *Anal. Chem.* **69** (1997), 2626-2630.

104. C.A. Emrich, H.Tian, I.L. Medintz, and R.A. Mathies, *Anal. Chem.* **74** (2002), 5076-5083.

105. E.T. Lagally, C.A. Emrich, and R.A. Mathies, *Lab on a Chip* **1** (2001), 102-107.

106. S. Yao, D.S. Anex, W.B. Caldwell, D.W. Arnold, K.B. Smith, and P.G. Schultz, *Proc. Nat. Acad. Sci.* **96** (1999), 5372-5377.

107. O. Hofmann, D. Che, K.A. Cruickshank, and U.R. Muller, *Anal. Chem.* **71** (1999), 678-86.

108. J. Wang, *Electrophoresis* **23** (2002), 713-718.

109. T.M. Phillips, *Electrophoresis* **25** (2004), 1652-1659.

110. J. Wang, G. Chen, M.P. Chatrathi, A. Fujishima, D.A. Tryk, and D. Shin, *Anal. Chem.* **75** (2003), 935-939.

111. H.R. Mobini Far, F. Torabi, B. Danielsson, and M. Khayyami, Masoud, *J. Anal. Toxico.l* **29** (2005), 790-793.

112. S.A. Pasas, N.A. Lacher, M.I. Davies, and S.M. Lunte, *Electrophoresis* **23** (2002), 759-766.

113. G. Chen, L. Zhang, and J. Wang, *Talanta* **64** (2004), 1018-1023.

114. D.-M. Tsai, K.-W. Lin, J.-M. Zen, H.-Y. Chen, and R.-H. Hong, *Electrophoresis* 26 (2005), , 3007-3012.

115. H.-L. Lee, and S.-C. Chen, *Talanta* **64** (2004), 750-757.

116. J.C. Fanguy, and C.S. Henry, *Electrophoresis* **23** (2002), 767-773.

CHAPTER 2 –MICROFABRICATION AND MICROMACHINING TECHNIQUES FOR MICROFLUIDICS

Micromachining techniques for fabricating microfluidic devices have been developed based on well-established techniques of micro/nano electronics industries [1,2]. The typical micromachining procedure consists of six main steps: film deposition, photoresist spin coating, photolithography, access holes drilling, and microchip bonding. In this chapter, these steps are illustrated with practical considerations.

1.1 Glass Micromachining

Glass has numerous advantages over polymeric materials that make it the first choice for fabrication microfluidic devisees. These advantages include its optical transparency, well-understood surface characteristics, such as electroosmotic flow similar to fused silica, high resistance to chemical reactivity and mechanical stress, superior heat dissipation capability, and high electrical insulation [3-7].

Figure 2.1 illustrates the typical experimental procedure for glass machining [1,2]. The pre-cleaned glass substrate is covered with a thin metal sacrificial layer (~200 nM). Chromium (Cr) is mostly used because of its relative easiness of deposition, either thermally or via sputtering, and low cost. After this deposition, a layer of positive photoresist is spun coated over the metal layer. The positive photoresist is made of polymeric materials that decompose when exposed to ultraviolet (UV) radiation, and become soluble in aqueous solutions of inorganic salt [1,2]. The contrast of positive photoresist is negative photoresist, which is basically a pre-polymer that polymerizes when exposed to UV radiation, and thus becomes insoluble in the developer solution, whereas unexposed materials can be washed

away. A baking process is then performed in order to evaporate the solvent and to harden the photoresist material.

The process by which a certain design is transferred to a substrate that is covered with photoresist material, by exposure to UV light, is defined as photolithography [1]. In this process, the substrate is exposed to UV light through a photomask for a period of time that depends on the thickness of the photoresist. The photomask contains the pattern that is to be transferred to the substrate; it could be made of glass covered with chromium or transparency films. Although transparency films are relatively inexpensive, they exhibit limited resolution (>20μm) in comparison to chromium photomasks (~500nm). After UV exposure, the substrate is soaked in developer solution for a short time followed by post baking. Then the metal is chemically wet etched.

In glass etching, the glass substrate's bare surface is etched either by a dry or wet chemical etching. The etching process could be isotropic, i.e. similar etching rate in all directions, or anisotropic where the etching rate depends on the direction [1,2]. The isotropic etching process, which is most frequently used, can be carried out by using a buffered solution of hydrofluoric acid (HF: NH4F; (1:1)), which results in a semi-circular shaped channel. This process involves a chemical reaction between the HF solution and the silicon atoms (Si) to form water soluble H_2SiF_6:

$$Si + HNO_3 + 6HF \longrightarrow H_2SiF_6 + HNO_2 + H_2O + H_2$$

The anisotropic etching process that results in V-grooves or vertically walls channels is achieved by using concentrated solution of potassium hydroxide (KOH). Figure 2.2

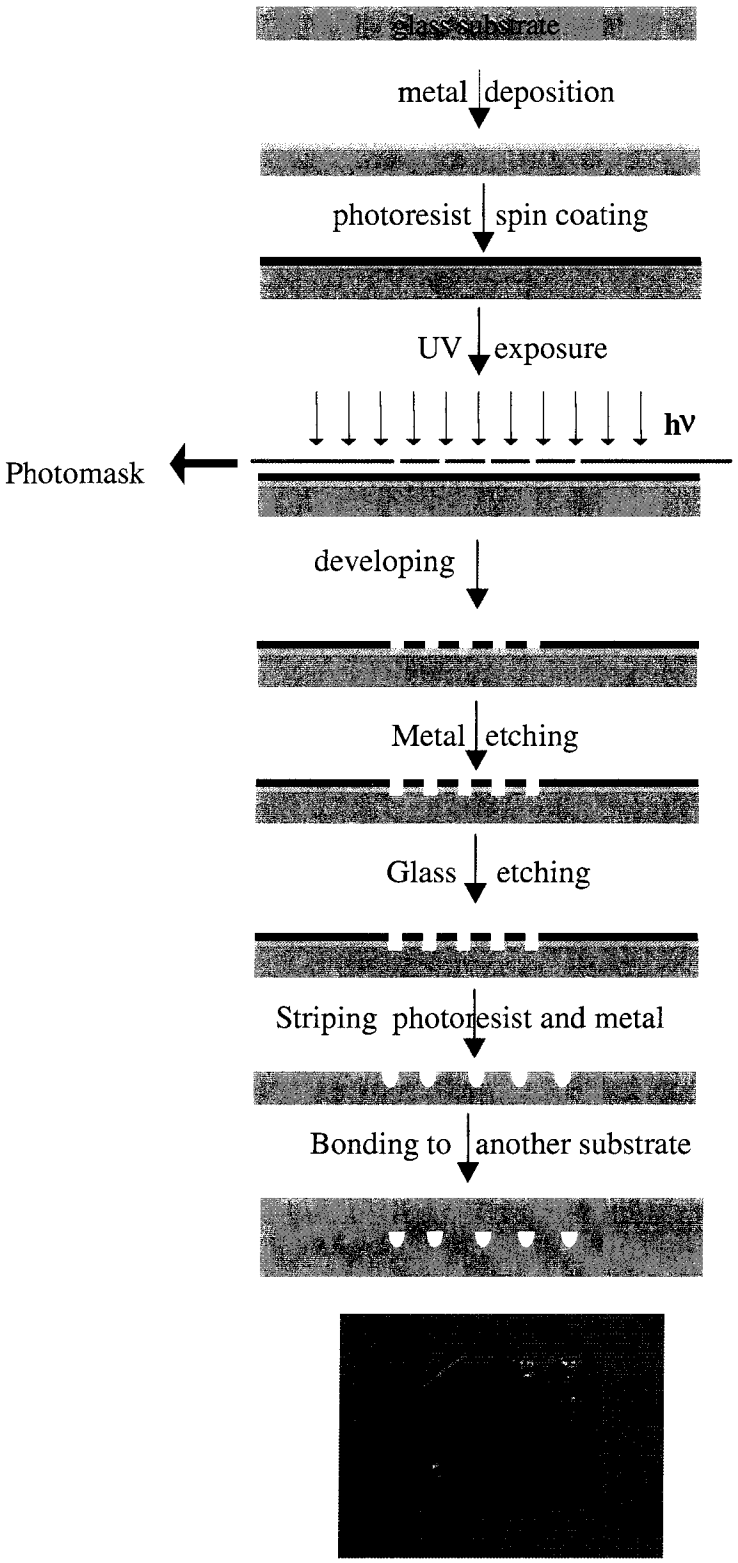

Figure2.1 Photolithography process for glass micromachining

shows scanning electro micrograph (SEM) images of isotropically etched glass substrates. As can bee seen from Figure 1.1.2, the microchannel has a semi-circular shape at the edges of the channels, which would have been vertical or V-shaped if KOH solution was used.

The other etching process is dry etching or plasma etching. In this process, reactive fluorine atoms are generated in the gaseous state at very low pressure ($<10^{-6}$ torr), which react with the silicon atoms and initiate the etching process [1]. The dry etching process is relatively more expensive than wet etching and needs complicated instrumentation. On the other hand, wet etching is simpler and can be carried out in regular laboratories. The concentration of the etching solution (etchant) is an important experimental issue to be considered before carrying out any etching process. While diluted buffered oxide (BOE) etchant solution has a slower etching rate than concentrated solution, it provides smoother surfaces and controlled operation [1,2]. Concentrated HF solution (49%) provide etching rates of ~10-15μm/min, whereas diluted HF solutions (~6%) provide etching rates of ~0.7μm/min [1]. The etching time depends on the desired depth of the channels, where channels with a depth of 15-20μm are most frequently used for microfluidics made of glass. Following the etching process, the remaining photoresist is washed away by soaking the substrate with acetone solution, followed by rinsing with water, then etching the remaining metal layer.

Prior to sealing the channels, by bonding the substrate to another substrate, access-holes are drilled into either the channels-substrate or the cover substrate. The bonding process is accomplished by using different techniques, but the most widely used is thermal bonding [3-7]. In thermal bonding, the two substrates are clamped together,

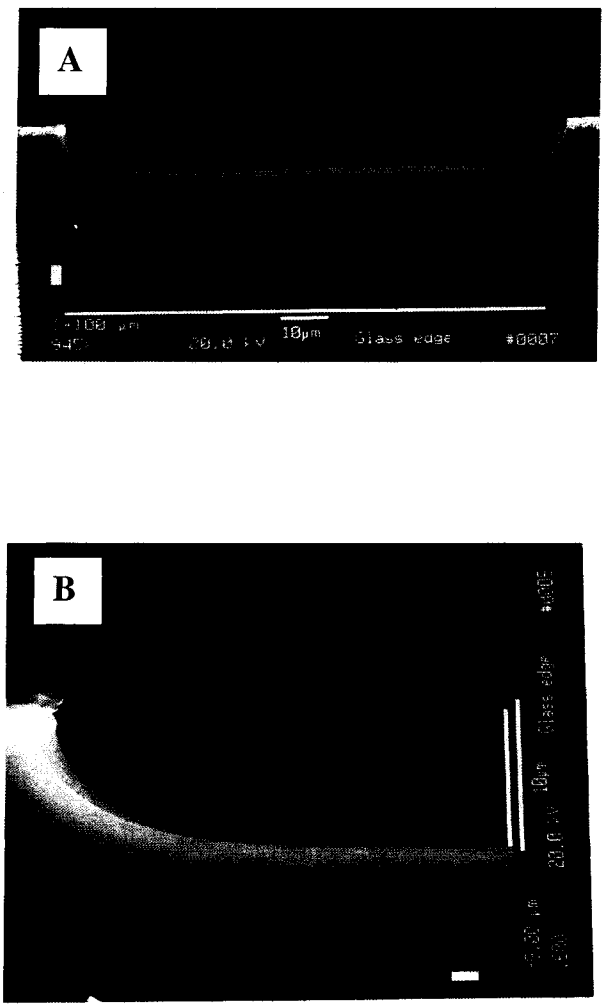

Figure 2.2 SEM images for cross section of microchannels created on glass substrate; (A) full profile, (B) microchannel's edge.

then loaded into a programmable oven. The temperature is ramped up slowly to approximately the melting point (mp) of the glass material, e.g. ~620 °C for soda lime glass. Other bonding techniques, such as anodic bonding [8] and using a lower melting point bonding layer between the two substrates [9] are two alternative techniques to avoid the high temperature bonding process, but they could be problematic in some cases where metals are deposited on the substrate surface.

1.2 Polymers Micromachining

Recently, different polymers have been used for fabricating microfluidic devices such as polyethylene terephthalate (PET) [10], polyethylene (PE) [11], poly (dimethyl siloxane) (PDMS) [12-16], and poly (methyl methacrylate) (PMMA) [17-19]. Although polymers exhibit some advantages over glass, such as they are inexpensive and need micromachining techniques rather than etching, but there are some drawbacks for using polymers; this includes paying more attention to their surface chemistry. They also have poor compatibility with organic solvents and with high temperatures since these polymers have low boiling points (~ 110 °C) as well [10,11,17-19]. Various micromachining techniques are used for fabricating microfluidic devices made of different polymeric materials; these techniques strongly depend on the elasticity and rigidity of the polymeric materials. These techniques include hot embossing [10,17], injection molding [19], and laser ablation [16]. Among those polymers used for microfabrication, PDMS is mostly used because of the easiness and low cost instrumentation needed for the fabrication process in comparison to other polymeric materials [12-15]. Therefore, a brief description is given to illustrate the micromachining

protocols for other polymers, whereas a detailed protocol is given to illustrate the fabrication process of PDMS.

1.2.1 Polydimethyl siloxane (PDMS)

Figure 2.3 shows the chemical structure of PDMS, which is featured by the presence of the methyl groups; accordingly the unmodified surfaces of PDMS are hydrophobic.

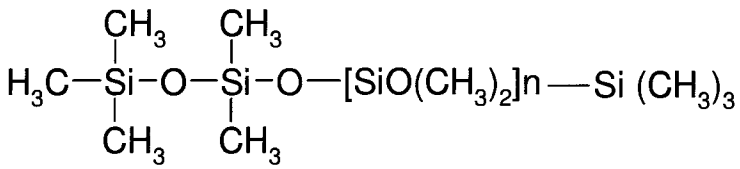

Figure 2.3 Chemical Structure of PDMS

In addition to the advantages of using PDMS mentioned above, PDMS exhibits some other features that have made it the first choice for manufacturing microfluidic devices made of polymeric materials; this includes being optically transparent down to ~ 260 nm, hence it is suitable for UV/Vis absorption and fluorescence detection, nontoxic, cures at low temperature, and can bond (seal) to different surfaces reversibly via van der Waals forces or irreversibly via covalent bonds [12,14].

The micromachining techniques used for fabricating PDMS microfluidic devices are a combination of photolithography and soft lithography techniques. The photolithography course of action is used to prepare a mold that contains the microchannels structure, whereas the soft lithography, specifically rapid prototyping and replica molding, are used to prepare the PDMS slabs with microchannels.

Figure 2.4 illustrates the typical experimental procedure for PDMS micromachining [14]. The first step is the preparation of the mold via photolithography process. A layer of

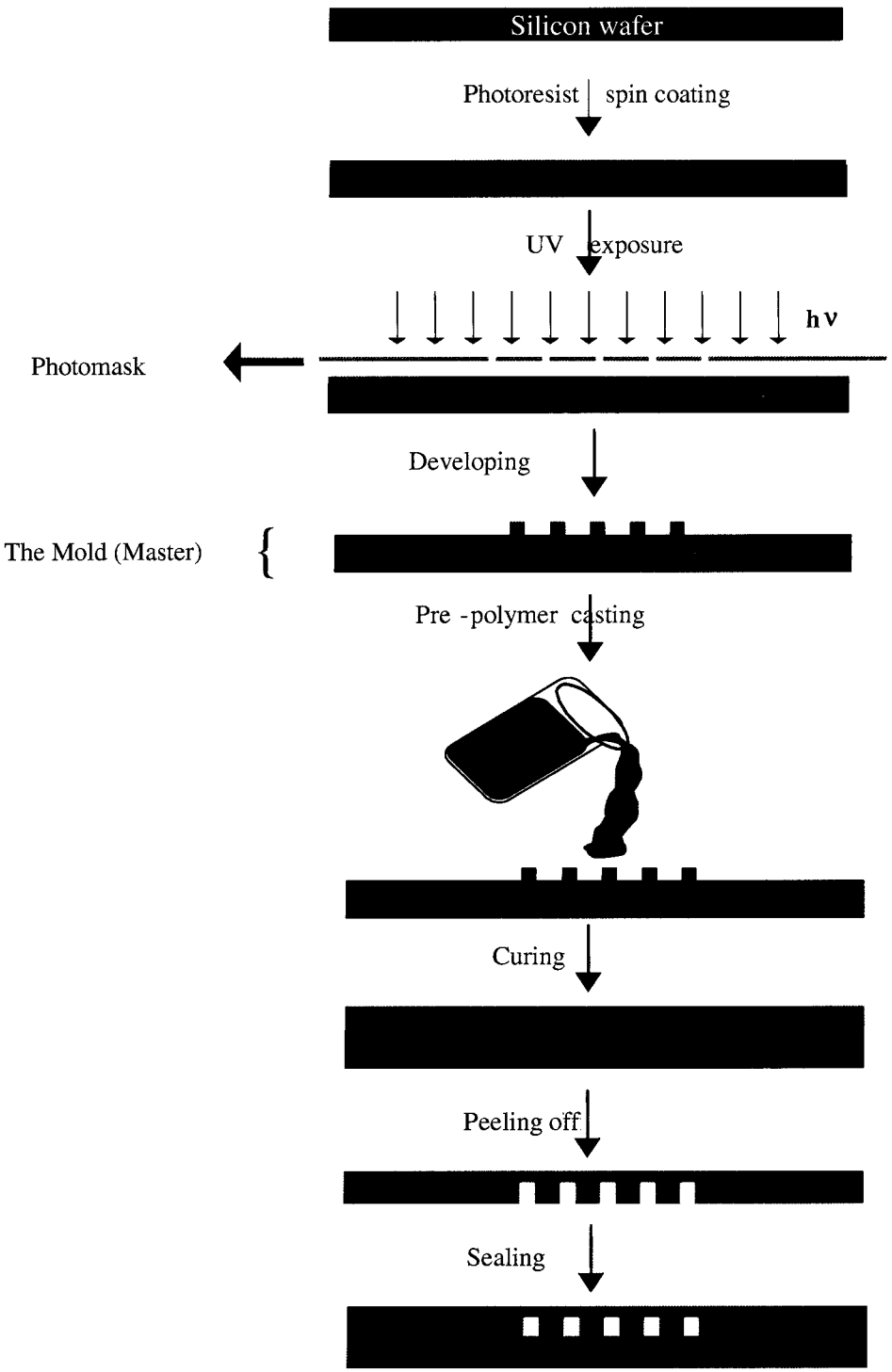

Figure 2.4 Rapid prototyping and replica molding processes for micromachining of PDMS

negative photoresist is spun coated on pre-cleaned glass substrate, followed by soft baking. Each brand of negative photoresist has different viscosity, which determines the range of applicable thickness of any brand. Choosing the right brand depends on the desired channel depth, where deeper channels necessitate using negative photoresist of higher viscosity [14]. The designed photo mask controls the width and the length of the channels. The substrate covered with the photoresist is exposed to UV light for a period of time that depends on the thickness of the photoresist layer. The polymerization process is activated by post baking the substrate at 95 °C. Thus far, the areas that have polymerized are those that define the microchannels, whereas the un-polymerized ones are washed away by soaking the substrate in developer solution.

Once the mold is fabricated, the next step is the process that is defined as replica molding. In this process a pre-polymer mixture is casted against the mold to generate a negative replica of the mold in the PDMS. The pre-polymer is a degassed mixture of the PDMS and the catalyst (10:1; v:v) . The substrate is baked at 60 °C for about one hour or at room temperature for 24 hours for curing. After the curing process, the PDMS slab is peeled off from the mold. Access holes can be formed with a hand-punch tool. The channels' profile depends on the mold's profile. Molds that are created according to the procedure above generate vertical profiles as can be seen in Figure 2.5 Semicircular profiles can be prepared with correspondingly shaped molds fabricated by the chemical wet etching procedure. Superlatively, the microchannels have dimensions similar to the master, which can be identified by using a profilometer. Figures 2.5 and 2.6 show results of profilometer measurements for a silicon master and a PDMS microchannel cross section made in our labs, respectively. Finally, sealing the PDMS replica to flat surface encloses the PDMS

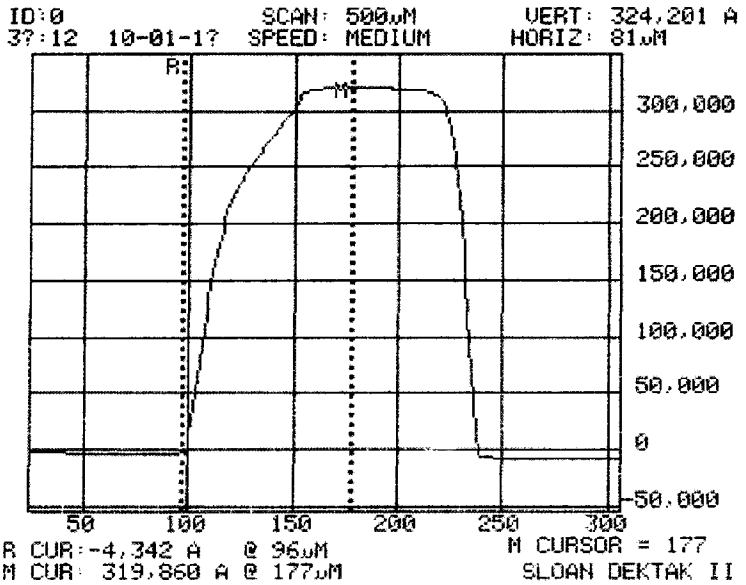

Figure 2.5 Profilometer image for microchannel's master on silicon wafer.

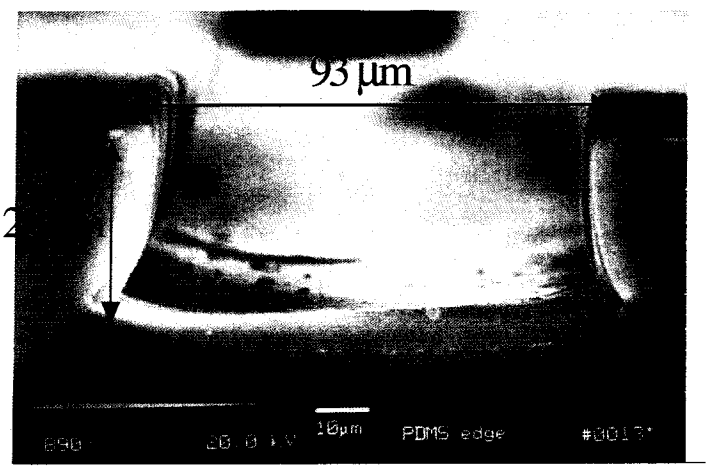

Figure 2.6 SEM image for cross section of microchannel on PDMS

microchannels. The bonding process can be done either reversibly or irreversibly. Cleaning both surfaces thoroughly with ethanol, dried by a stream of nitrogen or in an oven, then bringing both surfaces into contact attains reversible bonding. The reversible bonding is not relatively strong and does not permit the microdevice to withstand high pressure. For Irreversible bonding, the PDMS replica is exposed to air or oxygen plasma, which introduces negative charges to the PDMS surface, and consequently replacing the methyl groups with hydroxyl groups, Figure 2.7 [20]. The activated surface binds irreversibly to similarly treated surfaces such as glass or another PDMS slab. Interestingly, the irreversibly sealed microchip can withstand pressure that is one order of magnitude higher than reversibly bonded one. After the sealing process, the channels can retain their hydrophilicity for up to about one hour upon exposure to air, whereas keeping the microchannels wet, by water or buffer solution, enables the microchannels to retain their hydrophilicity for about a month [21]. IR analysis of the plasma treated PDMS surfaces, as a function of time after plasma exposure, has revealed a decrease in the OH peak intensity upon exposure to air [21]. These hydrophilic channels are necessary for the intricate separation of hydrophobic analytes such as proteins, and for having ideal electroosmotic flow as well.

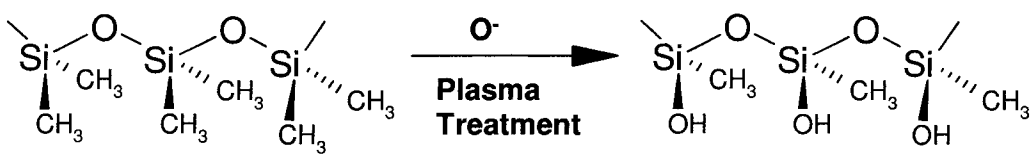

Figure 2.7 Oxidation reaction of PDMS

While surface modification of PDMS provides a promising solution for having hydrophobic microchannels, different techniques and protocols have been applied to solve

this problem, such as using surfactants [22], sol-gel modification with silicon materials [23], and coating with poly-vinyl alcohol [24].

1.2.2 Other Polymers

Other polymers, such as PMMA, are rigid materials and need special instrumentation for the fabrication process. Hot embossing is the most frequently used for fabricating microfluidics on rigid polymers. After fabrication of the mold, which mostly made of nickel, the substrate is mounted in the hot embossing system and pressure is applied [17-18]. The system is heated to a temperature just below the glass transition temperature of the material, T_g, after a short time; the temperature is ramped down to the room temperature. Another technique is injection molding, in which the polymer is melted then injected to a mold at high temperature, and is then cooled down [19]. Other techniques such as laser ablation have been applied for *direct* fabrication of rigid polymers [16]. One significant drawback of using rigid polymers is the bonding process, which is usually done by heating both substrates to a temperature just below the T_g, since such procedures might cause the microchannels to collapse [17-19].

1.3 Metals patterning and electrochemical plating

The metal layers in glass photolithography are considered necessary during the micromachining process for various reasons. During the chemical wet etching process, a metallic sacrificial layer, mainly chromium, is needed; since without the metal layer the photoresist layer cannot settle on the surface and more pinholes are expected [1,2]. Also, the metal layers are necessary for electrochemical measurements. Metals are deposited on the substrate's surface, followed by patterning protocol to create specific electrode designs and

characteristics. Metal deposition generally can be achieved either via sputtering or thermal evaporation.

Different problems are considered upon using either of the techniques mentioned above for metals deposition. Sputtering deposition requests specific targets for each metal, which is considered to be time consuming and expensive process. Although thermal deposition provides a solution for these problems, it still can hardly be used for some metals such as platinum and palladium. Furthermore, it is difficult to pattern these metals via traditional fabrication techniques.

Electroplating provides a sufficient remedy for all of these previously mentioned problems; it is reliable, fast, and more importantly inexpensive and can be carried out with simple instrumentation. The electroplating, or the electrochemical deposition, is a process by which a thin layer of a certain metal is deposited on the surface of another metal by electrolysis [25,26]. The process is carried out by dissolving a metallic salt in water with supporting electrolytes, such as sulfuric acid; the metallic salts dissociate into positively charged metallic ions and counter anions, then deposition potential (1-2 V) is applied from a power supply, or ideally from potentiostat for a short period of time (1-2 minutes). Typically, the metals that can be easily deposited and patterned, such as chromium and gold, are used as metallic seed layers so that specific desired metal layer can then be electrochemically deposited on top of these surfaces [25,26].

1.4 References

1. Marc J. Madou, *Fundamentals of Microfabrication: the Science of Miniaturization*, 2nd Ed., CRC press, New York (2002), Chap. 1.

2. Mark J. Jackson, *Microfabrication and Nanomanufacturing*, CRC press, New York (2006), Chap. 1.

3. S.C. Jacobson, R. Hergenroder, L.B. Koutny, R.J. Warmack, and J.M. Ramsey, *Anal. Chem.* **66** (1994), 1107-1113.

4. D.J. Harrison, A. Manz, Z. Fan, H. Luedi, H.M. Widmer, and H. Michael. *Anal. Chem.* **64** (1992), 1926-32.

5. I. Rodriguez, Y. Zhang, H.K. Lee, and S.F.Y. Li, *J. Chromatogr. A* **781** (1997), 287-293.

6. J.D. Ramsey, S.C. Jacobson, C.T. Culbertson, and J.M. Ramsey, *Anal. Chem.* **75** (2003), 3758-3764.

7. S.C. Jacobson, and J.M. Ramsey, *Anal. Chem.* **68** (1996), 720-723.

8. B.R. Fonslow, and M.T. Bowser, *Anal. Chem.* **77** (2005), 5706-5710.

9. H.Y. Wang, R.S. Foote, S.C. Jacobson, J.H. Schneibel, J.M. Ramsey, *Sens. Actuators B* **B45** (1997), 199-207.

10. Z. Wu, N. Xanthopoulos, F. Reymond, J.S. Rossier, H.H. Girault, *Electrophoresis* **23** (2002), 782-790.

11. S.L.R. Barker, M.J. Tarlov, H. Canavan, J.J. Hickman, and L.E. Locascio, *Anal. Chem.* **72** (2000), 4899-4903.

12. D.C. Duffy, J.D. McDonald, O.J.A. Schueller, and G.M. Whitesides, *Anal. Chem.* **70** (1998), 4974-4984.

13. R.S. Martin, A.J. Gawron, S.M. Lunte, and C.S. Henry, Charles, *Anal. Chem.* **72** (2000), 3196-3202.

14. J.C. McDonald, D.C. Duffy, J.R. Anderson, D.T. Chiu, H. Wu, O.J.A. Schueller, and G.M. Whitesides, *Electrophoresis* **21** (2000), 27-40.

15. D.C. Duffy, O.J.A. Schueller, S.T. Brittain, and G.M. Whitesides, *J. Micromech. Microeng.* **9** (1999), 211-217.

16. B.A. Fogarty, K.E. Heppert, T.J. Cory, K.R. Hulbutta, S.R. Martin, and S.M. Lunte, *Analyst* **130** (2005), 924-30.

17. L. Martynova, L.E. Locascio,M.K. Gaitan, G.W. Kramer, R.G. Christensen, and W.A. MacCrehan, *Anal. Chem.* **69** (1997), 4783-4789.

18. R.T. Kelly, and A.T. Woolley, *Anal. Chem.* **75** (2003), 1941-1945.

19. X.-M. Zhou, Z.-P. Dai, X. Liu, Y. Luo, H. Wang, and B.-C. Lin, *J. Separat. Sci.* **28** (2005), 225-233.

20. R.W. Stark, M. Sakai Stalder, and A. Stemmer, *Microelect. Eng.* **67–68** (2003) 229–236.

21. X.Q. Ren, M. Bachman, C. Sim, G.P. Li, and N. Allbritton, *J. Chromatogr. B* **726** (2001), 117-125.

22. C.D. Garcia, B.M. Dressen, A. Henderson, and C.S. Henry, *Electrophoresis* **26** (2005), 703-709.

23. G.T. Roman, T. Hlaus, K.J. Bass, T.G. Seelhammer, and C.T. Culbertson, *Anal. Chem.* **77** (2005), 1414-1422.

24. D. Wu, Y. Luo, X. Zhou, Z. Dai, and B. Lin, Bingcheng, *Electrophoresis* **26** (2005), 211-218.

25. Mordechay Schlesinger, and Milan Paunovic, *Modern Electroplating* (2000), John Wiley & Sons, New York, Chap.1.

26. Milan Paunovic, and Mordechay Schlesinger.*Fundamentals of Electrochemical Deposition* (1998), John Wiley & Sons, New York, Chap.1.

CHAPTER 3: DNA ADDUCTS AND RELATED BIOMARKERS

3.1 Introduction

Genotoxic carcinogens can react covalently with DNA to form DNA adducts, which can lead to mutations in critical genes, and subsequently, to the development of different diseases, such as cancer [1]. Some genotoxic carcinogens can directly bind to the DNA to create mutations, i.e. exogenous carcinogens, whereas others go through certain metabolic pathways to form active metabolites that can react with the DNA, i.e. endogenous carcinogens [2,3]. The role of DNA damage and their subsequent biomarkers, DNA adducts, are considered important in studies involving cancer, Parkinson's disease, and other aging-related diseases [4,5]. In this chapter a brief description of relevant DNA adducts and other related biomarkers that pertain to this thesis is presented. Figure 1 shows a summary for the process of formation of DNA adducts by genotoxic carcinogens [1].

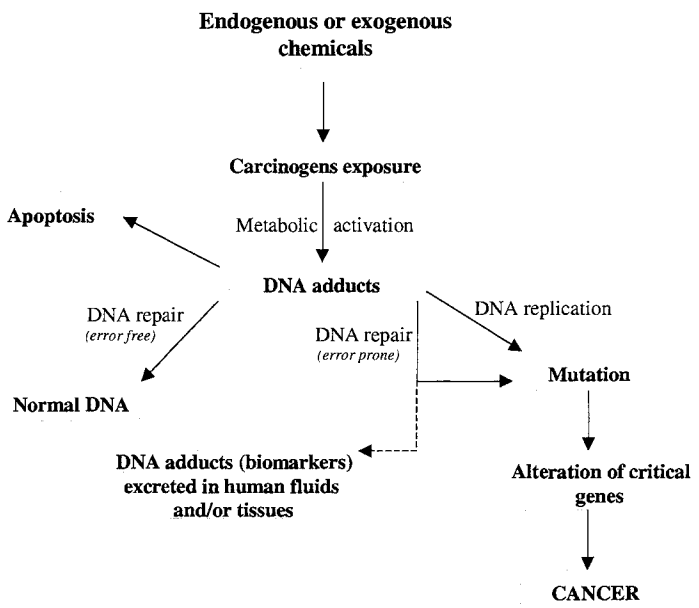

Figure 3.1: Schematic for the process of formation of DNA adducts by genotoxic carcinogens [1].

3.2 Dopamine-derived DNA adducts and related neurotransmitters.

Oxidative damage to cellular macromolecules has been proposed to perturb the metabolism of neurotransmitters, which eventually leads to the development of certain neurodegenerative diseases such as amyotrophic lateral sclerosis and Parkinson's disease [6-9]. The metabolic oxidation of catecholamines, such as dopamine (DA), leads to the formation of oxygen reactive metabolites, such as quinones and semiquinones [8,9]. The neurotoxicity observed in dopaminergic neurons of patients with Parkinson's disease may be related to the reaction of these reactive molecules with cellular macromolecules such as DNA, and thus initiate DNA damage through the formation of depurinating adducts [7-9]. Accordingly, the role of this kind of DNA damage is considered significant in initiating neurodegenerative disorders such as Parkinson's disease [9]. Figure 3.2 shows the chemical structures of DA-derived DNA adducts after reaction with guanine (Gua) and adenine (Ade).

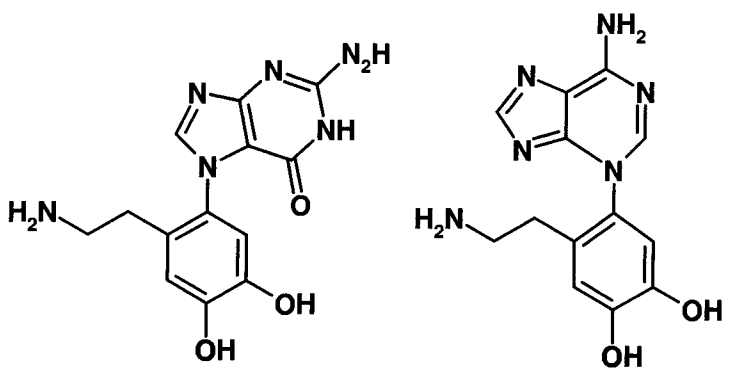

Figure 3.2: Chemical structure of DA-derived adducts: DA-6-N7Gua, and DA-6-N3Ade

3.3 8-Hydroxy-deoxyGuanosine (8-OH-dG)

Oxidative damage in a cell, tissue, or organ, is a steady-process known as oxidative stress (OS), caused by the reaction of reactive oxygen species (ROS), such as hydrogen peroxide radicals ($^{\cdot}O_2$) and hydroxy radicals ($^{\cdot}OH$), that result as a consequence of continuous metabolic reactions with cellular macromolecules [1,10-12]. The OS occurs because of imbalanced conditions of endogenous oxidants and antioxidants that result in an excessive amount of cellular oxidants [13]. The generated ROS can cause oxidative damage to lipids, proteins, and DNA, which results in the formation of adducts that can be identified and used as biomarkers for medical diagnostics [10-14]. Guanine has the lowest potential for oxidative stress among all nucleotides [10]. Therefore, different guanine adducts are generated, such as 8-hydroxy-2′-deoxyguanosine (8-OH-dG) (the oxidized product of DNA), and 8-OH-G (the oxidized product of RNA) [10,15]. Figure 3.3 lists the chemical structure of all guanine related oxidized products. Recently, 8-hydroxy-2′-deoxyguanosine (8-OH-dG) has emerged as a biomarker to characterize the extent of oxidative DNA damage. It has been shown that there is a pathogenic link between the oxidative DNA damage and a various degenerative diseases, such as cancer and other aging-related diseases [1,10,16,17]. More details regarding various detection techniques for (8-OH-dG) are presented and discussed in Chapter 5.

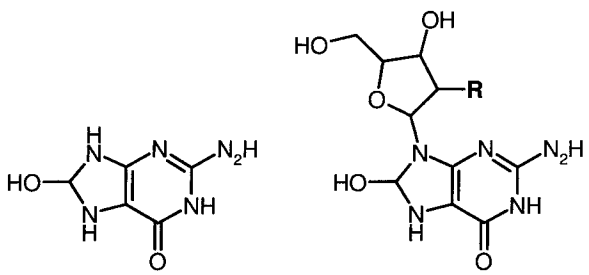

Figure 3.3: Chemical structure of guanine adducts: (A) 8-OH-Gua, and (B) 8-OH-dG (R= H); 8-OH-G (R = OH)

3.4 Catechol estrogens-derived (*CEQ-derived*) DNA adducts and conjugates:

Recently, it has been suggested that estrogens (E) are complete carcinogens capable of tumor initiation [18-21]. Estrogens (E) are linked with several cancers in humans and are known to induce tumors in animals [18,20,22]. E_1 and E_2 are produced by aromatization reaction of androstenedione and testosterone, respectively, catalyzed by cytochrome P450 (CYP) 19 aromatase [23-25]. E_1 and E_2 are biochemically interconvertible by 17β-estradiol dehyrogenase. Their metabolism leads to catechol estrogens and, to a lesser extent, 16α-hydroxylation [18]. Figure 3.4 summarizes the major metabolic pathways for principal natural estrogens.

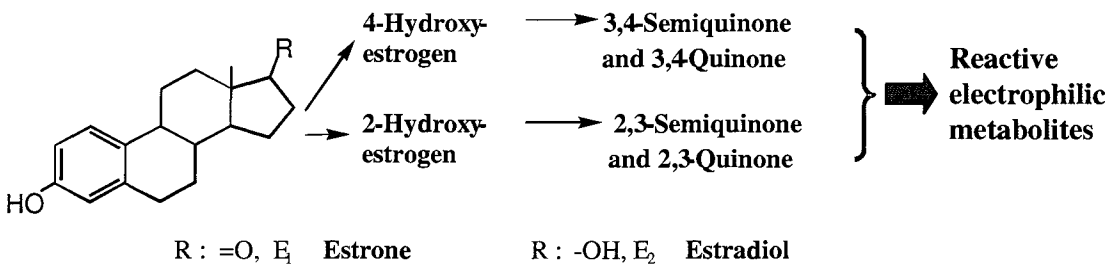

Figure 3.4: Major metabolic pathways for the principle natural estrogens

As can be seen from Figure 3.4, two catechol estrogens form based on metabolic conversion, 2-$OHE_1(E_2)$ as the primary product and 4-$OHE_1(E_2)$ as the secondary product [26-28]. These catechol estrogens are deactivated via various conjugation pathways; in the liver they are deactivated by conjugative reactions such as glucuronidation, sulfation and *O*-methylation, whereas in extrahepatic tissues, the major pathway of conjugation takes place by *O*-methylation catalyzed by metabolically prevalent catechol-*O*-methyltransferase (COMT) [29].

Conjugation of 4-OHE_1 (E_2) by methylation in extrahepatic tissues might become deficient because of the level and/or induction of CYP1B1 [30-32] and other 4-hydroxylases, which can cause 4-OHE_1 (E_2) to be the major metabolite, rather than the 2-OHE_1(E_2) and subsequently competitive catalytic oxidation of catechol estrogens to CEQ may occur. However, CEQ can be neutralized by reaction with GSH (see below). Another deactivating pathway for CEQ is their reduction to catechol estrogens by quinone reductase and/or cytochrome P450 reductase [33,34].

Catechol estrogens are oxidized to CEQ by peroxidases and cytochrome P-450 [35-37], a redox-cycling process that can also generate hydroxyl radicals that cause DNA damage [38,39]. CEQ that are derived from the catechol estrogens, 4-OHE_1 and 4-OHE_2, can react with DNA to form depurinating adducts at the N7 position of guanine and N3 position of adenine [18,20]. Considerably, the amount of stable adducts derived from the reaction of E_2-3,4-Q with DNA is only 0.02% the amount of depurinating adducts [20]. Thus, if the two deactivating processes discussed above are insufficient, CEQ may react with DNA to form stable and depurinating adducts [18,40]. The carcinogenic 4-OHE_1(E_2) [41-43] are oxidized to predominantly form the depurinating adducts 4-OHE_1(E_2)-1-N3Ade and 4-OHE_1(E_2)-1-N7Gua [18,20], whereas 2-OHE_1(E_2) are oxidized to form lower levels of the depurinating 2-OHE_1(E_2)-6-N3Ade adducts [31-33] and much lower levels of stable adducts [18,40]. Correspondingly, the imbalance between activating pathways and protective (deactivation) pathways that can instigate a substantial reaction of CE-3,4-Q with DNA, and thus initiate mutations that can lead to cancer [44]. The structures of major CEQ derived DNA adducts of interest are shown in Figure 3.5.

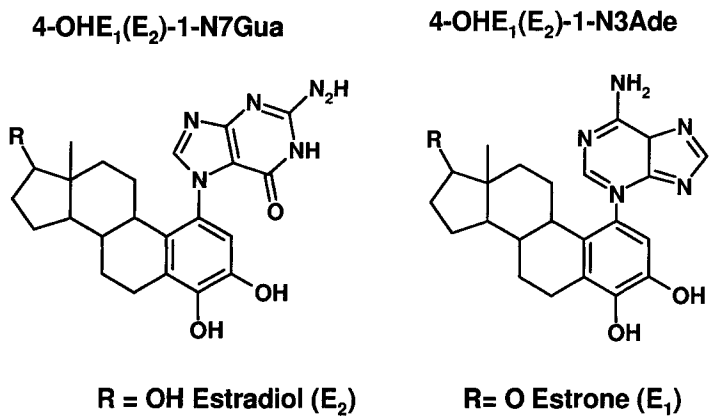

Figure 3.5: Chemical structures estrogen-derived DNA adducts.

The importance of various depurinating DNA adducts has been already demonstrated [45,46]. For instance, adducts derived from various polycyclic aromatic hydrocarbons (PAH), such DNA adducts formed by dibenzo[*a,l*]pyrene (DB[*a,l*]P), are converted into H-ras mutations by DNA damage repair errors, suggesting that the apurinic (AP) sites produced by depurinating DB[*a,l*]P-DNA adducts are converted into preneoplastic mutations in resting cells [44-46].

CEQ-derived GSH (γ-glutamyl-L-cysteinyl-glycine) conjugates are considered to be potentially useful biomarkers for catechol estrogen-induced DNA damage, which can indicate the risk of breast and other cancers (as identified in *in vivo* experiments [18,20]). Conjugation with GSH is considered a deactivation pathway that prevents damage to DNA [47], and is one of the most important detoxification pathways in biological systems. A large number of electrophilic compounds such as CEQ, conjugate with GSH nonenzymatically or, more effectively, via S-transferase-catalyzed reactions [18,48]. Thus, the conjugation reaction of CEQ with various sulfur nucleophiles, RSH, in which R is the Cys, NAcCys, or

GSH moiety, is considered of great interest in carcinogenesis. Once CEQ conjugates are formed, catabolism occurs via mercapturic acid biosynthesis. The conjugation reaction mechanism is summarized as the following: first, the glutamyl moiety of the GSH conjugate is removed by transpeptidation, catalyzed by γ-glutamyl transpeptidase; then the cysteinylglycine derivative is hydrolyzed to yield the cysteine conjugate; and lastly acetylation to the NAcCys conjugate and excretion in urine [18,48-50]. 4-OHE_1-2-NAcCys metabolites were already observed in human fluid samples (R. Jankowiak, unpublished results, 2006), therefore, identification and quantitation of CEQ-conjugates in urine have potential for assessment in the level of CEQ formed. Structures of 4-OHE_1, 4-OHE_2, and 4-OHE_1/4-OHE_2 derived –NAcCys conjugates are shown in Figure 3.6.

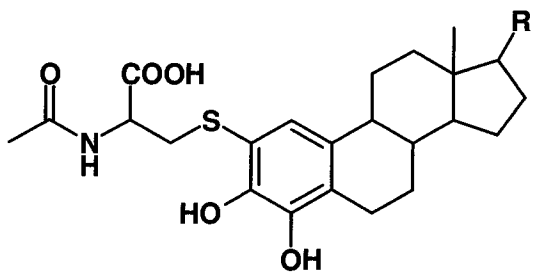

Figure 3.6: Chemical structures of 4-OHE_1- (R=O), 4-OHE_2-derived (R=OH) NAcCys conjugates

3.4 References

1. R. Singh, and P. Farmer, *Carcinogenesis* **27** (2006), 178-196.
2. K. Hemminki, *Arch. Toxiocol.* **52** (1983), 249-285.
3. A. Dipple, *Carcinogenesis* **16** (1995), 437-441.

4. G.N. Wogan, S.S. Hecht, J.S. Felton, A.H. Conney, and L.A. Loeb, *Semin. Cancer Biol.* **14** (2004), 473-486.

5. A. Luch, *Nat. Rev. Cancer* **5** (2005), 113-125.

6. G. Levay, and W.J. Bodell, *Carcinogenesis* **14** (1993), 1241-1245.

7. G. Levay, ; Q. Ye, and W.J. Bodell, *Exp. Neurol.* **146** (1997), 570-574.

8. B. Kalyanaraman, C.C. Felix, and R.C. Sealy, *Environ. Health Perspect.* **64** (1985), 185-198.

9. E.L. Cavalieri, K-M. Li, N. Balu, M. Saeed, P. Devanesan, S. Higginbotham, j. Zhao, M.L. Gross, and E.G. Rogan, *Carcinogenesis* **23** (2002), 1071-1077.

10. M.C. Peoples, and H.T. Karnes, *J.Chromatogr. B* **827** (2005), 5-15.

11. R. Floyd, J. Watsonand, P. Wong, D. Altmiller and R. Rickard, *Free Radio. Res. Commun* **1** (1986),163-172.

12. M. Shigenaga, C. Gimeno and B. Ames, *Proc. Natl. Acad. Sei.* **86** (1989), 9697-9701.

13. L.L. Wua, C-C. Chioud, P-Y. Change, and J.T. Wua, *Clin. Chem.Acta* **339** (2004), 1-9.

14. Y. Ma, G. Liu, M.Du, and I. Stayton, *Electrophoresis*, **25** (2004), 1473-1484.

15. S. Loft, K. Vistisen, M. Ewertz, A. Tjonneland, K. Overvad and H. Poulsen, *Carcinogenesis* **13** (1992), 2241-2247.

16. R. Rozalski, P. Winkler,D. Gackowski, T. Paciorek, H. Kasprzak, R. Olinski ,*Clin. Chem.* **49** (2003), 1218-1221.

17. S. Haghdoost, S. Czen, I. Naeslund, S. Skog, and M. Harms-Ringdahl, *Free Rad. Res.* **39** (2005), 153-162.

18. E.L. Cavalieri, E.G. Rogan, and D. Chakravarti, D. *Cell. Mol. Life Sci.* **59** (2002), 665-681.

19. Y. Markushin, W. Zhong, E.L. Cavalieri, E.G. Rogan, G.J. Small, E.S. Yeung, and R. Jankowiak, *Chem. Res. Toxicol.* **16** (2003), 1107-1117.

20. D. Roy, and J.G. Liehr, *Mutat. Res.* **424** (1999), 107.

21. R.F. Service, *Science* **279** (1998), 1631.

22. J.G. Liehr, *Endo. Rev.* **21** (2000), 4054-4058.

23. W.R. Miller, and J. O'Neill, *Steroids* **50** (1987), 537-548.

24. E.R. Simpson, M.S. Mahendroo, G.D. Means, M.W. Kilgore, M.M. Hinshelwood, S. Graham-Lorence, B. Amarneh, Y. Ito, C.R. Fisher, C.R., M.D. Michael, C.R. Mendelson, and S.E. Bulun, *Endocrine Rev.* **15** (1994), 342-355.

25. Jefcoate,C.R., Liehr, J.G., Santen, R.J., Sutter, T.R., Yager, J.D., Yue, W., Santner, S.J., Tekmal, R., Demers, L., Pauley, R., Naftolin, F., Mor, G., and Berstein, L. Tissue-specific synthesis and oxidative metabolism of estrogens. In: *JNCI Monograph 27* (2000)*: Estrogens as Endogenous Carcinogens in the Breast and Prostate* (E. Cavalieri and E. Rogan, Eds.), Oxford Press, 95-112.

26. F.P. Guengerich, *Annu. Rev. Pharmacol. Toxicol.* **29** (1989), 241-264.

27. C.P. Martucci, J.and Fishman, *Pharmacol. Ther.* **57** (1993), 237-257.

28. B.T. Zhu, and A.H. Conney, *Carcinogenesis* **19** (1998), 1-27.

29. P.T. Männistö, and S. Kaakola, *Pharmacol. Rev.* **51** (1999), 593-628.

30. U. Savas, K.K. Bhattacharyya, M. Christou, D.L. Alexander, C.R. and Jefcoate, *J. Biol. Chem.* **269** (1994), 14905-14911.

31. C.L.Hayes, D.C. Spink, B.C. Spink, J.Q. Cao, N.J. Walker, and T.R. Sutter, *Proc. Natl. Acad. Sci. USA* **93** (1996), 9776-9781.

32. D.C. Spink, B.C. Spink, J.Q.Cao, J.A. DePasquale, B.T. Pentecost, M.J. Fasco, M.J., Y. Li, T.R. and Sutter, *Carcinogenesis* **19** (1998), 291-298.

33. D.T. Diaphorase., *Chem. Scripta* **27A** (1987).

34. D. Roy, J.G. Liehr, *J. Bio. Chem.* **263** (1988), 3646-3651.

35. I. Dwivedy, P.D. Devanesan, P. Cremonesi, E.G. Rogan, and E.L. Cavalieri, *Chem. Res. Toxicol.* **5** (1992), 828-833.

36. B. Kalyanaraman, R.C. Sealy, K. and Sivarajah, *J. Biol. Chem.* **259** (1984), 14018-14022.

37. Liehr, J.G., Ulubelen, A.A., and Strobel, H.W. (1986). *J. Biol. Chem.* **261**, 16865-16870.

38. J.G. Liehr, and D. Roy, *Free Radical Biol. Med.* **8** (1990), 415-423.

39. L.M. Nutter, Y.Y. Wu, E.O. Ngo, E.E. Sierra, P.L. Gutierrez, Y.J. and Abul-Hajj, *Chem. Res. Toxicol.* **7** (1994), 23-28.

40. E. Cavalieri, K. Frenkel, J. Liehr, E. Rogan, and D. Roy, *Monogr. Natl. Cancer Inst.* **27** (2000), 75-93.

41. E.R. Simpson, M.S. Mahendroo, G.D. Means, M.W. Kilgore, M.M. Hinshelwood, S. Graham-Lorence, B. Amarneh, Y. Ito, C.R. Fisher, M.D. Michael, C.R. Mendelson, and S.E. Bulun, *Endocrine Rev.* **15** (1994), 342-355.

42. J.J. Li, and S.A. Li, *Fed. Proc.* **46** (1987), 1858-1863.

43. R.R. Newbold, and J.G. Liehr, Cancer *Res.* **60** (2000), 235-237.

44. D. Chakravarti, P.C. Mailander, K.-M. Li, S. Higginbotham, H.L. Zhang, M. Gross, J.L. Meza, E.L. Cavalieri, and E.G. Rogan, *Oncogene* **20** (2001), 7945-7953

45. D. Chakravarti, J.C. Pelling, E.L. Cavalieri, and E.G. Rogan, *Proc. Natl. Acad. Sci. USA* **92** (1995), 10422-10426.

46. E. Cavalieri, and E. Rogan, *The Handbook of Environmental Chemistry*, Vol. 3J: PAHs and Related Compounds; A. H. Neilson, ed.; Springer-Verlag, Heidelberg, pp. 81-117.

47. E.L. Cavalieri, S. Kumar, R. Todorovic, S. Higginbotham, A.F. Badawi, and E.G. Rogan, *Chem. Res. Toxicol.* **14** (2002), 1041-1050

48. K. Cao, P.D. Devanesan, R. Ramanathan, M.L. Gross, E. Rogan, and E.L. Cavalieri, *Chem. Res. Toxicol.* **11** (1998), 917-924.

49. M. Nakagomi, and E. Suzuki, *Chem. Res. Toxicol.* **13** (2000), 1208-1213

50. R. Todorovic, P. Devanesan, S. Higginbotham, J. Zhao, M.L. Gross, E.G. Rogan, and E.L. Cavalieri, *Carcinogenesis* **22** (2001), 905-911

CHAPTER 4: SEPARATION OF CATECHOLAMINES AND DOPAMINE-DERIVED DNA ADDUCT USING A MICROFLUIDIC DEVICE WITH ELECTROCHEMICAL DETECTION

A paper accepted for publication in *Sensors and Actuators B: Chemical,* (in press).

A.A. Dawoud, T. Kawaguchi, Y. Markushin, M.D. Porter, and R. Jankowiak

Abstract

Dopamine (DA) can produce quinones that form protein and depurinating DNA adducts; the latter are thought to be involved in some neurodegenerative diseases (e.g. Parkinson's disease) [E.L. Cavalieri et al. *Carcinogenesis,* **23**, 1071-1077, 2002]. Methods with high resolving power are needed to detect neurotransmitters (e.g. DA) and DA-derived DNA adducts in human fluids, as their presence is difficult to determine by standard chromatography with UV absorbance detection. We propose using microfluidic devices with an electrochemical (EC) detection system to determine the presence of DA, DA-6-N7Gua adduct, L-tyrosine, dihydroxyphenylalanine (L-DOPA), and catechol (used as an internal standard). A PDMS glass-based, hybrid microfluidic device for free solution electrophoresis with totally integrated electrodes as well as improved and simplified gated injection was fabricated and tested. The best position and optimal width for minimizing background current of the working electrode was experimentally established. Using a single power supply simplified the operation of the microfluidic device and provided control of the plug size (length), leading to increased separation quality. It is shown that excellent separation of the above analytes can be accomplished in a relatively short time; the response is linear in the range between 2 μM – 300 μM, and reproducible, with a limit of detection (LOD) for DA-6-

N7Gua adducts in the sub-femtomole range. Thus, future separation and identification of various neurotransmitters and/or their products in human fluids could be accomplished using microfluidic devices with electrochemical detection.

Abbreviations:

DA, Dopamine; DA-6-N7Gua; Dopamine-6-N7-Guanine; L-DOPAL, dihydroxyphenylalanine; PDMS, polydimethyl siloxane; EC, electrochemical detection

I. Introduction

Microfluidic chips, which first appeared in the early 1990s, are revolutionizing the analytical science landscape [1-9]. Current technologies offer "laboratories on a chip" that have already demonstrated several advantages over standard capillary electrophoresis (CE) systems, including minimal reagent and sample consumption [4,5], higher efficiency [7,8], speed and throughput, portability, integration, and increased parallelism and automation [4,11,12].

Microfluidic chips with an integrated electrochemical (EC) detection system exploit many of the advantages of miniaturization. In addition, they are more easily and more quickly fabricated than chips with integrated optical detection. EC detection also provides a precise method of analytical precision for sensing molecules that are difficult to detect with spectroscopic techniques.

CE combined with EC detection has been found to be a sensitive, selective technique for analyzing a large number of compounds [13,14], proteins, estrogen-derived metabolites [6], thiols [15], and neurotransmitters [16,17]. However, the observed electrophoretic current

is strongly affected by the detection current from CE. The challenge with this combination is decreasing the background in order to improve sensitivity [18].

Current research efforts are focusing on optimizing designs of various microfluidic devices using both chemical and physical techniques for biochemical applications [5,9]. Recent applications include nucleic acid size determination, genotyping, DNA sequencing, peptide and protein analysis, immunoassays, enzyme detection and characterization, neurochemistry, forensics and environmental studies, and clinical diagnostics [19]. Of particular interest to our laboratory are catecholamine neurotransmitters, such as dopamine (DA), which can produce semiquinones and quinones via autoxidation, metal ion oxidation, and peroxidative enzyme or cytochrome P450 oxidation [20,21]. For example, L-tyrosine is converted within nerve cells to dihydroxyphenylalanine (L-DOPA) and then to DA. DA-quinones can form protein adducts and depurinating DNA adducts [22]; the latter are thought to be involved in some neurodegenerative diseases (e.g., Parkinson's disease) [23]. In dopaminergic neurons, aggregation may be also promoted by DA-derived metabolites and perhaps by the formation of highly reactive DA-quinones [23]. In fact, Parkinson's disease is a progressive neurodegenerative illness that is associated with a profound loss of dopaminergic neurons in the nigrostrial pathway of the brain. Since catecholamines, DA, and DA-derived DNA adducts are weakly fluorescent at room temperature, native fluorescence detection methods are ineffective with this class of biomarkers [25]. Absorbance detection provides detection limits in the high micromolar range [24].and methodologies However, recent analysis of compounds with moderate redox potential properties (e.g., thiols and estrogens) revealed that high-performance liquid chromatography (HPLC) with electrochemical detection provides higher sensitivity [26].

Different electrochemical-based systems and methodologies have been developed to separate and detect neurotransmitters, where the electrochemical activity of these analytes has made them standard models for testing and evaluation of microchip-based electrophoresis separations [27,28]. We report the application of a microfluidic device combined with EC detection for separating and identifying dopamine-derived DNA adducts and various catecholamines. Since several catecholamines (e.g., epinephrine, norepinephrine, L-tyrosine, dopamine, and L-DOPA) are neurotransmitters, the ability to detect catecholamines may be very useful in diagnosing certain neurological diseases. To this point, it has been difficult to accurately detect and separate L-tyrosine, DA, L-DOPA, and DA-derived DNA adducts. This manuscript focuses on methods to further improve microfluidic devices for the sensitive, selective detection of DA and DA-derived DNA adducts. We have succeeded by using a microfluidic device with a totally integrated electrode system. Detection limits and possible improvements are discussed relative to the eventual use of these devices to analyze various neurotransmitters and their products.

II. Materials and Methods

2.1. Chemicals, reagents, and CEQ-DNA adduct standards. All chemicals were used as received. Dopamine and catechol were purchased from Acros; L-tyrosine, L-DOPA, and fluorescein were obtained from Sigma-Aldrich. Sodium hydroxide and boric acid were supplied by Fisher Scientific. The electrolyte solution used for the separations was a 10 mM borate buffer prepared with purified water (18 MΩ-cm, Millipore) and adjusted to pH 9.2 by sodium hydroxide. Stock solutions of analytes were prepared daily and diluted to the desired concentrations in this buffer.

The synthesis of the DA-derived adduct (4DA-6-N7Gua)(see Fig. 3) has been previously described.[23] Structural conformation of the adduct was obtained via UV, NMR, and mass spectrometry with the purity verified by both HPLC and CE. In order to minimize any heat-induced degradation, the adducts were stored at -80°C under an inert atmosphere (N_2 or Ar).

2.2. Fabrication of the microfluidic device. Wet etching and standard soft photolithography procedures were used to fabricate the microdevice, which consisted of a glass plate and a polydimethyl siloxane (PDMS) layer. All of the electrodes were formed on the glass plate, with the injection and separation channels molded in the PDMS layer [29].

a) Substrates and electrodes. Pre-cleaned soda lime glass slides (75 x 50 x 1 mm, Fisher Scientific), were used as electrode substrates and the lower portion of the microfluidic network of channels and solution reservoirs. The slides were treated under a 350 mTorr stream of air in a RF-plasma cleaner (YES-R1, Yield Engineering Systems) for 5 min; 1 nm of titanium and 200 nm of gold were then deposited onto the glass surface by resistive evaporation at 8 x 10^{-8} Torr. After back filling with high purity nitrogen, the coated substrates were removed from the evaporation chamber.

b) Photoresist coating and photopatterning. Following metal deposition, the substrate was coated with photoresist (AZ-5214, Microchem) using a spin coater (KW-4A, Chema Tech.) operating at 4,000 rpm for 40 s, and then baked at 95°C for 15 min. Using a photomask that was fabricated in-house, the substrate was then exposed to UV light (500 W at 365 nm; ABM Inc.) for 15 s. Finally, it was immersed in resist developer (Microchem) for 1 min, rinsed with water, dried in a stream of high purity nitrogen, and baked at 120°C for 20 min.

c) Gold etching process. The resist-patterned substrate was immersed in KI etchant, which consisted of 4 g of potassium iodine (J. T. Baker Chemical), 1 g of iodine (J. T. Baker Chemical), and 40 ml of water. This step removed gold from the areas exposed by the removal of photoresist. The substrate was then rinsed with acetone, methyl alcohol, and water, and dried with high purity nitrogen. The patterned gold strips were used as the electrodes for driving electrophoretic flow and for electrochemical detection; the details of the design (Fig. 1) are discussed below.

d) PDMS microchannel fabrication. The microchannel was fabricated in PDMS (Sylgard 184, Dow Corning) by micromolding. The mold consisted of a photoresist (SU-8025, Microchem) patterned on a 5-in silicon wafer (University Wafer). The wafer was coated with photoresist (SU-8025) using a spin coater operating at 2500 rpm for 30 s, and baked at 95°C for 7 min. The substrate was then photopatterned with UV light for 16 s (365 nm; 500 W). It was again baked for 2 min at 65°C and 7 min at 95°C before immersion into the developer (Microchem) for 7 min. Finally, the developed substrate was quickly rinsed with isopropyl alcohol (Fisher) and dried with high purity nitrogen.

The mold was filled with PDMS and baked at 65°C for 1 h. The PDMS slab was removed from the mold and four wells, each with a diameter of 3 mm, were formed in it with a sharp hand-punch (one reservoir each for the sample and buffer plus two for waste). Characterizations with a profilometer (Dektak IIA) indicated that the channel widths and heights were ~30 and ~90 μm, respectively.

e) Chip integration. To seal the two pieces together, both the PDMS slab and gold-patterned glass substrate were subjected to RF-plasma treatment under a 1-Torr stream of oxygen for 1 min. The PDMS slab was then bonded to the glass plate by bringing the two

components into conformal contact immediately after plasma treatment. All the above procedures were performed in a class 10/100 clean room.

f) Instrumentation and EC detection procedure. As shown in Fig. 1, the electrode plate has multiple gold electrodes: three for EC detection (reference [200 μm width], auxiliary [200 μm width]), and an array of working electrodes. The width and spacing of the working electrodes are 35μm respectively. The remaining four electrodes are for electrokinetic injection and for controlling electrophoretic flow. The optimal width and position of the working electrode in reference to the exit of the separation channel was experimentally established (see section III). In each case, the auxiliary electrode was designed with a surface area 5-6 times larger than that of the working electrode. The reference, auxiliary, and working electrodes were connected to a potentiostat (EG&G Princeton Applied Research model 273) with the potential of the gold pseudo-reference electrode determined by comparing it to a Ag/AgCl/saturated KCl electrode and periodically examining it for stability.

g) Electrophoresis. As soon as the bonding process was completed, the channels were filled with the running buffer and used without further pretreatment. First, the running buffer was loaded into the buffer waste reservoir, where it was delivered to all channels via capillary action. As detailed shortly, a gated injection procedure was used to introduce a sample plug into the separation channel. A 1.0-s injection time was used in all cases. Both the sample and the running buffer were replaced after each run. All separations were carried out using a Bertan Associates (model 205B-01R) power supply, with the electrophoretic current measured with an auto ranging picoammeter (Keithley, model 485).

h) Imaging apparatus. The apparatus for fluorescence-based imaging consisted of a Xenon UV lamp (50 W), suitable filters, and a CCD camera (Dalsa, Canada, model CA-D7), which was interfaced with a Leica microscope (DMLB model). The CCD camera was run by frame grabber software (Bit Flow) installed on a personal computer.

III. Results and Discussion

3.1. Design and optimization of CE microchip device. Figure 1 illustrates the locations of the microfluidic channels, the positions of the reservoirs, and the arrangement of all of the electrodes. The separation channels are between 3 and 6 cm in length, with electroosmotic flow employed for all fluid manipulation steps.

To decrease the coupling between the electrophoretic current and that for the faradaic reaction at the working electrode, both the location and width of the working electrode were optimized; an array design was used to locate the optimal positions. This iterative process involved fabricating and testing several microchips that consisted of working electrodes of varied widths deposited at different locations relative to the end of the separation channel. Positional control enabled assessment of the effectiveness of in-channel and end-channel detection schemes with respect to electrical isolation of the working electrode from the current flow in the electrophoretic separation. We found that the coupling of the electrophoretic current to the working electrode eliminated the necessity of in-channel detection formats.

In contrast, end-channel detection yielded a lower background current at the working electrode, which was located closer to the end of the channel [6]. This optimization implies that the electrophoretic potential distribution in the separation channel has a linear

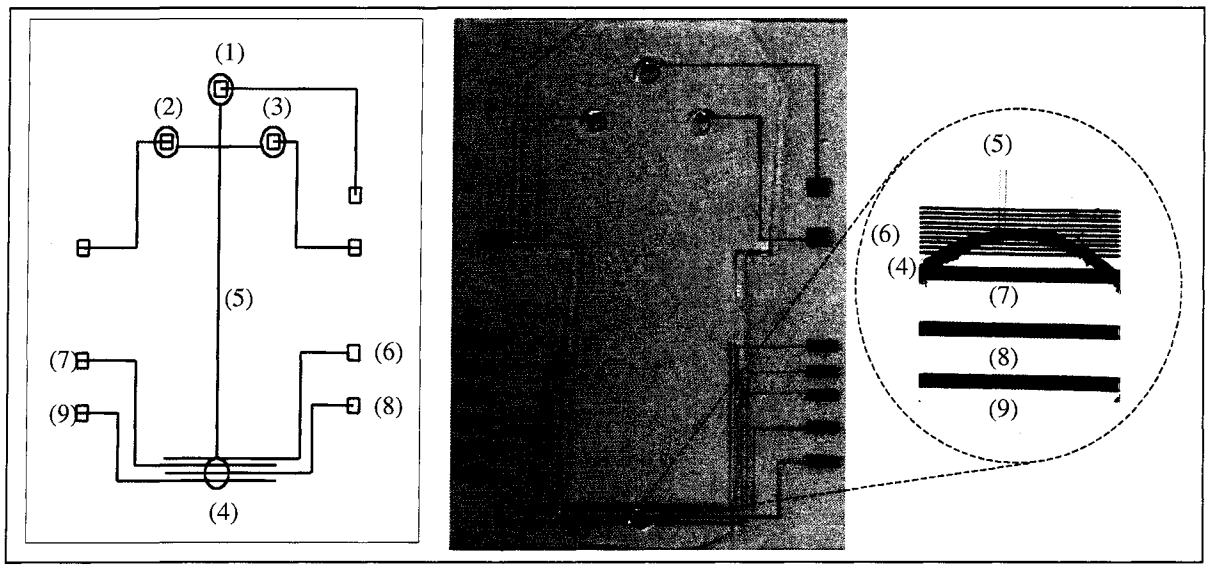

Figure 1. Left frame: Schematic representation of the CE microchip with a fully integrated electrochemical detection system: (1) sample reservoir and high voltage electrophoretic electrode; (2) buffer reservoir and buffer reservoir electrode; (3) sample waste reservoir and sample waste reservoir electrode; (4) running buffer waste reservoir; (5) separation channel; (6) working electrode; (7) reference electrode; (8) auxiliary electrode; and (9) electrophoretic ground electrode. Right frame: An image of an actual microfluidic device. The inset shows an expanded view of the electrochemical detection system (see text for details).

gradient between the electrode in sample/buffer reservoirs and waste reservoir, where the coupling is at its maximum level inside the channel. The potential drop at the end of the separation channel significantly decreases the coupling, and thus the background current. However, the observed elution band for dopamine had a long tail, which was attributed to the diffusion of the analyte in the reservoir.

Tests also showed that a lower background current extends the lifetime of the integrated microchip. However, the relative position of the working electrode (electrode 6 in Fig. 1) with respect to the channel-end is also important because it defines the strength of the coupling current. In other words, the coupling increases as the distance between the working electrode and the channel-end decreases. If the gap is too large, however, diffusional broadening of an elution band and decreasing signal intensity can occur. Based on experiments with designs in which the gap was systematically altered, we found that the best position for the working electrode was ~15 μm from the exit of a 90-μm wide separation channel. As noted earlier, the width of the working electrode is another important design parameter. An electrode that is too wide (e.g., ~60-100 μm) may increase the coupling between the two currents and subsequently increase the background current. Again, tests with several different designs revealed that the optimal width of the working electrode is ~35 μm. Finally, we tested various separation channel lengths since this parameter also affects the resolution of the separation process (results not shown). We concluded that field strengths up to 140 V/cm over a 5-cm separation channel could be safely applied to our microchips without any decrease in performance. The best resolution, however, was obtained with a channel length of 5-cm, as reported in a subsequent section.

3.2. Injection system: gated mode injection was used to introduce the sample plug into the separation channel. In this mode, one power supply is typically used to control the potential applied at the sample reservoir and a second power supply is employed to set the potential at the buffer reservoir [6]. Figure 2 shows an alternate approach that uses only one power supply. The electrical layout of the system in each of its operational steps is presented in the left column of Fig. 2, and experimental fluorescence images for the injection of a fluoresceine-containing solution are given in the right column. As detailed earlier, the figures in the top, middle, and bottom of each column correspond to the pre-injection, injection, and sample migration operational steps, respectively.

In addition to simplifying the instrumentation, the design shown in Fig. 2 reduces the Joule heating effect that can arise from electrophoretic sample injection. When the separation channel is notably longer than the injection channel, the current, and therefore the heat generated in the injection channel, can lead to delaminated electrode, gas evolution, and other problems. To reduce this problem, a resistor, R_1, was connected between the waste reservoir and ground. The resistor was used to ensure the compatibility of the electric fields along the separation and injection channels, thus minimizing the Joule heating effect. To keep a high current from passing through the injection channel, the waste reservoir was connected to ground with the series resistor R_1 (20 MΩ). Without the resistor, Joule heating often deforms the channels and leads to delaminated electrode bubble formation in the channel, blocking fluid flow. Blocked fluid flow resulted in cleavage of the bond between the PDMS and glass substrate. A detection reservoir that contains working, reference, and auxiliary electrodes connected to a potentiostat (not shown in Fig. 2) is held at ground potential.

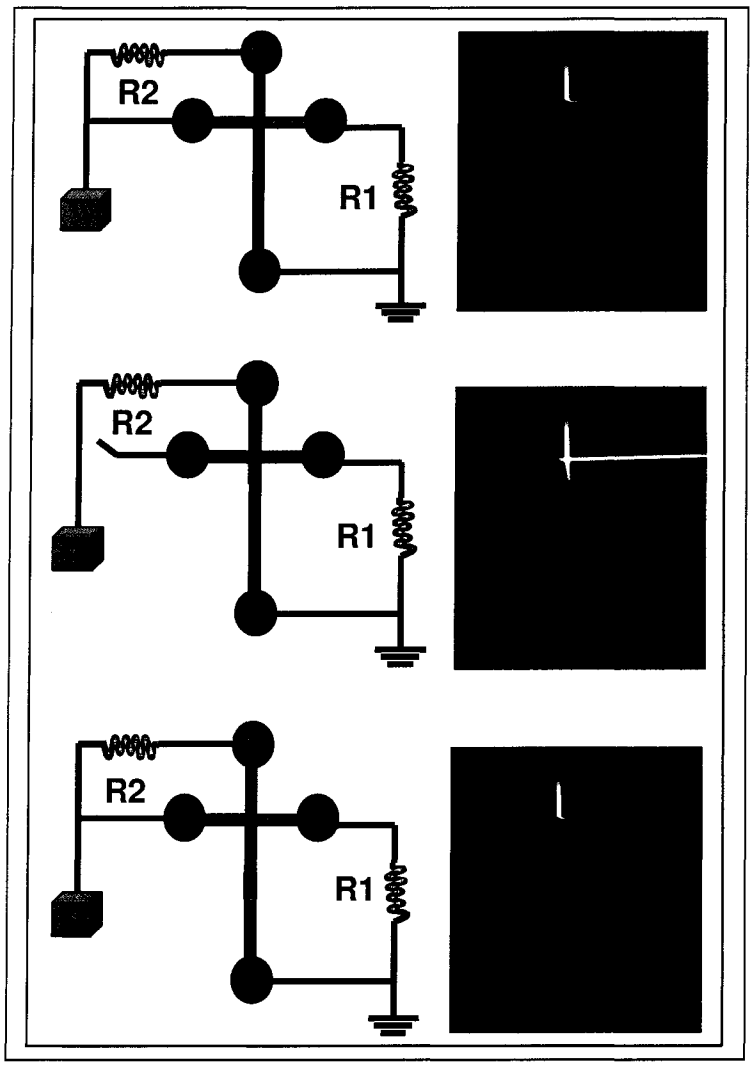

Figure 2. Illustration of the gated injection process using fluoresceine (100 μM fluoresceine in borate buffer) as the analyte. Operational schematics are shown in the left column and experimental data in the right column. The length of the sample plug is ~3 mm; injection time was 1 s.

Voltage has to be controlled over each reservoir with the configuration depicted on the left side of Fig. 2. First, the sample is introduced (pre-injection mode) by applying voltage to the sample (#1) and buffer (#2) reservoirs. Due to the presence of the variable resistor, R_2, (adjusted to 2.4 MΩ), the voltage to the sample reservoir is ~80% of that applied to the buffer reservoir. As a result, the sample flows only from sample to waste reservoirs, as visualized in the top panel on the right side of Fig. 2. The horizontal line (in the top right panel) is thinner than the vertical one due to the flow of buffer towards the sample waste (#3) and detection (#4) reservoirs. The middle panel shows the injection of a plug into the separation channel. To apply a high voltage to the buffer, reservoir #2 is floated for 1 s. This is easily accomplished by introducing an additional electric switch to the microchip design. With the switch, S, open, the sample plug (of several pL) moves into separation channel. This can be repeated many times; an example of plug injection is shown in the bottom right panel of Fig. 2. After the plug is injected, the switch, S, is closed, and the separation process begins.

3.3. Electrochemical detection. Catecholamines have a benzohydroquinone group or a phenol group within their structures, as shown in Fig. 3. The redox of quinone/ hydroquinone has been investigated [30]. In lower pH than its pK_a 9.85 [31], the redox reaction of quinone/hydroquinone is a 2-electron, 2-proton reaction process.

It has been shown that he coupling between electrophoretic and detection currents in microfluidic devices can change the apparent half-wave potential ($E_{1/2}$) of a redox couple [32]. Thus we considered the need for an investigation of the applied potential optimal for detecting eluents. Frames A and C of Fig. 4 show the hydrodynamic voltamograms for DA and DA-6-N7Gua, respectively. The blank solution was featureless, with the background;

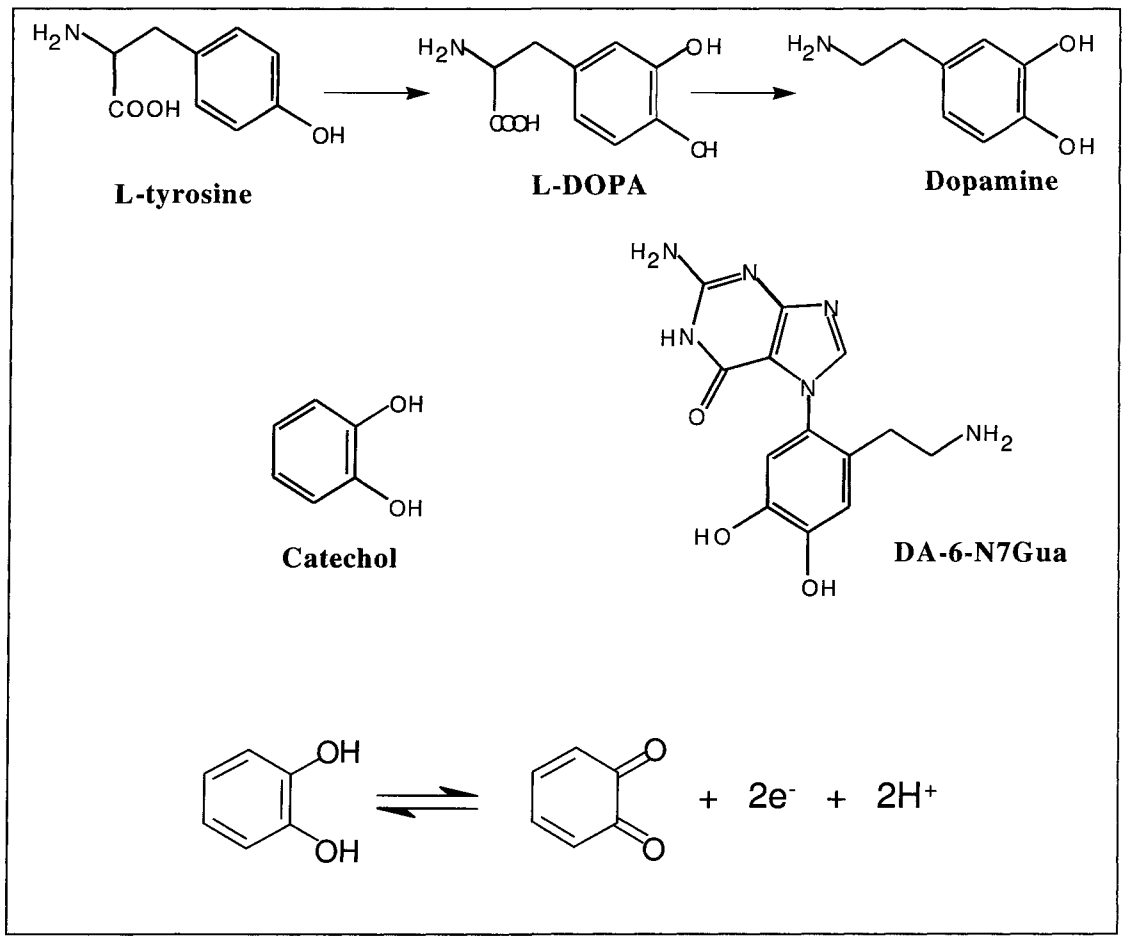

Figure 3. The chemical structures of L-tyrosine, dihydroxyphenylalanine (L-DOPA), dopamine (DA), catechol, and DA-derived DNA adduct (DA-6-N7Gua), and redox reaction of quinone/hydroquinone.

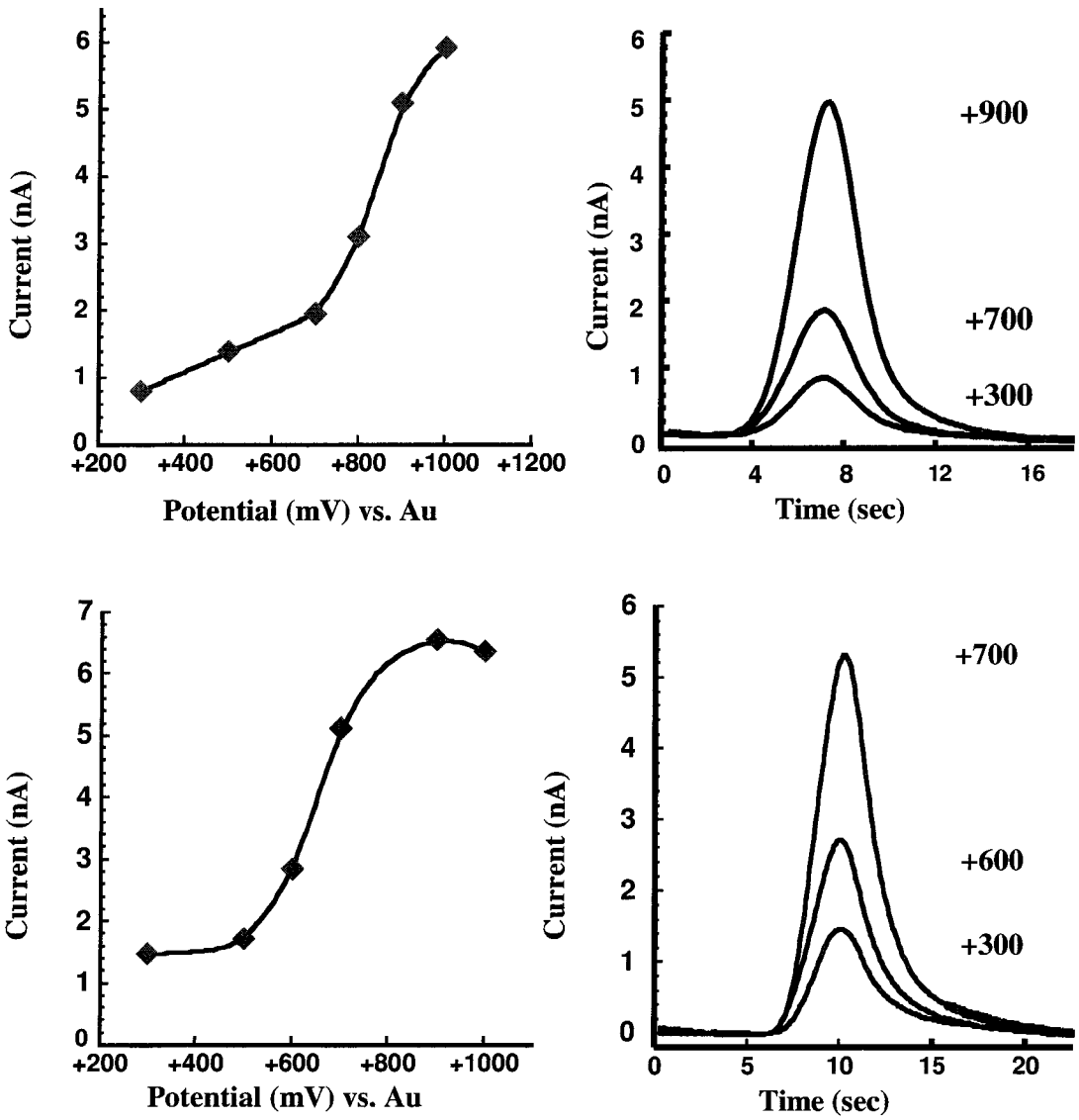

Figure 4. Hydrodynamic voltamogram (A) and electropherograms (B) of DA-6-N7Gua adduct (5×10^{-4} M), respectively. (C) and (D) are hydrodynamic voltamogram and electropherograms of DA (3.8×10^{-4} M), respectively. Separation conditions: 10 mM boric buffer (pH 9.2); separation field 200 V/cm; and injection time 1 s. Electropherograms of both standards were obtained at 3 different representative redox potentials.

current dependent on both the potential applied to the working electrode and the separation voltage; i.e., 800 V to 1500 V yielded ~1 nA of background current. It was possible to achieve a stable background current, as low as 800 pA with 140 V/cm separation field at low applied potential to the working electrode. The data points in Fig. 4 represent the peak current after subtracting the background current. The background current began increasing significantly at an applied potential of more than +1,000 mV, which arises from the formation of gold oxide [33]. As expected, both voltamograms show a redox potential shift to a higher value, approximately +500 mV, compared to cyclic voltamograms obtained for the same two analytes in a standard three-electrode electrochemical cell (data not shown). These data demonstrate that the redox potentials for DA-6-N7Gua and DA are about +1,000 mV and +900 mV, respectively. Thus, a potential of +1.0 V will be used to separate these compounds (*vide infra*); voltages higher than +1.0 V will only increase background current and cause instability in the system.

3.4. Injection and detection reproducibility. Figure 5 depicts seven repetitive injections, each at 1 s, of the DA-derived DNA adduct. The samples were introduced one after another (i.e., the system was not rinsed between injections). The reproducibility of the injection process is readily apparent. The elution bands varied in height by 0.6 nA, ranging from 8.0 nA (minimum) to 8.6 nA (maximum). A statistical analysis yields an average height of 8.3 ± 0.3 nA, a deviation of 3.5 %.

3.5. Separation of catecholamines and DA-6-N7Gua adduct and detection limits. Separations using different buffers and/or pH were performed with the goal of improving both the LOD (note: *this was abbreviated in the Abstract)* and sample resolution. We found that a running buffer of 10 mM 2-[N-morpholino] ethanesulfonic acid (MES) at pH 5.5

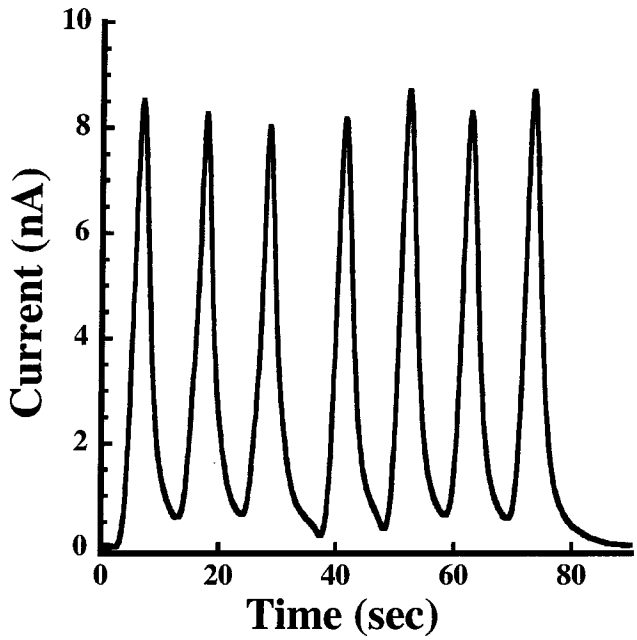

Figure 5. Seven consecutive injections of 1mM DA-6-N7Gua adduct (~10^{-4} M). Separation conditions: 10mM boric buffer (pH 9.2), electric field E = 200 V/cm, electrochemical potential (EC) = +1.0 V vs. Au electrode. A typical sample volume loaded into the reservoir was about 2-10 μL; injection time 1 s.

provided a stable background current. However, only two elution bands were observed; the first was composed of DA and tyrosine and the second of L-DOPA, catechol, and DA-6-N7Gua (data not shown). Other buffers (e.g., Tris-HCl [pH 7.1]) yielded a slightly improved separation but the background current at the working electrode was very large and unstable, preventing successful separation of all analytes. In turn, a borate buffer (pH 8.0) significantly enhanced the resolution of the separation process and provided a low, stable background current of ~10 nA. However, the best conditions, in terms of the stability and magnitude of the background current as well as resolution of the mixture, were obtained with 10 mM borate buffer (pH 9.2) using an electric field strength of 140 V/cm and potential of +1.0 V applied to the working electrode. Generally, the electrophoretic mobility depends on both, the molecule's ionic charge(q) and the radius(r) at constant viscosity(η), which is given by the following equation $\mu_e=q/6\pi\eta r$. Higher negatively charged molecules will migrate slower toward the cathode than other molecules. The separation process is dramatically affected by the pH of the running buffer, where under basic conditions the analytes become charged depending on their pKs values. Under our tested conditions we observed that the separation resolution was significantly enhanced upon changing the running buffer acidity into a basic regime (both borate and phosphate buffers). We believe that this enhancement is due to ionization of the analytes, in addition to different sizes of the tested analytes, DA and DA-derived DNA adduct. Furthermore, the resolution power of borate buffer can be attributed to some kind of complexation between the borate group and the analytes. The stability of the tested analytes during the operation conditions is also mentioned here, where under basic conditions some of the analytes decompose due to an undetermined oxidation process. We also noticed changes in the color of the prepared DA solution after long periods

of observation (> 1 hour), which necessitated the preparation of fresh solutions just before starting the separation process.

Figure 6 shows an electropherogram for the CE separation of the five-analyte mixture after the aforementioned optimization. The well-resolved peaks (1-5) in Fig. 6 correspond to dopamine, L-tyrosine, dopamine-derived DNA adduct, L-DOPA, and catechol, respectively. Higher concentrations of the borate buffer increased the background current without improving separation. The resolution obtained for DA (1) and catechol (5), compounds that are often used to test microfluidic devices with EC detection, is significantly better than previously reported [34-37]. Specifically, DA and catechol were barely baseline resolved [34], with a resolution ($R = 2\ (t_{rB} - t_{rA})/\ (W_A + W_B)$) of 1.5, 3.2 and 1.9 for references 25, 26, 31, respectively. (W is the baseline peak width and t_{rB} and t_{rA} are the migration times). Our results clearly show that the resolution for DA and catechol is around 7, which is significantly better than results from previous efforts [29]. The higher resolution was achieved by reduction of the current noise level (see above). It is also noted that the LOD for DA and the DA-derived DNA adduct were determined by separate analyte injections, where the LOD corresponds to the lowest concentration detected that gave a signal to noise ratio 3. Thus, the others analytes were used as separation models and standards; no attempts were made to separate these analytes near the detection limit concentration.

The number of theoretical plates at? $N = 5.54\ (t_R/W_{1/2})^2$, where t_R is the retention time and $W_{1/2}$ is the full width of the peak at its half maximum (FWHM), based on the electropherogram shown in Fig. 6, is about 5,000. This number, however, significantly increases for lower concentration of analytes, as this decreases peak tailing and FWHM. In

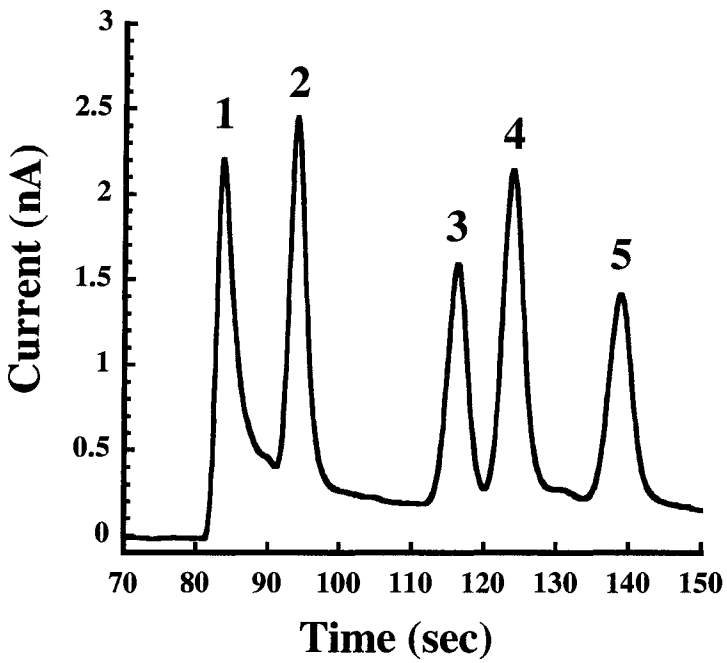

Figure 6. Electropherogram of a mixture of 200μM dopamine (1), L-tyrosine (2), DA-6-N7Gua adduct (3), L-DOPA (4), and catechol (5). Separation conditions: 10mM boric buffer, pH 9.2, electric field 140 V/cm, EC potential +1.0V vs. Au.

fact, the performance of any microfluidic device has to be evaluated in terms of both efficiency (i.e. the number of theoretical plates) and resolution, as the former may be very high but resolution may be very poor. For example, while separating various DNA fragments using fluorescence-based detection, Webster et al obtained a high number of theoretical plates (~30,000) with $R < 1$ [37].

The analytical performance of the microchip was tested over a large concentration range (from ~1 μM to 1 mM) of DA and DA-derived DNA. Calibration curves obtained from the peak areas (averaged over three injections) are shown in Fig.7. Frames A and B reveal a linear response for dopamine in the range of 2 μM (LOD) up to 350 μM (R^2=0.996), and for DA-derived DNA in the range of 5 μM (LOD) up to 250 μM (R^2=0.999). Thus, LOD is in the low micromolar range. Similar detection limits were obtained for phenols, which are often studied as model analytes as they are electroactive at moderate redox potentials. Detection limits obtained for the analytes of interest are still relatively high compared to alternative methodologies (e.g. HPLC with EC detection) where the LOD ranges from high nanomolar to low micromoler [24]. However, with a three-dimensional electrode system (research in progress), labeling of analytes with highly electrochemically active molecules to increase sensitivity of EC detection and various pre-concentration methods, a detection limit in the high nanomolar range (suitable for many *in vivo* studies) is anticipated.

IV. Conclusions

We have developed a PDMS glass-based hybrid microfluidic device with an EC detection system. Since the design of the CE and EC detection system was optimized at the

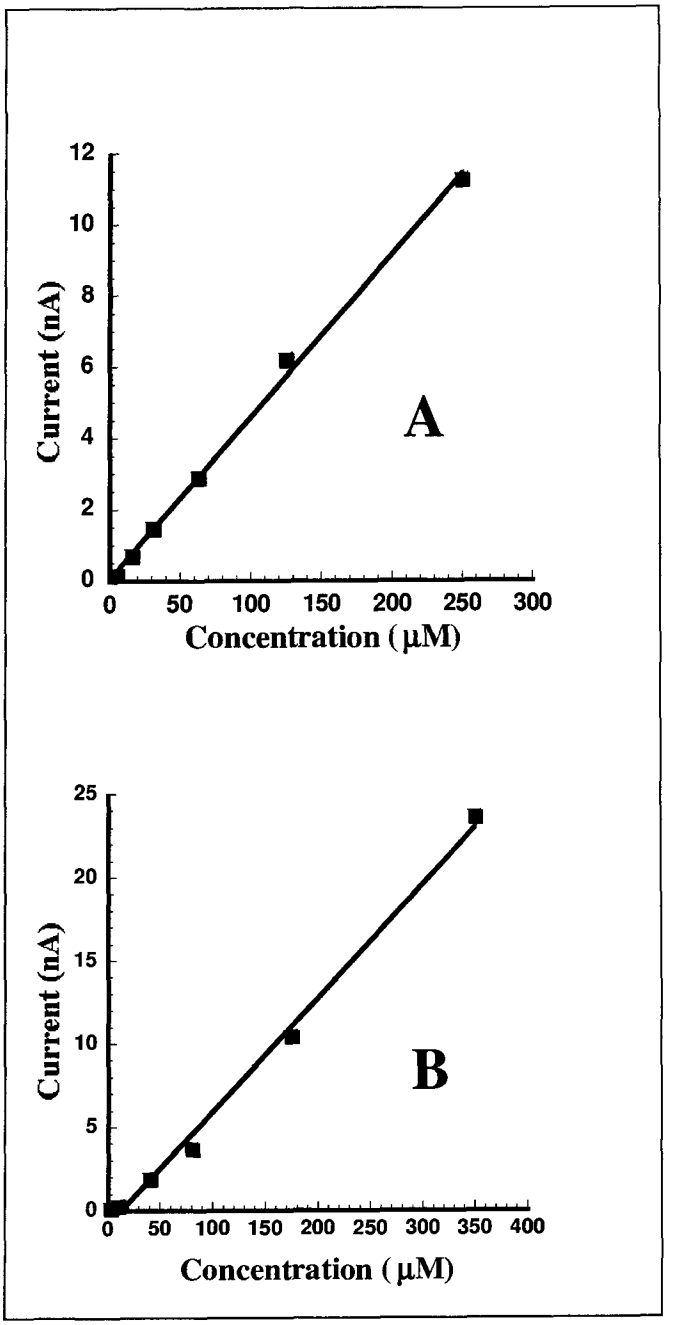

Figure 7. Calibration curves for DA-6-N7Gua adduct (A) and DA (B) showing the current (in nA) plotted vs concentration (in μM).

micro-meter level, the background current was significantly reduced, to ~1 nA. Minimized background current allowed us to use the small current range with the potentiostat. This step forward led not only to high resolution and high sensitivity, but also greater stability and an extended microchip lifetime. Better control of the plug length along with improved and simplified gated injection enhanced the accuracy and reproducibility of the separation process, providing greater separation quality. Using this system, we demonstrated the separation of catecholamines, which included dopamine, L-tyrosine, dopamine-derived DNA adduct, L-DOPA; catechol was used as an internal standard. The LOD for DA-6-N7Gua adducts is in the femtomolar range, with a concentration LOD in the low micromolar range. Current research focuses on further improvement of the LOD by employing carbon-based electrodes, where carbon fibers and/or modified carbon porous materials are placed at the end of the separation channel, creating a three-dimensional electrode detection system. It is anticipated that microfluidic devices with a carbon-based electrode detection system will further enhance detection limits providing simple devices for future detection of DA-derived biomarkers.

Acknowledgements.

This work was supported by a grant from the National Cancer Institute (Program Project Grant 2PO1 CA49210-12) and by the Microanalytical Instrumentation Center of Iowa State University through the W. M. Keck Laboratory for the Fabrication of Microminiaturized Analytical Instrumentation. We thank Prof. E.L. Cavalieri for providing DA-derived DNA adducts. Ames Laboratory is operated for the U.S. Department of Energy by Iowa State University under Contract No. W-7405-Eng-82.

References

1. A. Manz , N. Grabner, H.M. Widmer, Miniaturized total chemical analysis systems: A novel concept for chemical sensing, Sens. Actuators B. 1 (1990) 244-248.

2. A. Manz, D.J. Harrison, J.C. Rettinger, E. Verpoorte, H. Ludi, H.M. Widmer, Transducers 91, Digest of Technical Papers, IEEE 91 CH2817; IEEE: New York (1990) 939-941.

3. D.J. Harrison, A. Manz, P.J. Glavina, Transducers 91, Digest of Technical Papers, IEEE 91-CH2817-5; IEEE: New York (1990) pp 792-795.

4. G.J. Bruin, Recent developments in electrokinetically driven analysis on microfabricated devices Electrophoresis 21 (2000) 3931-3951.

5. A. Mello, On-chipchromatography: the last twenty years Lab. on a Chip 2 (2002) 48N-54N.

6. N.A. Lacher, K.E. Garrison, R.S. Martin, S.M. Lunte, Microchip capillary electrophoresis/ electrochemistry, Electrophoresis 22 (2001) 2526-2536.

7. D.J. Harrison, A. Manz, Z. Fan, H. Lüdi, H.M. Widmer, Capillary electrophoresis and sample injection systems integrated on a planar glass chip, Anal. Chem. 64 (1992) 1926-1932.

8. A.T. Woolley, R.A. Mathies, Ultra-High-Speed DNA Sequencing Using Capillary Electrophoresis Chips, Anal. Chem. 67 (1995) 3676-3680.

9. M.A. Burns, B.N. Johnson, S.N. Brahmasandra, K. Handique, D.T. Burke, An Integrated Nanoliter DNA Analysis Device, Science 282 (1998) 484-487.

10. R. Wilke, S. Büttgenbach, micromachined capillary electrophoresis chip with fully integrated electrodes for separation and electrochemical detection Biosensors and Bioelectronics 1 (2003) 149-153.

11. V. Dolník, S. Liu, S.J. Vladisl, Capillary electrophoresis on microchip, Electrophoresis 21 (2000) 41- 54.

12. M.P. Hughes, Strategies for dielectrophoretic separation in laboratory-on-a-chip systems, Electrophoresis 23 (2002) 2569-2582.

13. S.A. Pasas, N.A. Lacher, M.I. Davies, S.M. Lunte, Detection of homocysteine by conventional and microchip capillary electrophoresis/ electrochemistry, Electrophoresis 23 (2002) 759-766.

14. R.P. Baldwin, Recent advances in electrochemical detection in capillary electrophoresis , Electrophoresis 21 (2000) 4017-4028.

15. A. Wang, L. Zhang, S. Zhang, Y. Fang, Determination of thiols following their separation by CZE with amperometric detection at a carbon electrode, Journal of Pharmaceutical and Biomedical Analysis 23 (2000) 429-436.

16. A.T. Woolley, K. Lao, A.N. Glazer, R.A. Mathies, Capillary Electrophoresis Chips with Integrated Electrochemical Detection, Anal. Chem. 70 (1998) 684-688.

17. J. Bergquist, E. Josefsson, A. Tarkowski, R. Ekman, A. Ewing, Measurements of catecholamine-mediated apoptosis of immunocompetent cells by capillary electrophoresis, Electrophoresis 18 (1997) 1760-1766.

18. O. Klett, F. Bjoerefors, L. Nyholm, Elimination of High-Voltage Field Effects in End Column Electrochemical Detection in Capillary Electrophoresis by Use of On-Chip Microband Electrodes, Anal. Chem. 73 (2001) 1909-1915.

19. E. Verpoorte, Microfluidic chips for clinical and forensic analysis, Electrophoresis 23 (2002) 677-712.

20. B. Kalyanaraman, C.C. Felix, R.C. Sealy, Peroxidatic oxidation of catecholamines: a kinetic electron spin resonance investigation using the spin stabilization approach, Journal of Biological Chemistry 259 (1984) 7584–7589.

21. B. Kalyanaraman, C.C. Felix, R.C. Sealy, Semiquinone anion radicals of catechol(amine)s, catechol estrogens, and their metal ion complexes, Environ. Health Perspect. 64 (1985) 185–194.

22. K.A. Conway, J.C. Rochet, R.M. Bieganski, P.T. Lansbury, Kinetic Stabilization of the α-Synuclein Protofibril by a Dopamine-α-Synuclein Adduct, Science 294 (2001) 1346-1349.

23. E.L. Cavalieri, K-M. Li, N. Balu, M. Saeed, P. Devanesan, S. Higginbotham, J. Zhao, M.L. Gross, E.J. Rogan, Catechol ortho-quinones: the electrophilic compounds that form depurinating DNA adducts and could initiate cancer and other diseases, Carcinogenesis 23 (2002) 1071-1077.

24. J.T. Greenamyre, T.G. Hastings, Parkinson's--Divergent Causes, Science 304 (2004) 1120-1122.

25. Y. Markushin, W. Zhong, E.L. Cavalieri, E.G. Rogan, G.J. Small, E.S. Yeung, R. Jankowiak, Spectral Characterization of Catechol Estrogen Quinone (CEQ)-Derived DNA Adducts and Their. Identification in Human Breast Tissue Extract, Chemical Research in Toxicology 16 (2003) 1107-1117.

26. R. Todorovic, P. Devanesan, S. Higginbotham, J. Zhao, M.L. Gross, E.G. Rogan, E.L. Cavalieri, Analysis of potential biomarkers of estrogen-initiated cancer in the urine of Syrian golden hamsters treated with 4-hydroxyestradiol, Carcinogenesis 22 (2001) 905-911.

27. M. Schwarz, P.C. Hauser, Chiral On-Chip Separations of Neurotransmitters. Anal. Chem. 75 (2003), 4691-4695.

28. S. Wei, G. Song, J-M Lin, Separation and determination of norepinephrine, epinephrine and isoprinaline enantiomers by capillary electrophoresis in pharmaceutical formulation and human serum. J. Chromatography A 1098 (2005) 166-171

29. D.C. Duffy, J.C. McDonald, O.J. Sehueller, G.M. Whitesides, Rapid Prototyping of Microfluidic Systems in Poly(dimethylsiloxane), Anal. Chem. 70 (1998) 4974-4984.

30. Chambers, J.Q., Electrochemistry of Quinones, The Chemistry of the Quinonoid Compounds, Wiley, New York, 1974.

31. Y. Sato, M. Fujita, F. Mizutani, K. Uosaki, Electrochemical properties of the 2-mercaptohydroquinone monolayer on a gold electrode. Effect of solution pH, adsorption time and concentration of the modifying solution, J. Electroanal. Chem. 409 (1996) 145-154.

32. Klett, F. Bjoerefors, L. Nyholm, Elimination of High-Voltage Field Effects in End Column Electrochemical Detection in Capillary Electrophoresis by Use of On-Chip Microband Electrodes. Anal. Chem. 73 (2001) 1909-1915.

33. M.H. Holzle, U. Retter, D.M. .Kolb, The kinetics of structural changes in Cu adlayers on Au(111), J. Electroanal. Chem. 371 (1994) 101-109.

34. R.S. Keynton, T.J. Roussel, M.M. Crain, D.J. Jackson, D.B. Franco, J.F. Naber, K.M. Walsh, R.P. Baldwin, Design and development of microfabricated capillary electrophoresis devices with electrochemical detection, Analytica Chimica Acta 507 (2004) 95-105.

35. Y. Liu, J.A. Vickers, C.S. Henry, Simple and Sensitive Electrode Design for Microchip Electrophoresis/Electrochemistry, Anal. Chem. 76 (2004) 1513-1517.

36. C.C. Lai, C. Chen, F-H. Ko, In-channel dual-electrode amperometric detection in electrophoretic chips with a palladium film decoupler Journal of Chromatography A1023 (2004) 143-150.

37. J.R. Webster, M.A. Burns, D.T. Burke, C.H. Mastrangelo, Monolithic Capillary Electrophoresis Device with Integrated Fluorescence Detector, Anal. Chem. 73 (2001) 1622-1626.

CHAPTER 5: INTEGRATED MICROFLUIDIC DEVICE WITH AN ELECTROPLATED PALLADIUM DECOUPLER FOR ELECTROCHEMICAL DETECTION OF THE 8-HYDROXY-DEOXYGUANOSINE (8-OH-DG) DNA ADDUCT

A paper submitted for publication in *Lab on a Chip*

Abdulilah A. Dawoud, Toshikazo Kawaguchi, and Ryszard Jankowiak

Abstract

8-hydroxy-deoxyguanosine DNA adduct (8-OH-dG) is one of the most frequently used biomarkers reporting on the oxidative stress that leads to DNA damage. More sensitive and reliable microfluidic devices are needed for the detection of these biomarkers of interest. We have developed a capillary electrophoresis-based microfluidic device with an electroplated palladium decoupler that provides significantly improved detection limit, separation efficiency, and resolving power. The PDMS/glass hybrid device has fully integrated gold microelectrodes covered *in situ* with palladium nanoparticles using an electroplating technique. The performance and coverage of the electrodes electroplated with palladium particles were evaluated electrochemically and via SEM imaging, respectively. The performance of the device was tested and evaluated with different buffer systems, pH's and electric field strengths. The results showed that this device has significantly improved resolving power, even at separation electric field strengths as high as 600 V/cm. The detection limit for the 8-OH-dG adduct is about 20 attomoles; the concentration limit is on the order of 100 nM (S/N =3). A linear response is reported for both 8-OH-dG and dG in the range from 100 nM to 150 μM (~100 pA/μM) with separation efficiencies of ~120,000 – 170,000 plates/m.

***Abbreviations*:** dG, deoxyguanosine; 8-OH-dG, 8-hydroxy-deoxyguanosine; ED, electrochemical detection; CE, capillary electrophoresis; WE, working electrode; EG, electrophoretic ground; PDMS, poly(dimethylsiloxane); LOD, limit of detection.

1. Introduction

Exposure to chemicals has been linked to the oxidative damage to DNA that can cause physiological changes associated with degenerative diseases such as cancer and other age-related diseases [1,2]. The DNA damage results in the formation of urinary adducts that can be used as biomarkers for medical diagnostics [3]. Among the four DNA bases, guanine posses the lowest oxidation potential, that leads mainly to the formation of 8-OH-dG [4]. The analytical methods most often used for the detection of 8-OH-dG DNA adduct include: gas chromatography - mass spectrometry (GC-MS) [5], ELISA [6], and high performance liquid chromatography (HPLC) with electrochemical detection (ED) [7,8]. In particular, this last methodology (i.e. HPLC-ED) is often used since amperometric detection is several times more sensitive than UV-Vis optical detection [9]. However, the complexity of HPLC-ED and high operating cost limit the application of this methodology.

Recent studies have also shown the applicability of capillary electrophoresis with amperometric detection (CE-AD) for the separation and detection of the urinary 8-OH-dG adduct [10,11]. Two major difficulties with this approach exist: i) problems with aligning of the working electrode (WE) at the end of the separation channel; and ii) the interference and coupling that occur between the electrophoretic and detection currents. Such problems often lead to an unstable background current that leads to lower sensitivity and poor reproducibility. Different decoupling techniques have been applied to solve these problems

with the conventional CE-AD methodology. In the most frequently used remedy, the electrophoretic ground (EG) is placed before the working electrode [12-14].

The introduction of microfluidic chips has revolutionized the landscape of analytical sciences [15-19]; a wide range of analytes has been studied using microfluidic devices with electrochemical detection [20-23]. In our previous work, we developed a fully integrated microfluidic device with ED for the separation and detection of different neurotransmitters and dopamine-derived DNA adducts [24]. The working electrode (WE) was placed ~15 μm from the separation channel outlet in this device. This integrated microfluidic device offered an alternative solution for the aforementioned CE-AD problems, especially in the way that the decoupler is introduced [24].

The introduction of an electrophoretic ground electrode (i.e. cathode) into the separation channel to decouple the separation electric field from the electrochemical detector can be problematic as hydrogen gas bubbles will be generated at the cathode. To overcome this problem, electrode materials capable of absorbing hydrogen gas need to be used. Among all metals that can be used for the fabrication of solid-state metal-based decouplers palladium (Pd) is the most efficient in terms of adsorbing H_2 that can be produced at the EG. Unfortunately, Pd-based decouplers are hard to fabricate and process. In contrast, gold (Au) exhibits weak tendency to adsorb H_2, but it is easier to deposit and process. Electroplating also allows for deposition of additional metal on an already deposited metal layer. Although some research groups have used palladium as the decoupler for CE-ED on a chip [25-29], problems/difficulties associated with the fabrication procedure including optimization of the distance between the decoupler and the working electrode still exist. The above distance

strongly depends upon the separation electric field strength, limiting the universality of such devices.

In this work, we report the fabrication of a PDMS/glass microfluidic device employing ED with an electroplated Pd decoupler for the separation and detection of 8-OH-dG and dG. The distance between the decoupler and the WE was optimized by utilizing an array of microelectrodes. To the best of our knowledge, this is the first report on the detection of 8-OH-dG adduct on a chip using a microfluidic device with an electroplated Pd decoupler.

2. Experiment

2.1 Chemicals and reagents. All chemicals were used as received. 8-hydroxy-deoxyguanosine (8-OH-dG), deoxyguanosine (dG), 2-[N-morpholino]ethanesulfonic acid (MES), sodium tetrachloroaurate(III) dehydrate ($NaAuCl_4.2H_2O$), potassium hexachloropalladate(IV) (K_2PdCl_6), and potassium hexachloroplatinate(IV) (K_2PtCl_6) were purchased from Sigma-Aldrich. Sodium hydroxide, boric acid, perchloric acid, and sodium phosphate monobasic were supplied by Fisher Scientific. The individual electrolyte solutions for separations were 10 mM each of MES, borate, phosphate buffer prepared with purified water (18 MΩ cm, Millipore) and adjusted with sodium hydroxide to pH 5.5, 7.5, and 9.5 respectively.

2.2 Microchip. Details of the microchip fabrication procedure were published previously [24]. Briefly, PDMS slabs with channels were casted against SU-8025 photoresist-based mold on a 3 inches Si wafer. The electrodes were made of thermally deposited gold (200 nm) with 1 nm of titanium as an adhesion layer. The microdevice was assembled by bonding the

PDMS slab to the glass substrate after RF-plasma treatment under a 1-Torr stream of oxygen for 1 min.

2.3 Electroplating. 10mM aqueous solutions of K_2PdCl_6, $K_2Pt_2Cl_6$, and $NaAuCl_4 \cdot 2H_2O$, were used to electroplate Pd, Pt, and Au respectively. After filling the channels with the solution of the metal to be deposited, a square potential signal between –1800 mV and 0 mV, at a frequency of 2 Hz, was applied from a potentiostat.

2.4 Electrophoresis. 1mM stock solutions of 8-OH-dG and dG in the running buffer were prepared and kept in the refrigerator at 4°C. Fresh solutions were prepared daily by diluting the stock solutions with the running buffer. Prior to the separation, the microchannels were flushed for 5 min with NaOH, 10 min with deionized water, and 10 min with the running buffer. 10 mM of three buffers were used, MES (pH = 5.5), phosphate (pH = 7.5), and borate (pH = 9.5) buffers. The sample was injected into the separation via simplified gated-injection mode as previously described [24]. Injection time was 1 second for all runs.All separations were carried out using a Bertan Associates (model 205B-01R) power supply, with the electrophoretic current measured with an auto ranging picoammeter (Keithley, model 485) .

2.5 Electrochemistry. Three-electrode configuration was used for all EC measurements, which were made by a potentiostat from Gamry Instruments, Warminster, PA, model PCl4-FAS2. see results and discussion for more information regarding the electrodes arrangements.

2.6 Scanning electromicroscope imaging (SEM). The SEM images for the electroplated electrodes were obtained by conventional secondary electron imaging techniques utilizing a JEOL (Japan Electron Optics Laboratory) model 5910lv SEM. The specimens were not given any special coating or treatment. The conductors were all tied together and to machine

ground using colloidal silver paste along the edge of the mounting area. Magnifications and operation conditions were held constant for each of the areas of interest. Minimal problems due to charging were encountered by minimizing the time spent with the electron beam incident on the substrate regions.

3. Results and Discussion

Figure 1 shows a layout of the integrated microfluidic device. This device consists of a PDMS slab with two crossed channels. The separation channel is 3 cm long, and the distance from the crossing points to the other three reservoirs is 0.5 cm. The glass substrate supports an array of ten electrodes placed inside the microchannel (all 50μm wide with a 50 μm spacing between them), two 200 μm wide electrodes that serve as reference and counter (placed inside the waste reservoir), and three other electrodes for injection/separation placed inside the waste, buffer, and sample reservoirs. The depth and width of the microchannel are 35 and 75 μm respectively.

The electroplating process was carried out inside the channel. Figure 2 shows the SEM images for Pd particles, with different magnifications, formed on the surface of gold electrodes after 3.0, 1.5, and 0.5 minutes of deposition time (frames A, B, and C, respectively). As can be seen from the images of low magnification (left frames), there are two distinct regions. The first one, on both sides of the microchannel (center), corresponds to a bare gold surface that was protected by the PDMS. In the middle (channel) region, the surface is covered with Pd particles, which were electrically deposited. As the deposition

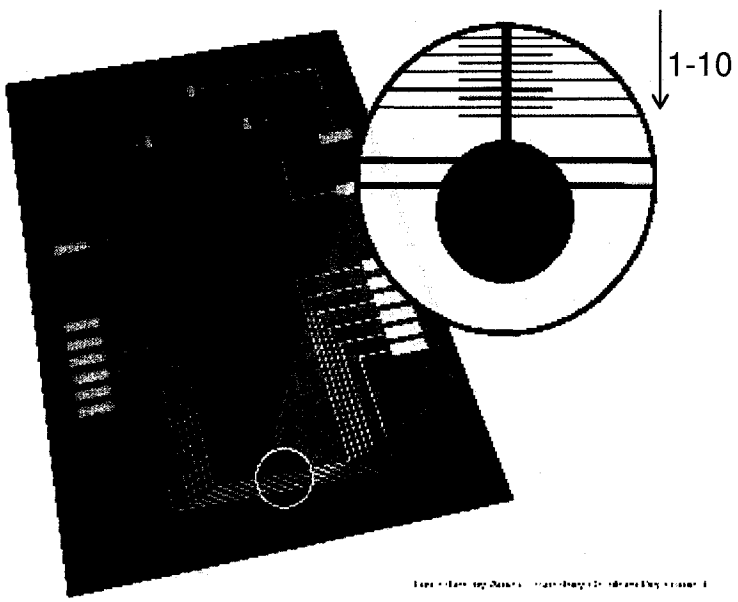

Figure 1: Schematic representation of the fully integrated microfluidic device with electrochemical detection system.

time was increased (moving from C to A), a significant increase in the size and the density of the particles was observed. The deposition time was changed in order to increase the surface area of the decoupler without increasing the width of the electrode. In order to estimate the relative increase in the surface area upon increasing the detection time, cyclic voltammograms of 50mM of perchloric acid ($HClO_4$) were generated as a function of deposition time. Figure 3 shows the cyclic voltammograms for three different deposition times. The insert shows the cyclic voltammogram of the gold electrode before the electroplating process for the same solution of $HClO_4$. The H_2 adsorption/desorption peaks are characteristic features of cyclic voltammograms for both Pt and Pd electrodes in aqueous solution, and cannot be observed for gold electrodes. Similar deposition procedures were applied for Au and Pt metals. Significant growth in peaks intensity was observed, which corresponds to an increased area of the decoupler by a factor of ~10. This increased surface area was accomplished by increasing the deposition time without increasing the width of the electrodes.

The performance of the decoupler was evaluated by using different buffer solutions of different pH's and different separation field strengths. Two important factors were considered: the surface area of the decoupler and the distance between the EG and the WE. The first test was performed without any electrochemical sensing, by just applying a separation electric field through the separation channel to test the stability of the decoupler and to find the maximum separation field that could be applied without the formation of hydrogen gas bubbles. Table 1 summarizes the results for all tested noble metals. As expected, Pd showed the best performance in terms of stability and operation lifetime.

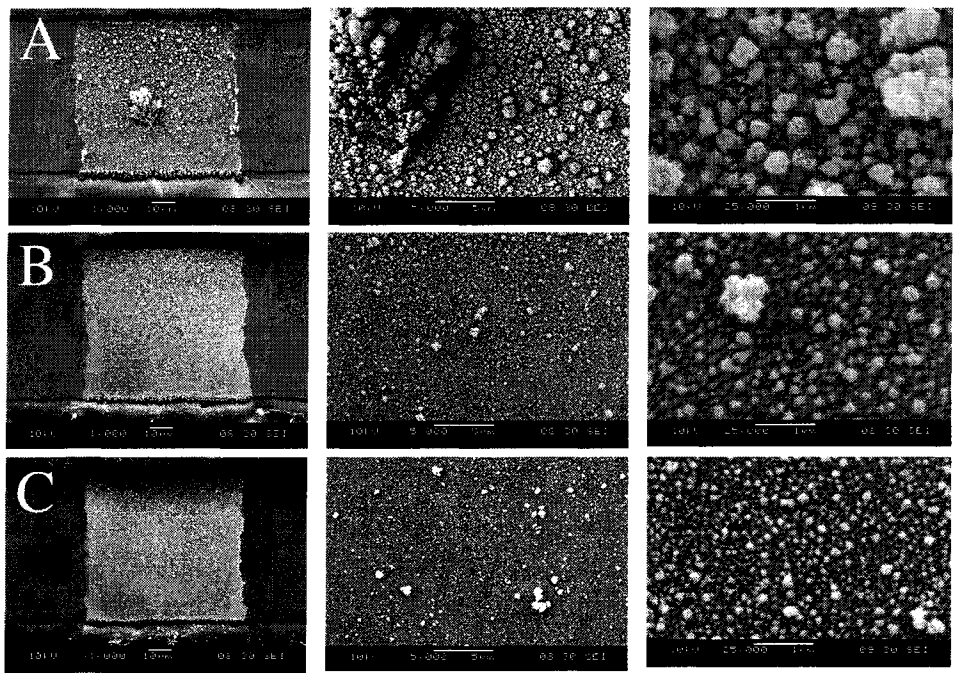

Figure 2: SEM images of channel electroplated with Pd particles. A magnification from left to right is 1,000; 5,000; and 25,000, respectively

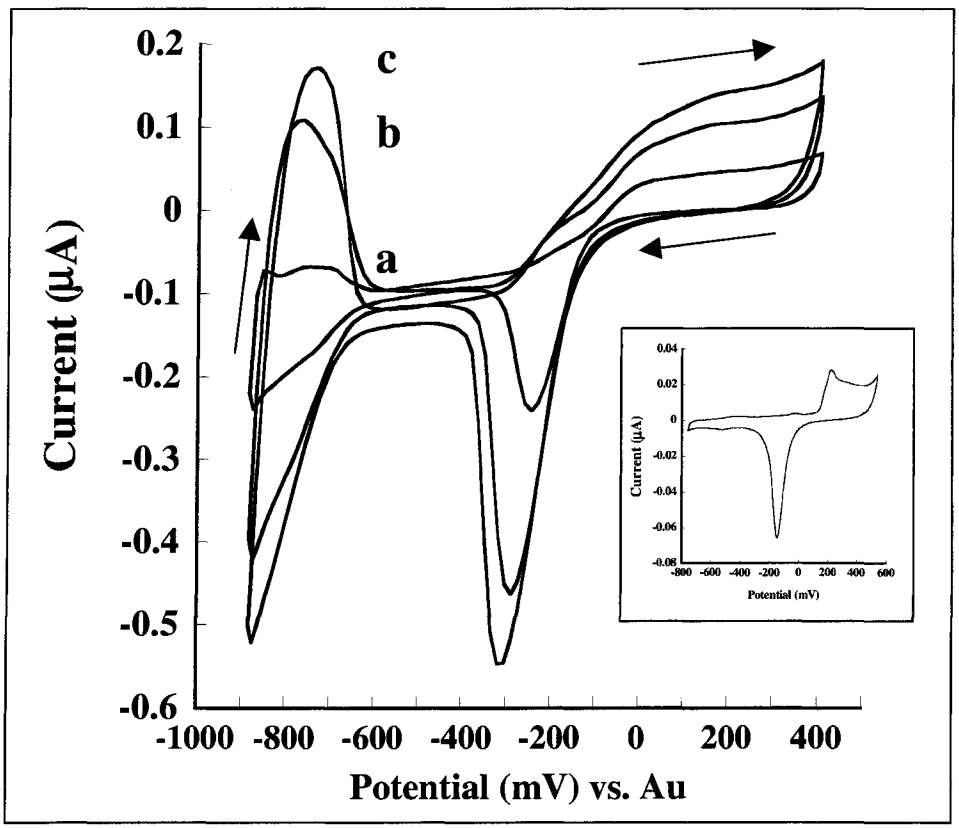

Figure 3: Cyclic voltammograms (CVs) of electroplated decoupler in 50 mM $HClO_4$ as a function of deposition time: 0.5 (a), 1.5 (b), and 3 min (c). The insert shows a CV for the Au electrode in the same solution.

Table 1: Summary of maximum applicable separation field (in V/cm) for different decouplers (Au, Pl, and Pd) in different buffers.

Buffer / Electrode	MES pH 5.5	Phosphate pH 7.5	Borate pH 9.5
Gold	70	<30	40
Platinum	150	30	100
Palladium	1000	200	600

Placing the electrophoretic ground (EG) before the WE would eliminate the interference between the detection and the electrophoretic current. Since the electroosmotic flow (EOF) vanishes at the EG, the sample plug will reach the WE under the influence of the hydrodynamic pressure created by the EOF. The distance between the EG and WE was optimized in order to achieve stable background current. As can be seen from the magnified detection zone in Figure 1, the first electrode is used as the decoupler while the WE could be selected as one of the remaining nine electrodes. This flexibility in the selection of electrodes was essential for optimizing the distance between the decoupler and the WE. Note that too short a distance can result in high interference with the electrophoretic current, whereas too great a distance leads to excess diffusion and band broadening, thus decreasing the resolving power of the system. Another /important factor in optimizing the performance of the microfluidic device is that the separation distance between the EG and the WE has to be optimized as a function of the separation field strength. It was found that the best detection conditions were obtained with a distance of ~600 μm between the EG and WE.

8-OH-dG is weakly fluorescent at room temperature, which makes fluorescence detection ineffective for detection of this biomarker. The electrochemical activity of 8-OH-dG augments ED as the more sensitive and efficient remedy for more ultra-sensitive

detection limits. Scheme 1 shows the redox reaction of 8-OH-dG in aqueous solution. The process is a 2-electron, 2-proton redox reaction that occurs on the surface of WE made of different materials [30,31].

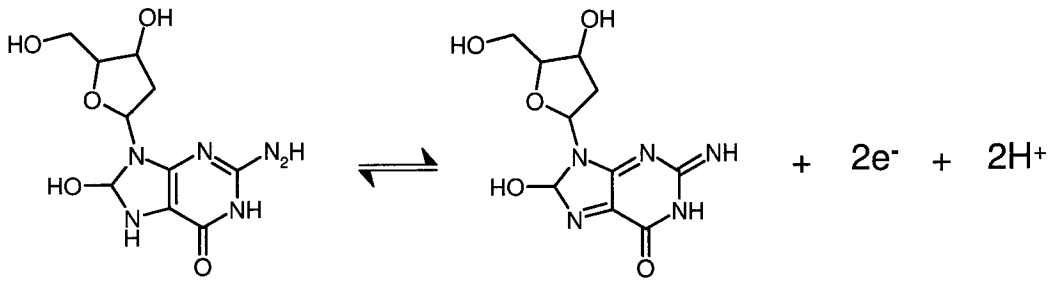

Scheme 1 The redox reaction of 8-OH-dG in aqueous solution

Before performing any further studies, it was crucial to determine the best detection potential that should be applied to the WE. Figure 4 shows the hydrodynamic voltammograms, which were generated simultaneously by injecting a mixture of 8-OH-dG and dG. It was found that 600 mV provides the maximum detection current for 8-OH-dG, whereas it was 1000 mV for dG. Since relatively higher background current was obtained upon increasing the detection potential from 900 mV to 1000 mV, the detection potential was set to 900 mV.

The durability of the decoupler strongly depends on the separation buffer. In this work, three buffer systems were used. MES has been the first choice for CE-ED because it provides very low electrophoretic current and thus less influence on the detection current. Although MES provides lower electrophoretic current, it shows weaker resolving power in comparison with other buffers such as phosphate and borate buffer. In particular, borate buffer has shown strong resolving power when used as the running buffer for the separation of diol compounds

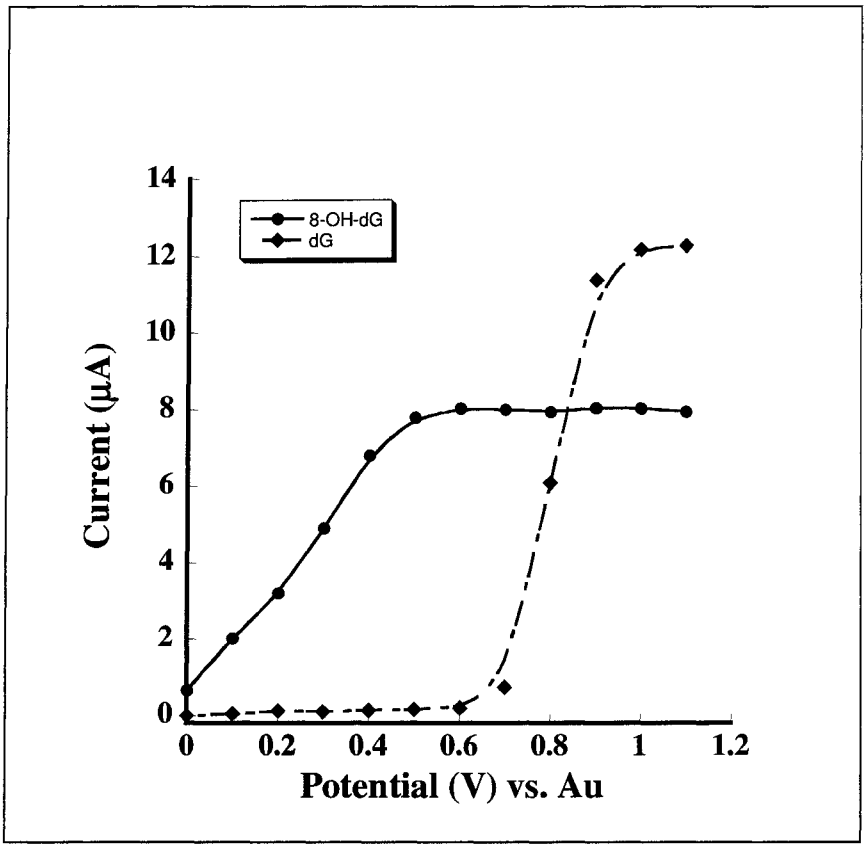

Figure 4: Hydrodynamic voltammogram of dG (75μM) and 8-OH-dG (50μM). Separation conditions: 10mM boric buffer, pH = 9.5, electric field 300 V/cm.

[32]. The borate group forms a complex with the diol compound that enhances the separation process. Interestingly, in our experiments baseline resolved peaks were only obtained in the borate buffer, but were not obtained with MES buffer. Using phosphate buffer instead generated a large electrophoretic current which went up from ~ 4 mA to 17 mA in just 15 minutes, which significantly increased the background current. Thus, no separation was attempted with phosphate buffer.

In order to study the effect of the separation voltage, all conditions were fixed except for the separation voltage. Figure 5 shows a typical electropherogram for both analytes at increasing magnitude of separation voltage. As it can be seen from Figure 5, a separation voltage up to 300 V/cm was applicable to achieve baseline-separated peaks. Interestingly, upon integrating each peak, no significant changes in the final values were found at different separation voltages, but higher resolving power and sensitivity were achieved, which can be attributed to minimizing the diffusion effect. The number of theoretical plates was found to be 170,000/m and 120,000/m for dG and 8-OH-dG, respectively. Figure 6 shows 10 repetitive injections of 8-OH-dG, which signifies the stability of the microchip. Both the detection current and the decoupler were very stable allowing performing the analyses for an extended time. Statistical analysis yields an average of 6.74 ± 0.20, a deviation.

The analytical performance of the microchip was studied by injecting a mixture of dG and 8-OH-dG of different concentrations. Figure 7 shows typical electropherograms for increasing concentrations of dG and dG 8-OH-dG. Calibration curves for both analytes (see Figure 8) were obtained from the peak areas (averaged over three injections). The dotted and solid curves correspond to dG and dG 8-OH-dG; respectively; these data reveal a linear response

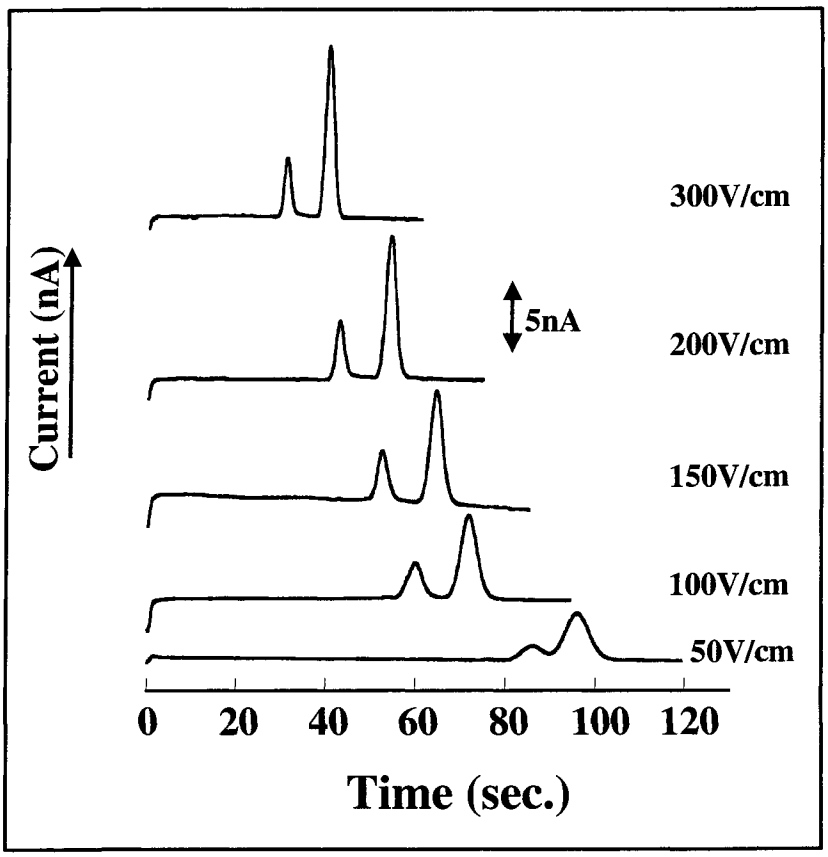

Figure 5: Effect of separation voltage on the separation of dG (50μM) and 8-OH-dG (100μM). Separation conditions: 10mM boric buffer, pH = 9.5, electric field 300 V/cm, EC potential +0.9 V vs. Au.

for dG (R^2 = 0.995) and 8-OH-dG (R^2 = 0.997) in the range of 100 nM (LOD) to 140 μM. Two electropherogram for the separation at the LOD level are shown in the insert of Figure 8; curves a and b correspond to two levels of concentrations, 100 and 200 nMrespectively.

4. Conclusions

We have developed an integrated PDMS/glass device with electrochemical detection with gold microelectrodes using a PD decoupler which was electroplated *in situ* for more efficient separation of dG and 8-OH-dG. The electroplated Pd decoupler provided stable detection background current. Low noise level (~5 pA) has allowed detecting approximately 100 nM of 8-OH-dG. The above detection limit is close to the concentration of 8-OH-dG in urine samples of healthy individuals. Since the level of this adduct in diseased individuals is significantly elevated, we anticipate that our microchip could be used in future clinical applications.

Acknowledgement

This work was supported by a grant from the National Cancer Institute (Program Project Grant 2PO1 CA49210-12) and in part by the NIH COBRE award 1 P20 RR15563, and matching support from the State of Kansas.

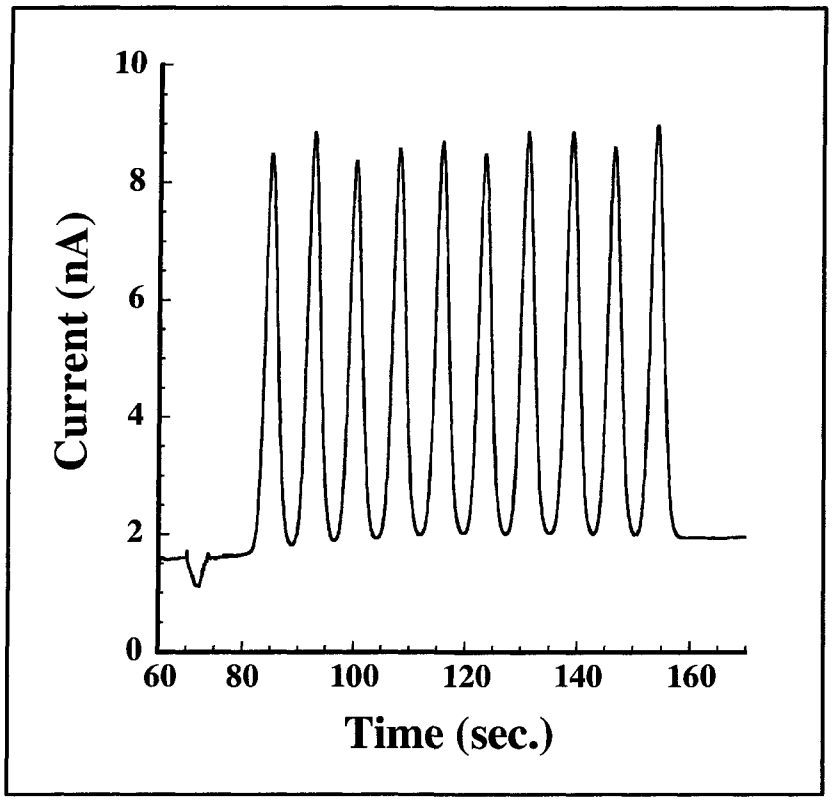

Figure 6: Ten consecutive injections of 8-OH-dG (50μM). Separation voltage is 150 V; other separation conditions are the same as in Figure 5.

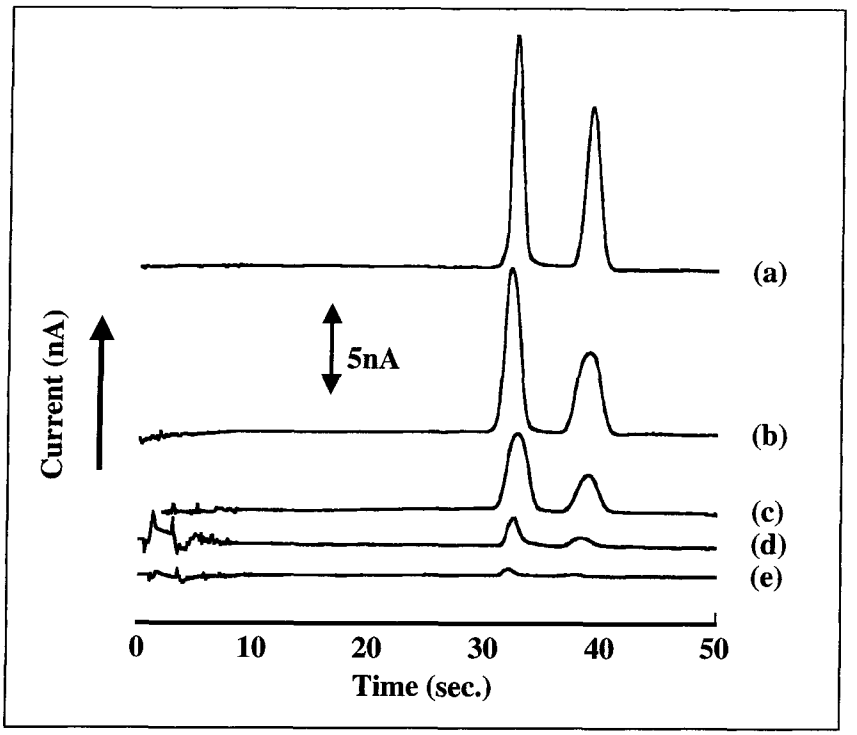

Figure 7: electropherograms of increasing levels of dG and 8-OH-dG in the range of 1μM to 150μM. Separation conditions are the same as in Figure 5.

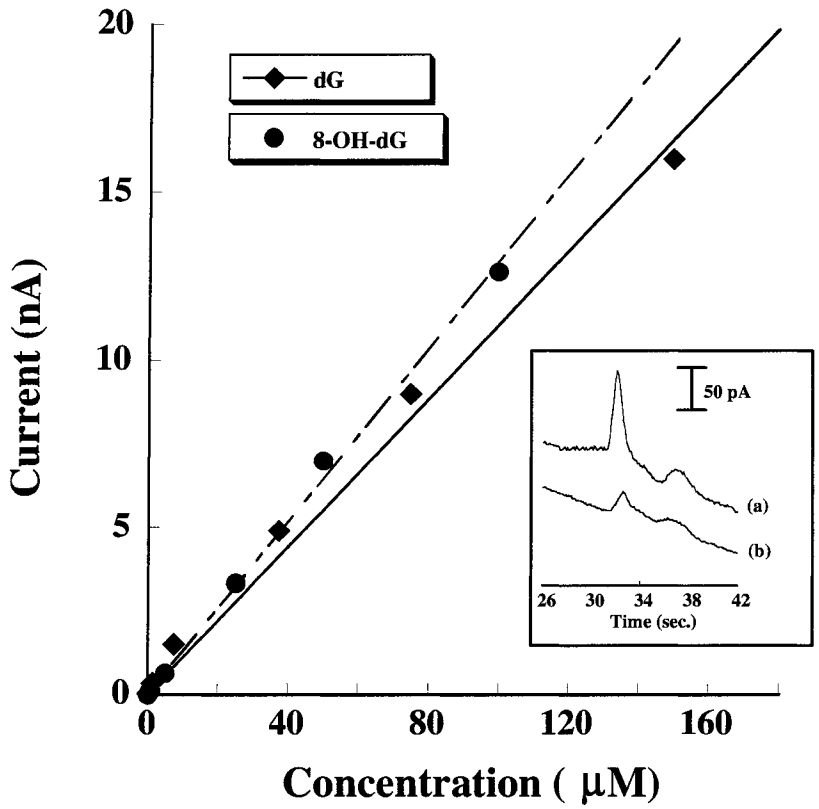

Figure 8: Calibration curves for dG and 8-OH-dG. The insert: electropherograms at the LOD for dG and 8-OH-dG. Separation conditions are the same as in Figure 5.

References

1. R. Floyd, J. Watsonand, P. Wong, D. Altmiller and R. Rickard, *Free Radio. Res. Commun*, 1986, **1**, 163-172.

2. M. Shigenaga, C. Gimeno and B. Ames, *Proc. Natl. Acad. Sei.*, 1989, **86**, 9697-9701.

3. S. Loft, K. Vistisen, M. Ewertz, A. Tjonneland, K. Overvad and H. Poulsen, *Carcinogenesis*, 1992, **13**, 2241-2247.

4. L. Wu, C. Chiou, P. Chang and J.Wu, *Clin. Chim. Acta*, 2004, **339**, 1-9.

5. H. Lin, A. Jenner, C. Ong, S. Huang, M. Whiteman and B. Halliwell, *Biochem. J.*, 2004, **380**, 541-584.

6. S. Adachi, M. Zeisig and L. Moller, *Carcinogenesis*, 1995, **16**, 253-258.

7. D.S. Arnett, D.M. Osbourn,K.D. Moore, S.S. Vandaveer and C.E. Lunte, *J. Chromatog. B* 2005, **827**, 16-25.

8. T. Hofer and L. Moller, *Chem. Res. Toxicol.*, 2002, **15**, 426-432.

9. H. Helbock, K. Beckman, M. Shigenaga, P. Walter, A. Woodall, H. Yeo and B. Ames, *Proc. Natl. Acad. Sci.*, 1998, **95**, 288-293

10. D. Weiss and C.E. Lunte, *Electrophoresis*, 2000, **21**, 2080-2085.

11. S. Mei, Q. Yao, L. Cai, J. Xing, G. Xu and C. Wu, *Electrophoresis*, 2003, **24**, 1411-1415.

12. H. Hisamoto, T. Horiuchi, K. Uchiyama, M. Tokeshi, A. Hibara and T. Kitamori, *Anal. Chem.*, 2001, **73**, 5551-5556.

13. A. Guenther, S.A. Khan, M. Thalmann, F. Trachsel and K.F Jensen, *Lab Chip*, 2004, **4**, 278-286.

14. J.M Gordillo, M. Perez-Saborid and A.M. Ganan-Calvo, *J. Fluid Mech,.* 2001, **448**, 23-51.

15. A. Manz , N. Grabner and H.M. Widmer, *Sens. Actuators B: chemical*, 1990, **1**, 244-248.

16. A. Manz, D.J. Harrison, J.C. Rettinger, E. Verpoorte, H. Ludi and H.M. Widmer, Transducers 91, Digest of Technical Papers, IEEE 91 CH2817; IEEE: New York, 1990 939-941.

17. D.J. Harrison, A. Manz, Z. Fan, H. Lüdi and H.M. Widmer, *Anal. Chem.*, 1992, **64** 1926-1932.

18. N.A. Lacher, K.E. Garrison, R.S. Martin and S.M. Lunte, *Electrophoresis*, 2001, **22**, 2526-2536.

19. M.A. Burns, B.N. Johnson, S.N. Brahmasandra, K. Handique and D.T. Burke, *Science*, 1998, **282**, 484-487.

20. M. Schwarz and P.C. Hauser, *Anal. Chem.*, 2003, **75**, 4691-4695.

21. R.S. Keynton, T.J. Roussel, M.M. Crain, D.J. Jackson, D.B. Franco, J.F. Naber, K.M. Walsh and R.P. Baldwin, *Anal. Chimica Acta*, 2004, **507**, 95-105.

22. A.J. Blasco, I. Barrigas, M.C. Gonzalez and A. Escarpa, *Electrophoresis*, 2005, **26**, 4664-4673.

23. Q.L. Zhang, J.J. Xu, H.Z. Lian, X.Y. Li and H.Y. Chen, *Analy. Bioanaly. Chem.*, 2000, **384**, 265-270.

24. A. Dawoud, T. Kawaguchi, Y. Markushin, M. Porter and R. Jankowiak, *Sens. Actu.B: Chem.*, 2006, in press.

25. J.A. Vickers and C.S. Henry, *Electrophoresis*, 2005, **26**, 4641-4647.

26. M.L. Kovarik, M.W. Li and S.R. Martin, *Electrophoresis*, 2005, **26**, 202-210.

27. N.A. Lacher, S.M. Lunte and R.S. Martin, *Anal. Chem.*, 2004, **76**, 2482-2491.

28. C-C. Wu, R-G Wu, J-G. Huang, Y-C. Lin and H-C. Chang, *Anal. Chem.*, 2003, **75**, 947-952.

29. D-C. Chen, F-L. Hsu, D-Z. Zhan and C-H. Chen, *Anal. Chem.*, 2001, **73**,758-762.

30. J. Langmaier, Z. Samec and E. Samcova, *Electroanalysis*, 2003, 15, 1555-1560.

31. A.M.O. Brett, J. A. P Piedade and S.H.P Serrano, *Electroanalysis*, 2000, **12**, 969-973.

32. J.P. Landers, R.P. Oda and M.D. Schuchard, *Anal. Chem.*, 1992, 64, 2846-2851.

CHAPTER 6. SEPARATION AND ELECTROCHEMICAL DETECTION OF CATECHOL ESTROGENS-DERIVED DNA ADDUCTS WITH ON-CHIP CAPILLARY ELECTROPHORESIS

Manuscript in preparation (to be submitted to *Electrophoresis*)

Abdulilah A. Dawoud and Ryszard Jankowiak

6.1 Introduction:

Estrogens are associated with several cancers and are known to induce tumors in humans [1-3]. Estrogens are produced by aromatization reaction of androstenedione and testosterone, respectively, catalyzed by cytochrome P450 (CYP) 19 aromatase [4-6]. They are biochemically interconvertible by 17β-estradiol dehyrogenase. Their metabolism leads to catechol estrogens and to a lesser extent, 16α-hydroxylation [1]. Two catechol estrogens form on metabolic conversion, 2-OHE_1 (E_2) as the major one and 4-OHE_1(E_2) as the minor one [7-9]. Catechol estrogens are oxidized to catechol estrogen quinones (CEQs) by peroxidases and cytochrome P-450 [3,10,11], a redox-cycling that can also generate hydroxyl radicals that cause DNA damage [12].

CEQs derived from the catechol estrogens, 4-OHE_1 and 4-OHE_2, can react with DNA to form depurinating adducts at the N7 position of guanine and N3 position of adenine [1,13-16]. The CEQs can be deactivated via various conjugation pathways. Among these is the conjugation with GSH, which is considered as one of the most important detoxification pathways in biological systems. Conjugation of CEQs with various sulfur nucleophiles, RSH, in which R is the Cys, NAcCys, or GSH moiety forms DNA adducts that are excreted in urine [17,18], and thus, identification and quantitation of CEQ-conjugates in urine have potential for assessment of the level of CEQ formed. Schematic structures of DNA adducts

of interest, 4-$OHE_1(E_2)$-1-N3Ade, 4-$OHE_1(E_2)$-1-N7Gua, and 4-OHE_2-derived –NAcCys conjugates of interest are shown in figure 6.1

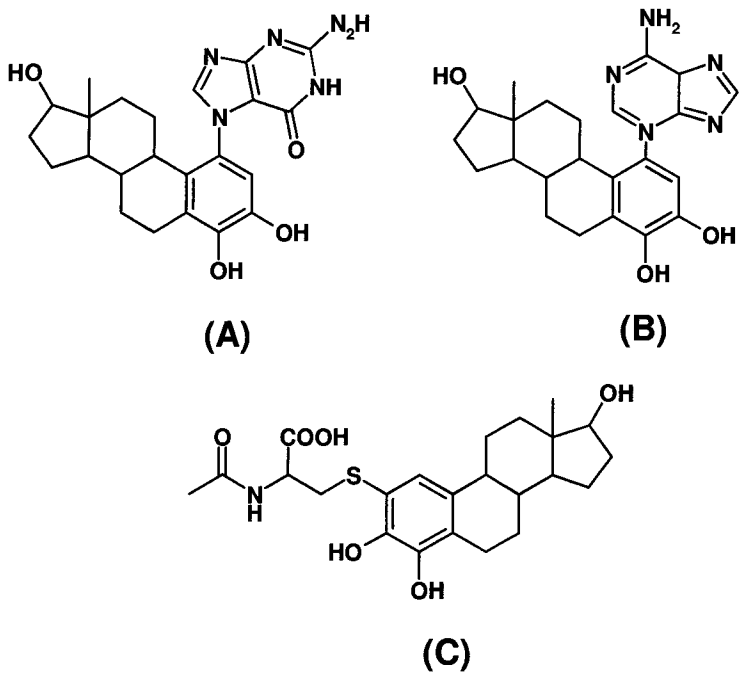

Figure 6.1: Chemical structures of (A) 4-OHE_2-1-N7Gua, (B) 4-OHE_2-1-N3Ade, and (C) 4-OHE_2-NAcCys

These DNA adducts have weak fluorescent properties at room temperature, which makes fluorescence detection inconvenient. Electrochemical/amperometric detection provides an efficient remedy and methodology for the detection of these adducts of interests because of their inherent electrochemical activity. For example, recent analysis of potential biomarkers of estrogen-initiated cancer in urine and in kidney tissue of Syrian golden hamsters treated with 4-OHE_2 revealed that high-performance liquid chromatography

(HPLC) with electrochemical (EC) detection provides high specificity [1,19,20]. Thus, electrochemical detection is a sensible separation and detection methodology for the identification of these adducts.

For the last decade, on-chip analysis has revolutionized the landscape of chemical analysis [21-25]. We have reported the development of fully integrated microfluidic device with electrochemical detection (end-channel) for the separation and detection of dopamine-derived DNA adducts and related neurotransmitters [27]. The limit of detection (LOD) was in the low micromolar range (~2 μM). Further improvement in detection limit and noise reduction was achieved via decoupling the electrophoretic and the detection currents by applying *in situ* electroplating of palladium decoupler [28]. The decoupler improved detection current stability by at least one order of magnitude and allowed LOD in the low nanomolar range (~100 nM).

In this paper, we present sensitive electrochemical detection system integrated on a capillary electrophoresis-based microfluidic device that should provide an excellent methodology for identification of estrogen-derived biomarkers. These devices could be used in future clinical applications. This is the first report that is solely devoted for the separation and detection of DNA adducts using a microfluidic device.

6.2 Experimental Section

6.2.1 Chemicals and reagents

All chemicals were used as received. 8-hydroxy-deoxyguanosine (8-OH-dG), deoxyguanosine (dG), 2-[N-morpholino]ethanesulfonic acid (MES), potassium hexachloropalladate(IV) (K_2PdCl_6), and sodium dodecyl sulfate (SDS), were obtained from

Sigma-Aldrich. Sodium hydroxide, boric acid, perchloric acid, and sodium phosphate monobasic were supplied by Fisher Scientific. The 4-OHE_2-1-N3Ade, 4-OHE_2-1-N7Gua, and 4-OHE_2-derived NAcCys conjugates were synthesized according to previously published procedures. The individual electrolyte solutions for separations were MES, and borate, 10mM each, prepared with purified water (18 MΩ cm, Millipore) and adjusted with sodium hydroxide to pH 5.5 and 9.5, respectively.

6.2.2 Microchip and Pd decoupler:

PDMS/glass hybrid microchip was used with gold electrodes fabricated on the glass layer, whereas the microchannels were on the PDMS layer. An array of electrodes was utilized for the detection. Details of the fabrication procedure regarding the microchip and the decoupler were published previously [27,28].

6.2.3 Electrophoresis

100μM stock solutions of each analyte was prepared in water and kept in the refrigerator at 4°C. Fresh solutions were prepared daily by diluting the stock solutions with the running buffer. Prior to the separation, the microchannels were flushed for 5 min with NaOH, 10 min with deionized water, and 10 min with the running buffer. 10 mM of three buffers were used, MES (pH = 5.5), and borate (pH = 9.5) buffers. The sample was injected into the separation via simplified gated-injection mode as previously described [24]. Injection time was 1 second for all runs. All separations were carried out using a Bertan Associates (model 205B-01R) power supply, with the electrophoretic current measured with an auto ranging picoammeter (Keithley, model 485).

6.245 Electrochemistry

A three-electrode configuration was used for all EC measurements, using a Gamry

Instruments potentiostat, Warminster, PA, model PCI4-FAS2.

3. Results and Discussion

The separation process was carried out on microchips of different separation channels lengths, 3 cm and 4.5 cm. The microchannels' depth and width were 35 and 75 μm, respectively. Also two running buffers were used for the separation process, MES and borate buffer. The sample plug was injected into the separation channel by a gated mode; injection time was either 1 or 2 seconds for all separations. Before performing any separation process, it was necessary to find the optimal detection potential for the analytes. For this purpose, hydrodynamic voltammograms were generated for 4-OHE_2-1-N3Ade and 4-OHE_2-NacCys. The results are shown in Figure 6.2. As can be seen from Figure 6.2, the optimal detection potentials were 800 mV and 1000 mV for 4-OHE_2-1-N3Ade and 4-OHE_2-NacCys, respectively. Therefore, a potential of 900mV was used for further analysis.

For the separation process, a mixture 4-OHE_2-1-N7Gua, 4-OHE_2-1-N3Ade, 8-OH-dG, and 4-OHE_2-NacCys, injected via gated injection; injection time was 1 sec. Not surprisingly, separation with MES buffer did not adequately resolve all four adducts and only two peaks were observed. Using borate buffer allowed for better resolving power than MES, where 4 peaks were obtained. Figure 6.3 shows the corresponding electropherogram (see Chapter 4). As can be seen from Figure 6.3, the peaks of 4- OHE_2-1-N3Ade and 4-OHE_2-1-N7Gua are not determined within the limit to observe the FWHM of both peaks. Increasing the separation channel from 3 to 4.5 cm has slightly enhanced the separation process.

Based on work that has been published by our group [29], buffer additives are necessary to separate the corresponding analytes. Two approaches were tested in order to

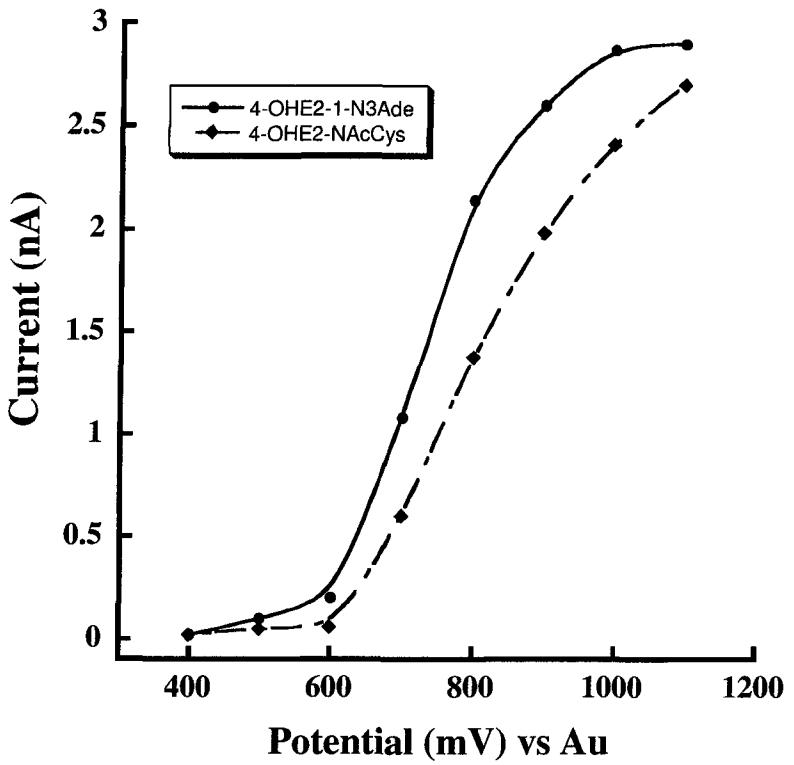

Figure 6.2: Hydrodynamic voltammograms of 4-OHE_2-1-N3Ade and 4-OHE_2-NAcCys. Separation conditions: 5mM boric buffer, pH = 9.5, electric field - 200 V/cm.

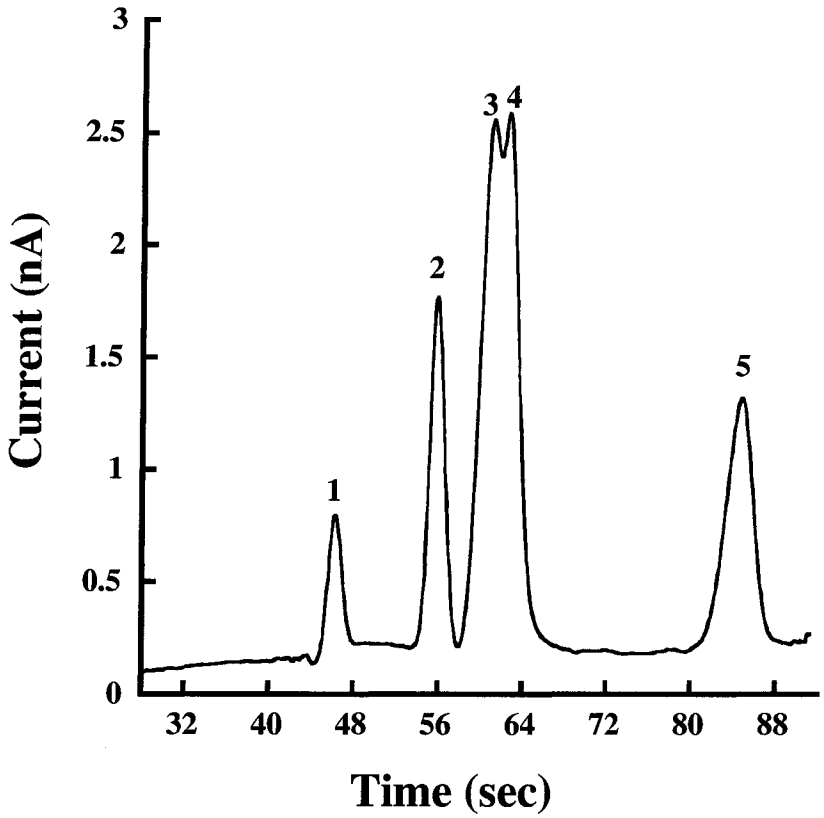

Figure 6.3: Electropherogram of a mixture of 25 μM of 8-OH-dG (2), OHE_2-1-N3Ade (3), 50 μM of 4-OHE_2-1-N7Gua (4), and 25 mM of 4-OHE_2-NacCys (5). Separation conditions: 5mM boric buffer, pH 9.5, electric field 200V/cm, and EC potential +900 mV vs. Au. Peak #1 is the EOF peak

enhance the separation process. First, 25mM of SDS was added to the running buffer. The high ionic strength that resulted after the addition of the SDS caused the electrophoretic current to increase significantly from 2μA to ~ 12μA, which noticeably disturbed the detection current and thus no sharp peaks were obtained. Furthermore, PDMS as weak heat dissipation material, resulting in joule heating inside the capillary channels and thus, causing the formation of air bubbles, eventually destroying the chip. Addition of acetonitrile, as an organic modifier, was tested and evaluated (see Chapter 2). No enhanced resolution was obtained.

Estradiol (E_2) and 4-OHE_2 were tested as potential analytes for separation. The difficulty associated with the analysis of these analytes was one-measurement phenomenon, i.e. after the oxidation process and the generation of the corresponding peak, there was a huge drop in the background current and very weak signal was obtained for the second injection process. As can be seen from Figure 6.4, there was a reduction in the second peak of about 86%. After the oxidation process, highly active radicals are formed in the transition state, where these radicals react to form a polymer on the electrodes' surfaces and cause electrodes passivation [30,31]. Therefore, no attempts were made to mix E_2 or 4-OHE_2 with the DNA adducts mixture (see above).

Interestingly, the detection of 4-OHE_2-NAcCys is achievable, although NAcCys is not. The reason for this is the high potential needed to detect thiol compounds on the bare electrode surface. Specifically, the presence of the free (un-bonded) thiol group causes NacCys to bind to the gold surface at moderately applied potentials. For 4-OHE_2-NacCys, the thiol group is used to form the final product, where it is not free any more, and the resultant oxidation current corresponds to the catechol hydroxy groups.

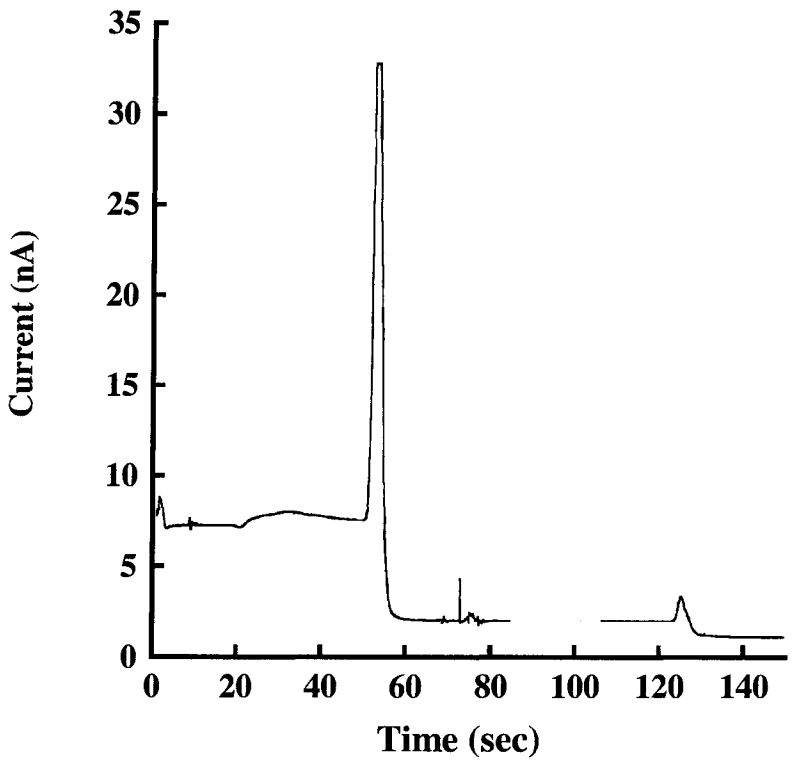

Figure 6.4: Electropherograms of two injections of 500mM E_2.Separation conditions: 4:1 borate, acetonitrile, pH = 9.5, electric field 200V/cm, EC potential +900mV vs. Au.

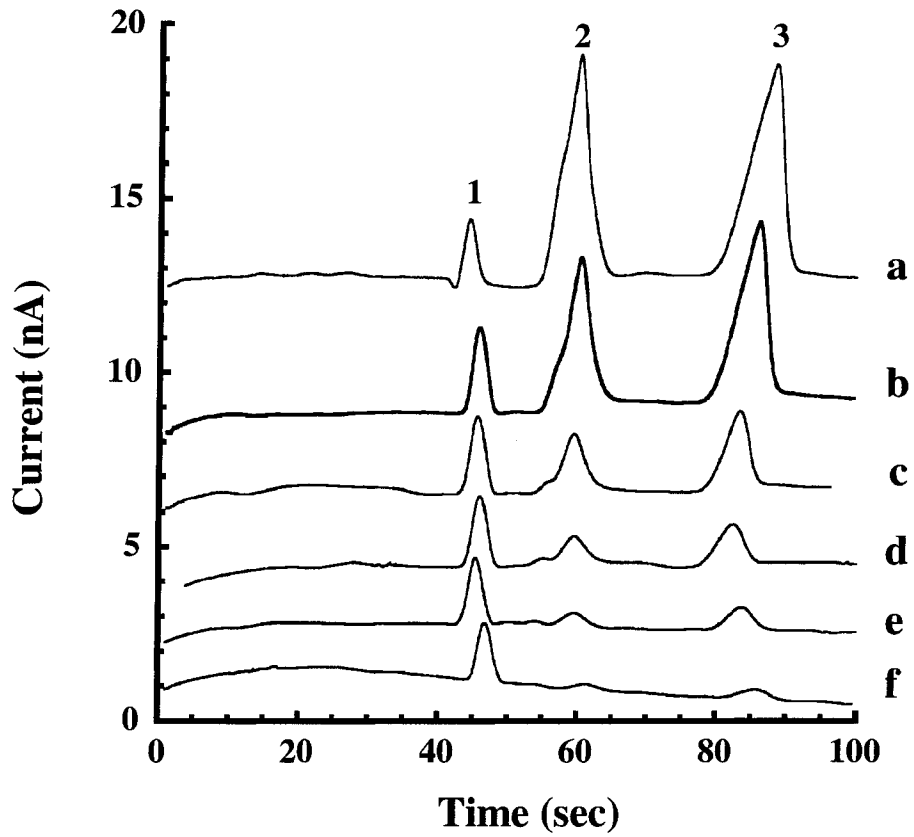

Figure 6.5 Electropherograms a-f correspond to increasing levels of 4-OHE_2-1-N3Ade (1) and 4-OHE_2-NAcCys(2), in the concentration range of 0.8μM to 50μM. Separation conditions are the same as in Figure 6.3. Peak #1 is the EOF peak.

Figure 6.5 shows typical electropherograms for increasing level of 4-OHE_2-1-N3Ade and 4-OHE_2-NacCys. Calibration curves for both analytes were obtained from their integrated peak area (averaged over three injections). Figure 6.6 reveals a linear response for 4-OHE_2-1-N3Ade (R^2 = 0.992), 4-OHE_2-NAcCys (R^2 = 0.987) in the range of 400 nM (LOD) to 50 μM. The electropherogram for the separation at the LOD level is shown in the insert of Figure 6.6.

6.4 Conclusions:

We have used capillary electrophoresis-based microfluidic devices for the separation and electrochemical detection of estrogen-derived DNA adducts of interest. The experiments have revealed a detection limit in the nanomolar range, the concentration detection limit is <500 nM, which could have potential applications in future medical diagnostics. Further improvements are still needed in order to enhance the resolving power of our system and to bring down the detection limit to the low nanomolar range.

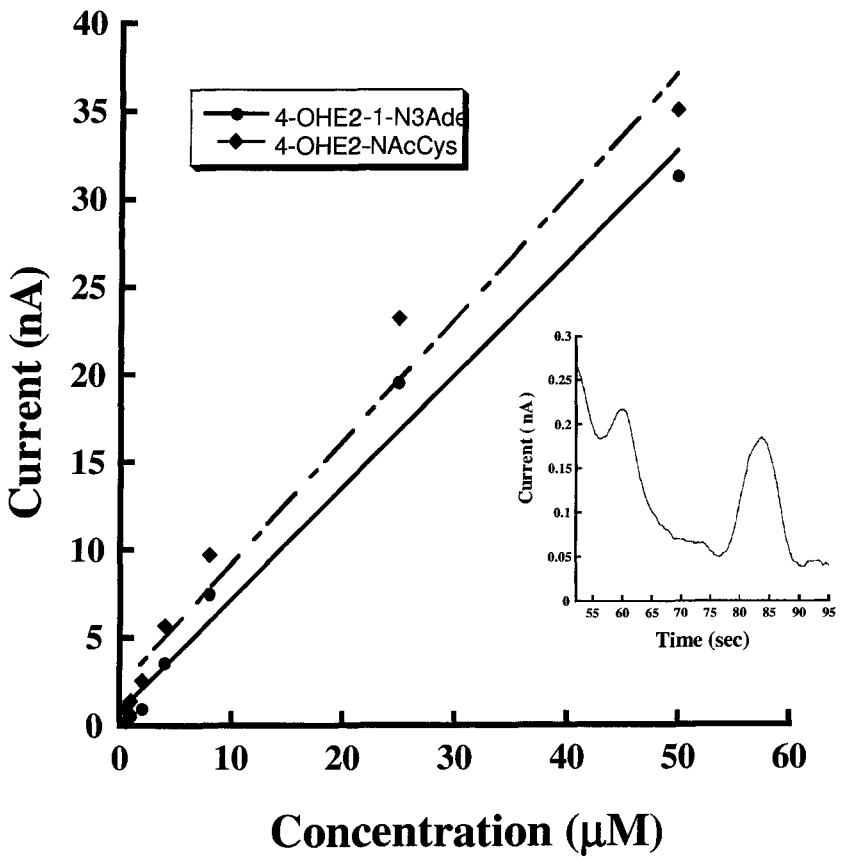

Figure 6.6: Calibration curves for 4-OHE_2-1-N3Ade, and 4-OHE_2-NAcCys. The insert shows the electropherogram generated at the LOD of 4-OHE_2-1-N3Ade and 4-OHE_2-NAcCys. Separation conditions are the same as those in Figure 6.3.

6.5 References:

1. E.L. Cavalieri, E.G. Rogan, and D. Chakravarti, D. *Cell. Mol. Life Sci.* **59** (2002), 665-681.

2. D. Chakravarti, PC. Mailander, K.-M.Li, S. Higginbotham, H.L. Zhang, , M. Gross, J.L. Meza, E.L. Cavalieri, and E.G. Rogan, *Oncogene* **20** (2001), 7945-7953.

3. I. Dwivedy, P.D. Devanesan, P. Cremonesi, E.G. Rogan, and E.L. Cavalieri, *Chem. Res. Toxicol.* **5** (1992), 828-833.

4. International Agency for Research on Cancer Group, IARC Monographs on Evaluation of Carcinogenic Risk of Chemicals to Humans, International Agency for Research on Cancer, Lyon, France; Sex Hormones (II) Vol. **21**, pp. 173-221 (1979).

5. J.G. Liehr, Endo. *Rev.* **21** (2001), 4054-4058.

6. E. Cavalieri, E. Kohli, M. Zahid, and E.G. Rogan,Greater reactivity of estradiol-3,4-quinone *vs* estradiol-2,3-quinone with DNA in the formation of depurinating DNA adducts. *Proc. Am. Assoc. Cancer Res.* **44** (2003), (2^{nd} edition), 180.

7. F.P. Guengerich, *Annu. Rev. Pharmacol. Toxicol.* **29** (1989), 241-264.

8. C.P. Martucci, and J. Fishman, *Pharmacol. Ther.* **57** (1993), 237-257.

9. B.T. Zhu, A.H. and Conney, *Carcinogenesis* **19** (1998), 1-27.

10. B. Kalyanaraman, R.C. Sealy, and K. Sivarajah, *J. Biol. Chem.* **259** (1984), 14018-14022.

11. Liehr, J.G., Ulubelen, A.A., and Strobel, H.W. (1986). *J. Biol. Chem.* **261**, 16865-16870.

12. D. Roy, and J.G. Liehr, *Mutat. Res.* **424** (1999), 107.

13. E.L. Cavalieri, D.E. Stack, P.D. Devanesan, R. Todorovic, I. Dwivedy, S. Higginbotham, S. Johanson, K. Patil, and E. Rogan, *Proc. Natl. Acad. Sci.* **94** (1997), 10937-10942.

14. K-M.Li, , P.D. Devanesan, , E.G. Rogan, , and E.L. Cavalieri, *Proc. Amer. Assoc. Cancer Res.* **39** (1998), 636-643.

15. D. Stack, J. Byun, M.L. Gross, E.G. Rogan, and E. Cavalieri, E. *Chem. Res. Toxicol.* **9** (1996), 851-859.

16. R. Jankowiak, D. Zamzow, D.E. Stack, E.L. Cavalieri, G.J. and Small, *Chem. Res. Toxicol.* **11** (1998), 1339-1345.

17. E.L. Cavalieri, S. Kumar, R. Todorovic, S. Higginbotham, A.F. Badawi, and E.G. Rogan, *Chem. Res. Toxicol.* **14** (2002), 1041-1050

18. K. Cao, P.D. Devanesan, R. Ramanathan, M.L. Gross, E. Rogan, and E.L. Cavalieri, *Chem. Res. Toxicol.* **11** (1998), 917-924.

19. R. Todorovic, P. Devanesan, S. Higginbotham, J. Zhao, M.L. Gross, E.G. Rogan, and E.L. Cavalieri, *Carcinogenesis* **22** (2001), 905-911.

20. P. Devanesan, R. Todorovic, J. Zhao, M.L. Gross, E.G. Rogan,and E.L. Cavalieri, Carcinogenesis **22** (2001), 489-497.

21. A. Manz, N. Grabner, H.M. Widmer, *Sens. Actuators B.* **1** (1990), 244-248.

22. A. Manz, D.J. Harrison, J.C. Rettinger, E. Verpoorte, H. Ludi, H.M. Widmer, Transducers 91, Digest of Technical Papers, IEEE 91 CH2817; IEEE: New York (1990), 939-941.

23. D.J. Harrison, A. Manz, P.J. Glavina, Transducers 91, Digest of Technical Papers, IEEE 91-CH2817-5; IEEE: New York (1990), pp 792-795.

24. G.J. Bruin, *Electrophoresis* **21** (2000), 3931-3951.
25. A. Mello, *Lab. on a Chip* **2** (2002), 48N-54N.

26. W. R. Vandaveer, S.A. Pasas-Farmer, D.J. Fischer, C.N. Frankenfeld, and S.M. Lunte, *Electrophoresis* **25** (2004), 3528-3549.

27. A. Dawoud, T. Kawaguchi, Y. Markushin, M. Porter and R. Jankowiak, *Sens. Actu.B: Chem.*, 2006, in press.

28. A. Dawoud, T. Kawaguchi, and R. Jankowiak, submitted to *Lab on a Chip.*

29. Y. Markushin, P. Kapke, M. Saeed, H. Zhang, A. Dawoud, E.G. Rogan, E.L. Cavalieri, and R. Jankowiak, *Chem. Res. Toxicol.* **18** (2005), 1520-1527.

30. D.P. Manica, Y. Mitsumori, and A.G. Ewing, *Anal. Chem.,* **75** (2003), 4572–4577.

31. A. Collier, J. Wang, D. Diamond, and E. Dempsey, *Anal. Chim. Acta* **550** (2005), 107-115.

APPENDIX: HYPERSELECTIVE AND TARGETED SEPARATION OF ANALYTES USING DYNAMIC MULTIPLE EQUILIBRIUM GRADIENTS (DMEG) APPROACH

A paper published in *NSTI Nanotech **2005**, Technical Proceedings*, Vol. I, pp. 640-643.

Y. Markushin, A. Dawoud and R. Jankowiak

ABSTRACT

Separation of closely related analytes can be significantly enhanced by introducing a new dynamic multiple equilibrium gradients (DMEG) approach. Namely, low-voltages applied as running waveforms to specifically designed grids of electrodes microfabricated along the separation channel (e.g. a thin capillary) can increase peak capacity and separation of molecules in complex mixtures.

Keywords: capillary electrophoresis, microfluidic devices, equilibrium gradient

A.1 Introduction. Although a number of powerful separation techniques, such as chromatography, electrophoresis, field flow fractionation, and equilibrium gradient methods (EGM) are available for the separation of mixtures of various chemicals and proteins, there is a growing need for new techniques that can provide even greater resolving power and peak capacity. Recent advances in separation sciences have been driven by the demands of genomics and proteomics research; these areas of research continue to introduce new challenges for developing rapid methods for more selective separations. Many

comprehensive reviews analyzing the lab-on-a-chip technology and its many applications have been published [1-5]. Multi-layer electrode structures are also being developed for selective manipulation of particles and cell suspensions using the traveling field dielectrophoresis (DEP) effect [6]. DEP is the motion of a particle due to the interaction between a non-uniform electric field and its induced dipole moment in the particle [6-8]. Electro-hydrodynamic (EHD) planar wave pumps have also been constructed using the concept of the moving electrostatic wave applied to poly-Si bus bars [9]. To generate non-uniform electric fields for the purpose of fluid pumping and/or separation of particles, the electrodes are deposited on one side of a channel (or surface) and a very high frequency (~1 MHz) external electric field is imposed to induce a dipole moment in a particle in a medium.

The potential of EGM in chemical and separation sciences has not been fully explored as yet, although a linear field intensity gradient in which analytes are brought to unique equilibrium points by a force gradient and a counter force (a hydrodynamic flow) along the separation pathway has been recently described and tested experimentally [10-14]. In this case the electric field gradient is established using an array of electrodes for which voltages are individually adjusted [12,13]. A disadvantage of the EGM approach is that resolution and peak width cannot be improved simultaneously. Experimental designs utilizing EGM [12,13,15] are limited in resolving power because of a simple stair-step electric field gradient with discontinuities at the electrodes that is not practical. Besides, it is not easy to keep the profile constant over a long distance of the separation column and extended separation time, as the opposing hydrodynamic flow and its broadening effects significantly hamper the extent of electrofocusing. Though novel technologies continue to be developed, including the

Protein Chip Arrays and multiplexed microchip gel electrophoresis [16-19], many laboratories rely on

traditional conventional capillary electrophoresis (CE). Therefore, industrial and biomedical communities continue to articulate a need for new, more selective separation methods for chemical analyses. We are at a stage where further advances can only be explored through the development of new principles and/or novel platform architectures such as those described in this manuscript.

A.2 Results and Discussion. It is demonstrated that separation of analytes can be significantly enhanced by introducing a new dynamic multiple equilibrium gradients (DMEG) approach. In this methodology relatively low-voltages applied as running waveforms to specifically designed grids of electrodes microfabricated along the separation channel (or thin capillary) can increase peak capacity and separation of molecules in complex mixtures. The running waveforms (applied to the electrodes) create moving electric field gradients, which results in very efficient separation and transport of analytes to the detection area. Figure 1 shows a schematic of our simplified experimental setup with which the proof-of-principle data were obtained. A thin capillary (o.d., 150 μm; i.d., 75 μm; length, 10 cm) was placed between two glassy plates with 300 chromium electrodes on each side. For simplicity the electrodes were grouped into sets of four; they were connected in such a way that electrode #1 in each group is connected to all other #1 electrodes, electrode #2 to all #2's, and so on. The electrode width and the gap between electrodes were about 5 and 350 μm, respectively. Saw-tooth type waves were applied along the capillary outfitted with electrodes. The best results were obtained when the waveform of the top electrodes was slightly shifted in reference to the electrodes on the bottom plate (see Figure A.1).

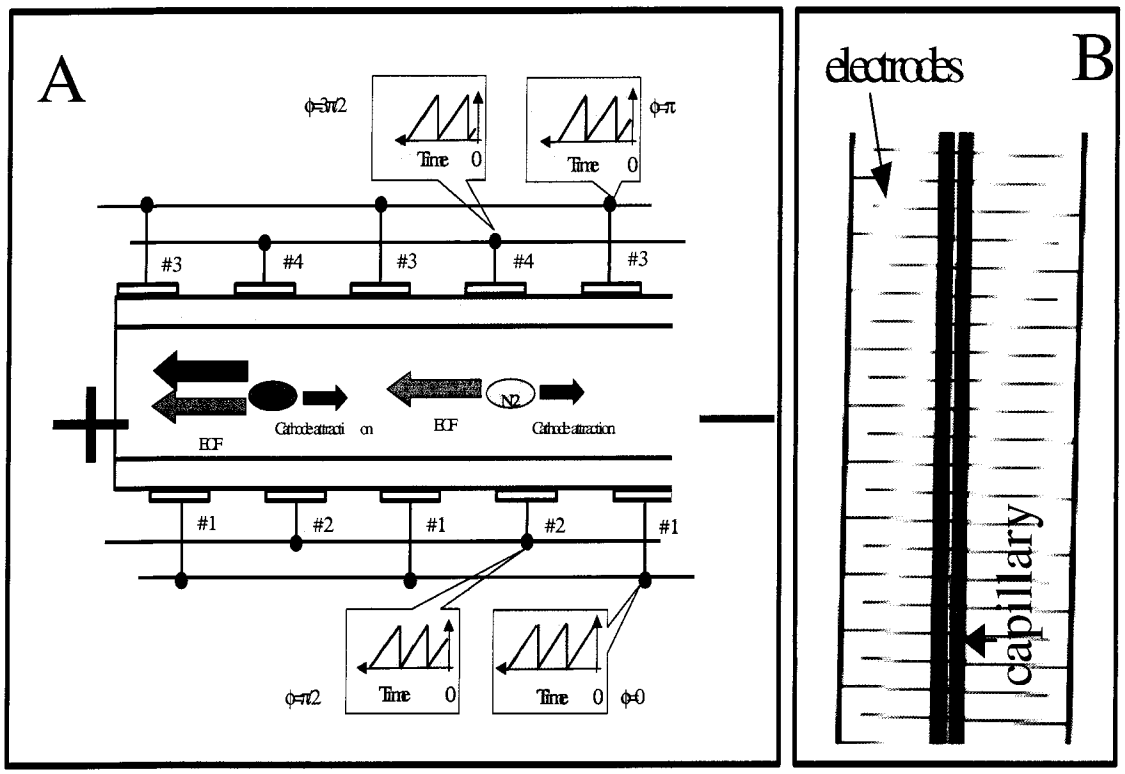

Figure A.1. Frame A: Schematic of our simplified prototype device (only a few electrodes are shown for simplicity). N1 and N2 are two negatively charged analytes with slightly different mobilities. The thick black arrow corresponds to the additional force due to the electric field gradient fulfilling the equilibrium gradient condition for this particular analyte (N1). (Focusing is explained in Figure 2). The saw-tooth voltage applied to electrodes 1,2,3, and 4 at time zero has the phase shift (ϕ) of $0,\pi/2$, π, and $3\pi/2$, respectively. The time course of the phase-shifted signals to create running waves is also shown for an easy inspection. EOF = electroosmotic flow. **B:** An image of a section of capillary and electrodes on the bottom plate.

An example of fluorescence based electropherograms obtained for a mixture of four closely related analytes: 1) 2',7'-dichlorofluorescein diacetate, 2) 4(5)-carboxyfluorescein, 3) 3',7'-dichloro-fluorescein, and 4) 4',5'-dichlorofluorescein is shown in Figure A.2. Curve (a) corresponds to an electropherogram obtained using conventional CE without running waves. The sample ($c \sim 10^{-5}$ M) was hydrodynamically injected, resulting in ~20 nL injection volume. Standard CE separation was carried out at –2.1 kV in 4 mM of sodium tetraborate running buffer, and fluorescence electropherograms were acquired during CE separation. As shown in curve (a), under these experimental conditions the analytes 1-4 could not be separated. However, CE separation combined with the running waves (λ = 1,400 μm, f = 0.1 Hz, and gradually increasing wave amplitude (from 0 to ± 540 V) in a sweeping mode provided excellent separation of all analytes. The fluorescence intensity of the broad peak in curve (a) is the same as the combined intensity of the very narrow peaks 1, 2, 3, and 4 in chromatogram (b). This result is striking as further improvements are anticipated. The significantly narrowed peaks illustrate the electric field gradient induced focusing effect. The extent of focusing strongly depends on λ, the shape of the running waves, device design, and electric field strength, all of which can be controlled experimentally. The electrodes act as capacitors and the applied waveforms generate strong electric field (estimated experimentally to be $\sim 10^{-2}$ V/μm), which drives the separation. It is shown that the separation of molecules with $\Delta\mu/\mu$ of $\sim 5 \times 10^{-4}$ can be accomplished. Electropherogram (c) was also acquired by CE combined with the same running waves but with fixed amplitude of ± 400 V. As a result only the analyte with the fastest electrophoretic mobility is "fished-out" from the mixture. This

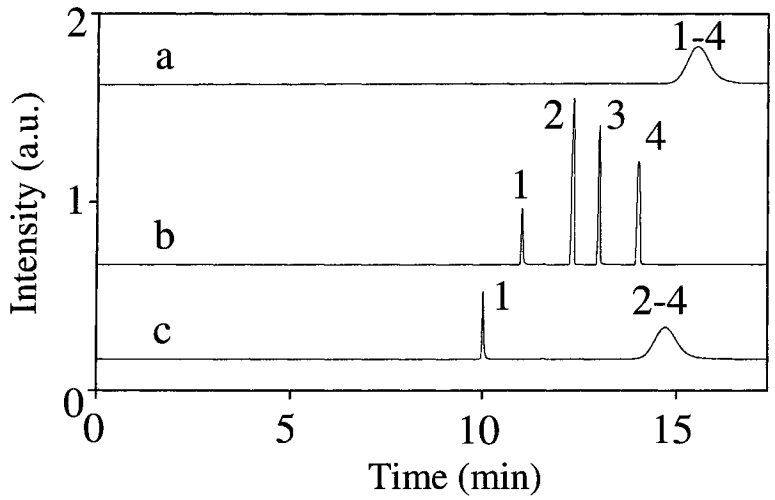

Figure A.2. CE fluorescence based electropherograms obtained for a mixture of four analytes without (curve a) and with running waves (curve b and c) obtained under different experimental conditions (see text for details).

illustrates for the first time that targeted separation of analytes in complex mixtures is feasible.

These results demonstrate that the application of a DMEG approach to CE and/or various microfluidic devices (research in progress) will lead to separation with significantly improved peak capacity and resolution.

A.3 References

1. V. Dolník, S. Liu and S. J. Vladisl, *Electrophoresis*, **21**, 41 (2000).
2. G. Bruin, *Electrophoresis*, **21**, 3931 (2000).
3. M. P. Hughes, *Electrophoresis*, **23**, 2569 (2002).
4. M.A. Schwarz and P.C. Hauser, *Lab on a Chip*, **1**, 1 (2001).
5. I. L. Medintz, B.M. Paegel and R. A. Mathies, *J. Chromatogr. A*, **924**, 265(2001).
6. F.M. Moesner and H. Higuchi, *IEEE Industry Application Society*, Annual Meeting, New Orleans, **vol. 3**, pp.2004-2011 (1997).
7. M.S. Talary, J.P.H. Burt, J.A. Tame and R. Pethig, *J. Phys. D: Appl. Phys.* **29**, 2198 (1996).
8. Y. Huang, X-B. Wang, J.A. Tame and R. Pethig, *J. Phys. D: Appl. Phys.* **26**, 1528 (1993).
9. G. Fuhr, T.Schnelle and B. Wagner, *J. Micromech. Microeng.* **4**, 217 (1994).
10. Giddings, *J.C. Sep. Sci. Technol.* 1979, 14, 871-882.
11. Tolley, H.D., Wang, Q, LeFebre, D.A. and Lee, M.L., *Anal.* Chem. 2002, 74, 4456-4463.
12. Ivory, C.F. *Sep. Sci. Technol.* 2000, 53(11), 1777-1793.
13. Huang, Z. and Ivory, C.F., *Anal. Chem.* 71, 300-309 (1999).
14. A.J. link, J. Eng, D.M. Schielte, E. Carmack, G.J. Mize, D.R. Morris, B.M. Garvik, J.R. Yates III, *Nat. Biotechnology* 17, 676 (1999).

15. A. Kolin, In Electrofocusing and Isotachophoresis, B.J. Radola, and D. Graesslin, Eds.; de Gruyter: Berlin, 3-33 (1977).

16. Emrich, C. A.; Tian, H.; Medintz, I. L.; Mathies, R. A. *Analytical Chemistry* **2002**, *74*, 5076-5083.

17. Lagally, E. T.; Mathies, R. A. *Journal of Physics D: Applied Physics* **2004**, *37*, R245-R261.

18. Grover, W. H.; Skelley, A. M.; Liu, C. N.; Lagally, E. T.; Mathies, R. A. *Sensors and Actuators, B: Chemical* **2003**, *B89*, 315-323.

19. Paegel, B. M.; Blazej, R. G.; Mathies, R. A. *Current Opinion in Biotechnology* **2003**, *14*, 42-50.